Dynamics of Andeev states in a normal metal-superconductor ring : supercurrent fluctuations and spectroscopy of the minigap

Bastien Dassonneville

Université Paris-Sud

Ecole Doctorale de Physique de la Région Parisienne
Laboratoire de Physique des Solides

Discipline : Physique des Solides

Thèse de doctorat

Soutenue le 13 janvier 2014 par

Bastien Dassonneville

Dynamics of Andreev states in a normal metal - superconductor ring:

Supercurrent fluctuations and spectroscopy of the minigap

Directrice de thèse :	Hélène Bouchiat
Composition du jury :	
Président du jury :	Marco Aprili
Rapporteurs :	Jérôme Cayssol
	Hervé Courtois
Examinateurs :	Mikhaïl Feigel'man
	Cristian Urbina

Contents

Je voudrais pas crever
Avant d'avoir connu
Les chiens noirs du Mexique
Qui dorment sans rêver
Les singes à cul nu
Dévoreurs de tropiques
Les araignées d'argent
Au nid truffé de bulles
Je voudrais pas crever
Sans savoir si la lune
Sous son faux air de thune
A un coté pointu
Si le soleil est froid
Si les quatre saisons
Ne sont vraiment que quatre
Sans avoir essayé
De porter une robe
Sur les grands boulevards
Sans avoir regardé
Dans un regard d'égout
Sans avoir mis mon zobe
Dans des coinstots bizarres
Je voudrais pas finir
Sans connaître la lèpre
Ou les sept maladies
Qu'on attrape là-bas
Le bon ni le mauvais
Ne me feraient de peine
Si si si je savais
Que j'en aurai l'étrenne
Et il y a z aussi
Tout ce que je connais
Tout ce que j'apprécie
Que je sais qui me plaît
Le fond vert de la mer
Où valsent les brins d'algues
Sur le sable ondulé
L'herbe grillée de juin
La terre qui craquelle
L'odeur des conifères
Et les baisers de celle
Que ceci que cela

La belle que voilà
Mon Ourson, l'Ursula
Je voudrais pas crever
Avant d'avoir usé
Sa bouche avec ma bouche
Son corps avec mes mains
Le reste avec mes yeux
J'en dis pas plus faut bien
Rester révérencieux
Je voudrais pas mourir
Sans qu'on ait inventé
Les roses éternelles
La journée de deux heures
La mer à la montagne
La montagne à la mer
La fin de la douleur
Les journaux en couleur
Tous les enfants contents
Et tant de trucs encore
Qui dorment dans les crânes
Des géniaux ingénieurs
Des jardiniers joviaux
Des soucieux socialistes
Des urbains urbanistes
Et des pensifs penseurs
Tant de choses à voir
A voir et à z-entendre
Tant de temps à attendre
A chercher dans le noir
Et moi je vois la fin
Qui grouille et qui s'amène
Avec sa gueule moche
Et qui m'ouvre ses bras
De grenouille bancroche
Je voudrais pas crever
Non monsieur non madame
Avant d'avoir tâté
Le goût qui me tourmente
Le goût qu'est le plus fort
Je voudrais pas crever
Avant d'avoir goûté
La saveur de la mort.

Boris Vian

Au suivant

Remerciements

Je tiens tout d'abord à remercier du fond du coeur l'ensemble du groupe Meso pour la formidable ambiance qui y règne. J'ai énormément apprécié de travailler (ou pas) avec vous. Hélène est une chef géniale: on ne sait pas trop ce qu'elle fait, ça discute, ça s'énerve gentiment et au final voilà une superbe tartiflette ou un délicieux saumon... mais ça serait tout a fait réducteur de ne considérer Hélène que comme une chef, il faut aussi l'imaginer en exploratrice dans la jungle (ce qu'elle aurait pu devenir si le sort en avait décidé autrement, en tout cas voilà qui expliquerait le léger désordre de nos salles de manip). Et même si on a apparemment un sens de l'humour différent (la première de mes blagues que tu as compris, c'était trois mois avant ma soutenance si je me souviens bien), c'est toujours un plaisir de discuter avec toi. Meydi m'a beaucoup aidé au tout début de mon arrivée dans le groupe et m'a transmis une partie de son savoir lors de discussions qui avaient même parfois lieues avant le café. Ca a été un grand plaisir de te retrouver au Japon et d'être avec toi à Tokyo sous la neige. J'espère qu'on aura l'occasion de manger des vrais sushi ensemble et qu'entretemps j'aurai un peu progressé en japonais. Sophie est géniale quand il s'agit d'avoir quelque chose de simple: dans la vie pratique, les plans foireux et les systèmes D qui font galérer ne lui résistent pas, dans la vie théorique, elle a toujours cette volonté d'expliquer les choses simplement avec ses fameux "dessins bébés". Elle est aussi pleine d'enthousiasme, je me souviens de ton "mais c'est super t'as des résultats !" en voyant mes premières données qui m'avait beaucoup encouragé alors que c'était à peine le début d'un commencement de quelque chose. Richard quand à lui est l'exemple même de la clarté et de la concision. Si vous avez besoin de vous remettre les idées en place, ne cherchez pas plus loin il aura une explication sans fioritures pour vous. Vous pouvez même lui poser des questions sur les couches culottes, c'est devenu un expert! Mais il n'est pas seul, Sandrine est là entre deux dessins de bobines supra et de frigos. Vous vous doutez donc que j'ai appris beaucoup sur les bébés tant mon ignorance était grande sur le sujet. A special thank to Alik because he knows the secrets of FIB-deposited W. Without him I would not have measured anything. He also taught me many useful proverbs such as "I know but what to do !" and the always true "better is the enemy of good" and his special technic to keep a fresh mind: gymnastic. Julien m'a accompagné pendant deux ans et j'adorais quand il ramenait les petits-pains et les croissants pour le petit déj ou le fromage pour le midi. Je me suis bien marré avec Chuan que j'adore lui raconter des plagues et parce qu'elle est trop forte à tous les jeux. Si un jour elle en a marre de comprendre les secrets des électrons, elle n'aura qu'à faire des compets de billard ou de poker. L'ambiance des salles

enfumées lui convient aussi bien que celle, plus confinée, des salles blanches. J'espère que tu ne m'en veux pas de la tête que j'ai fait quand j'ai goûter à tes "bonbons" qu'on peut manger "quand tu veux" pendant le café post-déjeuner (composition des "bonbons": yak séché et épices, un peu surprenant quand on s'attend à du chocolat ou du caramel. Ca à un goût de bouffe pour chat mais on finit par aimer). Thanks to Katsuyoshi, I had fun with you racing in the stairs of the lab. You are my reference for Paris good restaurants. It was very nice of you to guide Meydi and me in Kanamura though you've been there dozens of time. Thanks also to Shamashis who helped me (whithout knowing it) to keep a good level in english, even if I know my accent is terrible. Il y a aussi des jeunes qui viennent d'arriver, Raphaëlle qui a toujours des chaussettes à la dernière mode et assorties à son mug à soupes chimiques. Anil qui continue ce que j'ai commencé et qui ira sans doute beaucoup plus loin que moi. Anil et Raphaëlle sauront prolonger l'esprit qui régnait dans le bureau où j'ai vécu, je leur fais confiance.

Merci à Marco Aprili, Jérôme Cayssol, Hervé Courtois, Mikhaïl Feigel'man et Cristian Urbina d'avoir accepté de faire partie de mon jury. Leurs questions et leurs remarques m'ont permis de clarifier et d'améliorer mon manuscrit de thèse.

Un merci particulier également à Julien Bobroff, Frédéric Bouquet et l'ensemble du groupe de vulgarisation avec qui j'ai eu le plaisir de faire du hoverboard et autres lévitations supraconductrices en mangeant de la meringue. Il faut maintenant que je l'avoue, il y a de cela quelques années quand je ne savais trop que faire de tout ce temps que sera ma vie, j'ai vu une affiche avec un aimant qui lévite au-dessus d'un supraconducteur et j'ai été fasciné. Je pense donc que c'est un peu à cause d'eux que je suis là aujourd'hui...

Merci à l'ensemble des habitants du labo que je croisais tous les jours (parfois même le week-end...) avec sourire. En particulier merci aux thésards du labo avec qui j'ai pu partager quelques bowlings et foots en salle arrosés de bière (avec modération) et de pizzas.

Merci aux autres thésards rencontrés en école d'été ou en conférence. Je me rappelle très bien cette fin août où je me demandais ce que je partais bien faire perdu en plein milieu des Alpes. J'avais peur de me retrouver seul avec la physique, ça n'a pas été le cas. Ca a été un plaisir de vous revoir régulièrement aux écoles d'étés et autres GdR.

Voilà le moment de remercier l'ensemble de mes potes, d'où qu'ils viennent et où qu'ils soient. Il y a la bande (élargie) du lycée avec qui j'ai passé des soirées dantesques et ruiné ma jeunesse (mais elle est faite pour ça, à quoi servirait-elle si on ne l'usait pas?). En plus on a parfois des bonnes nouvelles, comme l'apparition de nouveaux membres (qui l'eut cru?). J'espère que vous viendrez me voir même si je suis parti vers l'est (alors que tout le monde me pense à l'ouest). Il y a l'ensemble assez mal défini des scientifiques que j'ai rencontré dans cette magnifique banlieue du sud de Paris (il manquait une parenthèse ici). Heureusement que vous étiez là pour rendre sympa ce petit coin de paradis (je déconne presque) perdu (là je ne déconne pas). J'ai eu la chance énorme de partager ma vie quotidienne avec Cédric, Romain et une touche de Solène. Ca s'est fait presque par hasard, sur un pourquoi pas quand je cherchais à faire une coloc, ça s'est transformé en une superbe ambiance. En un hymne: vive le κ ! Dans ce milieu inhomogène que forme la masse de mes amis, je dois souligner la présence de Benjamin, fortement anis au trope avec qui j'ai

partagé les plaisirs de l'escalade. Merci à lui et à Clément d'avoir accepté la présence de ma soeur à l'appart, ça a dû être difficile pour vous d'avoir deux Bastien à la maison. Dans le genre escalade, je dois aussi remercier Doudou et Mary qui étaient toujours là pour me motiver pour aller au viaduc alors que c'est un endroit où on se fait mal au mains et qu'après on ne peut plus manger de biscuits tranquillement. Enfin un remerciement spécial à Yoan avec qui j'ai partagé ma chambre au LPS. C'était super de pouvoir parler avec lui tout en travaillant. J'ai beaucoup de respect pour ton engagement et j'espère que tu arriveras à construire ton petit coin en accord avec tes convictions (désolé de faire dans le sentimental, je ne dis pas là maintenant combien je me suis amusé avec lui; ça il le sait). Dans le genre amis, il y a l'espèce plus rare qu'on pourrait qualifier d'alien soit parce qu'ils le sont vraiment (dans le genre philosophe physicien sportif de haut niveau qu'est ce bon vieux bab) soit parce qu'on ne voit pas comment j'ai pu un jour les rencontrer et avoir une conversation avec eux (la Phiso Dallas multitâche ou la Philo danseuse Katkat) et la constellation McBabethienne-Moumougalienne les entourant. Je commence à raconter n'importe quoi alors le mot de la fin pour les amis revient au Génepi, où j'ai rencontré des gens sympas qui m'ont ouvert l'esprit à des questions que je ne me posais même pas.

Je vais essayer d'arrêter de raconter n'importe quoi et remercier ma famille. C'est avec vous que j'ai grandi depuis que je suis haut comme trois pommes et puis après quand je grimpais au pommier. Je dois vraiment remercier ma maman de m'avoir fait réciter mes verbes irréguliers en anglais, même si je soupçonne au vu de ses lectures de chevet que c'était aussi pour son propre plaisir qu'elle faisait ça. Merci à elle de nous avoir laissé libres de faire ce qu'on voulait, parfois après un "oh non !" indigné. Merci aussi à Céline, Gautier et Rémy; il paraît qu'on se ressemble mais je dois reconnaître que c'est bien pire que ce que tout le monde pense: je nous ai longtemps vu comme quatre émanations d'une même entité. Merci à mon père pour ses talents de bâtisseur et à Aline qui le soutien.

Pour finir, merci aux personnes qui ont contribué à faire de moi ce que je suis aujourd'hui mais qui ne sauront probablement jamais qu'elles sont ici remerciées: merci Adrien, Pierre et Alexia.

Et puis quand même merci au lecteur, sans lui tout ça ne servirait à rien.

1

Introduction

About 100 years ago, superconductivity was discovered by K. Onnes with the vanishing of the resistance of a piece of Hg when cooled down to $4K$ in liquid helium. The complete disappearance of resistance is most sensitively demonstrated by experiments with persistent currents in superconducting rings [1]. Once set up, they have been observed to flow without measurable decrease for a year. A lower bound of some 10^5 years for their decay time has been established. The true hallmark of superconductivity is however the so-called Meissner effect: a magnetic field is expelled from a macroscopic[1] superconductor, this is the perfect diamagnetism of a superconductor. This property is impressively demonstrated by the levitation of a magnet above a superconductor (see fig.1.1) [2].

These features can be understood within the framework of Ginzburg-Landau theory of phase transitions [3]. When going from a normal (non-superconducting) to a superconducting state, the gauge symmetry is broken and a *macroscopic wave function* $\Delta e^{i\varphi}$ with a unique phase φ emerges over the whole piece of superconducting metal. Δ is an energy gap in the density of states of the superconducting metal, as predicted by the microscopic theory of Bardeen, Cooper and Schrieffer (BCS theory) [4]. Meissner effect can be understood as follows: via the potential vector, the magnetic field creates a phase gradient that induces screening currents. These screening currents exclude the magnetic field from the bulk of the superconductor, therefore the magnet is repelled.

In 1962, Josephson predicted that two superconductors separated by a thin insulating layer (a SIS junction) support a non-dissipative current at equilibrium [7]. This effect, now called dc Josephson effect, was observed soon after [8]. Further studies have shown that the effect extends beyond Josephson's predictions and can exist if superconductors are connected by a weak link (a region where superconductivity is weak and where a phase drop can occur) of any physical nature [9]. In the following, we will focus on normal metal weak links (a SNS junction, see fig.1.1). Once again, the supercurrent originates from a phase gradient, here between two bulk superconductors.

Since the observation of superconductivity, non-dissipative currents are often associated with superconductivity yet superconductors are not the only systems that exhibit a non-dissipative behavior. Surprisingly, a small loop (a micron-sized loop) of a non-superconducting material threaded by a magnetic field at low temperature ($T < 1K$), also carries a persistent current (see fig.1.1). This is only possible thanks to quantum coherence: as in a superconducting

[1] larger than the magnetic field penetration length

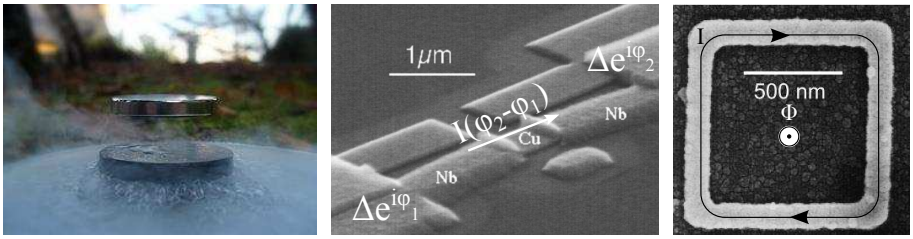

Figure 1.1: **Left:** Magnet (shiny plate) levitating over a YBaCuO plate (black plate, superconductor at -96^oC) in a liquid nitrogen bath. **Middle:** A SNS junction. A phase drop occurs in a region where superconductivity is weak, called a weak link. Due to the phase gradient, there is a non-dissipative current flow at equilibrium. After [5]. **Right:** A small normal metal ring (here, silver) threaded by a magnetic flux supports a persistent current I. After [6].

ring, there is phase sensitivity leading to non-dissipative currents. Such systems where the quantum coherence is preserved are called mesoscopic systems.

The existence of such persistent currents in normal rings, predicted in [10, 11, 12], was first greeted with skepticism. Its observation indeed depends on the way the experiment is performed: if leads are attached to the ring in order to perform transport experiments, a resistive behavior is observed [13]. Non-invasive measurements have to be performed, for instance by measuring the magnetic field created by the persistent current of one or an assembly of rings [14, 15, 16].

In the case of SNS junctions, superconducting leads does not break the phase coherence in N and most experiments probing their physics rely on the study of the switching from the non-dissipative to the dissipative state [17, 18, 19]. However the system is then in a strongly out-of-equilibrium regime; it is thus impossible to access its equilibrium properties.
These two remarks emphasize that **transport experiments are not optimal to elucidate the physics of a phase coherent system.** What kind of measurement is appropriate to unveil the physics of a phase coherent sample?

An alternative to transport experiments is to thread a non-connected ring with a time dependent flux oscillating at the frequency ω and measure the magnetic susceptibility $\chi(\omega) = \chi'(\omega) + i\chi''(\omega)$. In the linear response regime the susceptibility is related to the ac conductance G by $\chi = i\omega G$. The current response of mesoscopic rings to a time-dependent flux is the subject of several theoretical investigations [12, 20, 21, 22, 23]. The essential physics can be grasped thanks to a very simple two-levels model.

1.1 AC conductance of a flux-sensitive system: a simple model

SNS junctions and mesoscopic rings are phenomenologically analogous; both display a non-dissipative current at equilibrium. That reflects the phase dependence of their energy spectrum (see fig.1.2 for typical spectra) related to specific phase-dependent boundary conditions. Superconductors have indeed a gap Δ in their density of states and are similar to phase-conjugation mirrors in

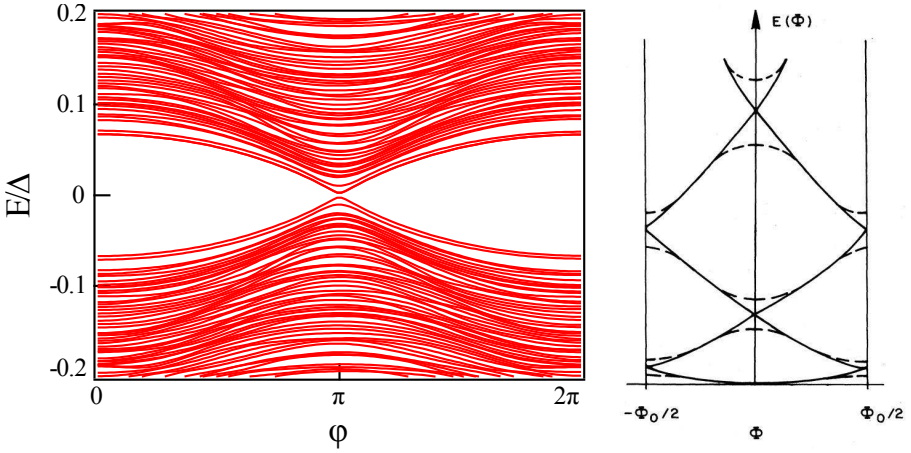

Figure 1.2: **Left:** Spectrum of a diffusive SNS junction with the normal part longer than the superconducting coherence length. **Right:** Electron energies of an isolated loop as a function of the flux. The ballistic loop is represented by full lines, the loop with additional elastic scattering by dashed lines. From [12].

a Fabry-Pérot cavity leading to the formation of phase-sensitive electron-hole bound states in the weak link called Andreev bound states [24, 25, 26, 27]. On the other hand, an electron in a mesoscopic ring experience periodic boundary conditions leading to energy quantization. Its phase sensitivity leads to a phase-dependent spectrum. This similarity between SNS junctions and mesoscopic normal rings has been underscored by several authors (e.g. [11, 28, 29, 30, 31]). There are however some major differences:

- the nature of the quasiparticles differs in these two cases : they are independent electrons in the case of purely normal rings whereas they are a superposition of an electron and a hole conjugated by time-reversal symmetry in the case of a SNS junction. The periodicity is therefore $\Phi_0 = \frac{h}{e}$ for a normal ring and $\Phi_0 = \frac{h}{2e}$ for a NS ring. In both cases one can define the phase φ as $\varphi = -2\pi\frac{\Phi}{\Phi_0}$ where Φ is the flux through the ring [2].

- In both cases the single level current i_n is given by the curvature of the energy level E_n:

$$i_n = -\frac{dE_n}{d\Phi} \tag{1.1}$$

  Due to the electron-hole symmetry in a SNS junction, all levels of negative energy carry current in the same direction; positive energy levels carry current in the opposite direction. In contrast, the sign of the single level currents alternates between adjacent levels in a normal ring. The sign of the total current therefore depends on the position of the chemical potential as observed experimentally [32] and on the particular realization of disorder in the ring.

[2] i.e. $\varphi = -e\Phi/\hbar$ in a normal ring and $\varphi = -2e\Phi/\hbar$ in a NS ring. We keep the same notation on purpose to emphasize the similarity of physical phenomena at play.

To elucidate the physics of such systems with a phase-dependent spectrum, we first derive their linear current response to a time dependent phase driving within a two levels model. We show with this simple model that there are two processes contributing to conductance: the first is related to the relaxation of populations driven out-of-equilibrium by the phase-driving, the second is related to induced transitions. We leave aside Zener tunneling processes because they are non-linear. This simple model qualitatively accounts for our findings in NS rings.

model: a phase-dependent two level system

To capture the physics of systems with a phase-dependent spectrum, we consider the simplest model: a single electron confined to a 1D ring threaded by a magnetic field. Due to the periodic boundary conditions, the eigenenergies of the system are quantized and, due to its ring geometry [33], they are Φ_0-periodic where $\Phi_0 = \frac{h}{e}$ is the flux quantum. At equilibrium, such a loop

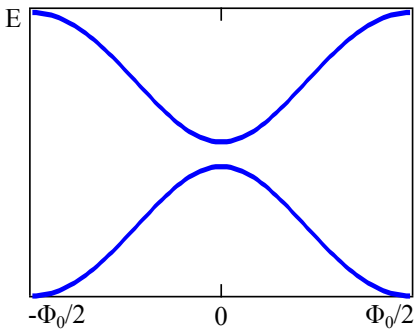

Figure 1.3: The physics of a phase-coherent system (e.g. a SNS junction or a normal mesoscopic ring) is captured in a simple two level model. The major feature of such a system is the phase dependence of its energy levels that leads to the emergence of a non-dissipative current at equilibrium.

displays persistent currents due to the flux-sensitivity of the energy levels E_n and the single-level current is:

$$i_n = -\frac{dE_n}{d\Phi} \tag{1.2}$$

The total current is then the sum of the single-level currents weighted by their occupation probability $\rho_n(E_n(\varphi), T)$. For a two levels system it reads:

$$I(\varphi, T) = \rho_1 i_1 + \rho_2 i_2 \tag{1.3}$$

AC Josephson effect

As emphasized by Bloch and by Buttiker, Imry and Landauer [34, 35, 11], applying a flux linearly increasing with time through a coherent ring leads to an ac current. This is due to the antisymmetry of the i_n with flux over one period ($-\Phi_0/2 \leq \Phi \leq \Phi_0/2$). This is the ac Josephson effect: the flux Φ leads to a dc voltage V such as

$$V = -\frac{d\Phi}{dt} \tag{1.4}$$

We have not yet considered the coupling of the system to a thermal bath (for instance a phonon bath). In the following we describe this coupling by an inelastic scattering time τ_{in}.

Relaxation of populations driven out-of-equilibrium by a time-dependent phase biasing

We first consider the equilibrium situation at a fixed flux Φ. If the coupling to the thermal bath is weak enough, the levels E_n acquires a finite lifetime τ_{in} and inelastic scattering induces transitions between the states. For a two levels system with $E_2(\Phi) = -E_1(\Phi)$ the current oscillates between i_1 and $i_2 = -i_1$. Inelastic scattering therefore cause fluctuations in the persistent current but do not destroy it [12].

If the system is now driven out of equilibrium, the rate of change from the out-of-equilibrium distribution toward the equilibrium distribution is determined by the lifetime τ_{in} of the states. To elucidate the physics further, we consider the response of a loop to an oscillating flux superimposed to a static flux [20]:

$$\Phi = \Phi_{dc} + \Phi_{ac} e^{-i\omega t} \tag{1.5}$$

with Φ_{ac} small compared to Φ_0.

In the presence of a time-dependent flux through the loop the occupation probabilities ρ_n become time-dependent. Inelastic scattering events cause transitions between these two levels and drive the system toward the instantaneous equilibrium $f_n(\Phi(t)) = f(E_n(\Phi(t)))$ with $f(E)$ the Fermi distribution. The master equation reads:

$$\frac{\partial \rho_n(t)}{\partial t} = -1/\tau_{in} \left[\rho_n(t) - f_n(\Phi(t))\right] \tag{1.6}$$

In the linear response regime we have:

$$f_n(\Phi(t)) = f_n(\Phi_{dc}) + \frac{\partial f_n}{\partial \Phi} \Phi_{ac} e^{-i\omega t} \tag{1.7}$$

and

$$\rho_n(t) = \rho_n(\Phi(t)) + \delta\rho_n e^{-i\omega t} \tag{1.8}$$

with $\rho_n(\Phi(t)) = f_n(\Phi(t))$. We now determine ρ_n to first order in Φ_{ac}:

$$\delta\rho_n = \frac{1}{1 - i\omega\tau_{in}} \frac{\partial f_n}{\partial \Phi} \Phi_{ac} = \frac{1}{1 - i\omega\tau_{in}} \frac{\partial f_n}{\partial E_n} \frac{\partial E_n}{\partial \Phi} \Phi_{ac} \tag{1.9}$$

and calculate the current to this order, using $i_n = -\frac{dE_n}{d\Phi}$:

$$\delta I = \sum_n i_n \delta\rho_n = -\frac{i\omega\tau_{in}}{1 - i\omega\tau_{in}} \sum_n i_n^2 \frac{\partial f_n}{\partial E_n} \Phi_{ac} \tag{1.10}$$

The magnetic susceptibility χ_D reads:

$$\chi_D = \frac{\delta I}{\Phi_{ac}} = -\frac{i\omega\tau_{in}}{1 - i\omega\tau_{in}} \sum_n i_n^2 \frac{\partial f_n}{\partial E_n} \tag{1.11}$$

Anticipating on the following, we denote this contribution to the susceptibility $\chi_D$and call it diagonal contribution since it involves only the diagonal elements i_n of the current operator. Its real part χ'_Dcontributes the non-dissipative response whereas its imaginary part χ''_Dcontributes the dissipative response.
In the original derivation by Büttiker [20], an effective ac conductance $\alpha(\Phi, \omega, T)$ has been calculated rather than a magnetic susceptibility χ_D. These two quantities are related by:

$$\chi''_D(\Phi, \omega, T) = \omega\alpha(\Phi, \omega, T) \tag{1.12}$$

As pictured in fig.1.4, it exhibits a very specific phase dependence with a double peak. This strong 2^{nd} harmonic reflects its dependence on the square of the single-level currents. It contributes the susceptibility both to its non-dissipative and dissipative parts. On the one hand, χ'_Dmodifies the phase-dependence of the adiabatic response $\chi_J = \frac{\partial I_J}{\partial \Phi}$ but does not modify its amplitude since $i_n(\Phi = p\frac{\Phi_0}{2}) = 0$ with p integer. On the other hand, χ''_Dreflects the emergence of dissipation at finite frequency. Its amplitude is maximal for frequencies close to the inelastic scattering rate. We also emphasize that due to the energy derivative of the Fermi distribution, this contribution is zero at zero temperature.

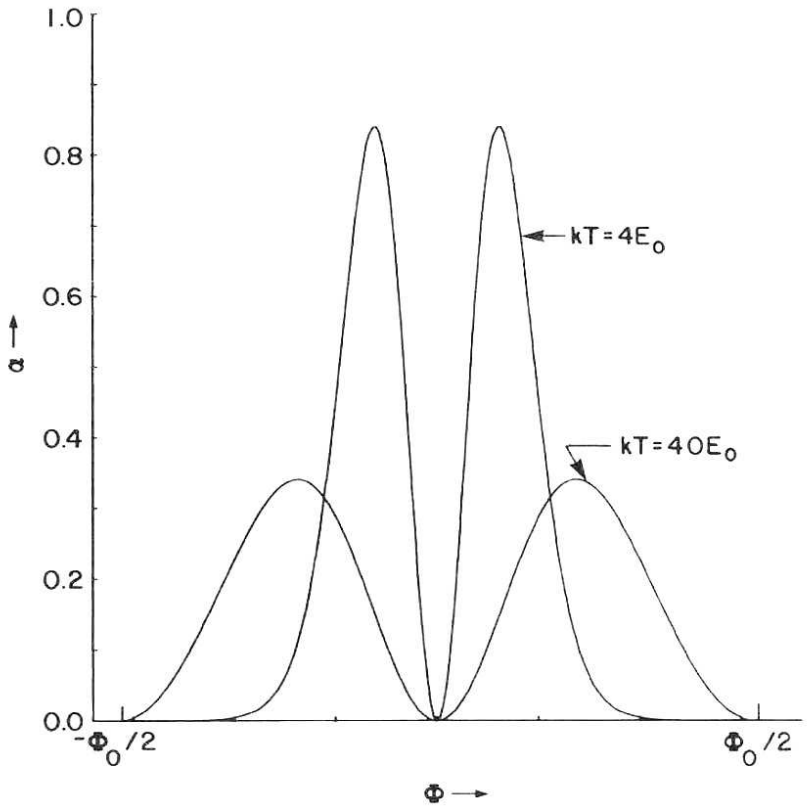

Figure 1.4: Effective ac conductance $\alpha(\Phi, \omega, T)$ related to the relaxation of populations for two different temperatures (in units of E_0, the level spacing). Note the dip around $\Phi = 0$. From [20]

Microwave-induced transitions in the spectrum

Another contribution to the ac conductance is due to the absorption of power by induced transitions. This contribution is non-negligible only when the microwave field is resonant with the energy difference between levels. The conductance of a phase-dependent two level system at frequency ω is zero excepts when $\hbar\omega = E_2(\varphi) - E_1(\varphi)$ where it peaks. Following the Kubo formula, the susceptibility related to this process,χ_{ND}, reads:

$$\chi_{ND} = \sum_{n,m\neq n} |J_{nm}|^2 \frac{f_n - f_m}{\epsilon_n - \epsilon_m} \frac{i\hbar\omega}{i(\epsilon_n - \epsilon_m) - i\hbar\omega + \hbar\gamma_{nm}} \tag{1.13}$$

where γ_{nm} describe the relaxation of the coherences due to interlevel transitions. We call this contribution the non-diagonal susceptibility since it depends on the non-diagonal elements of the current operator J_{nm}. The conductance $\sigma = \frac{\chi"_{ND}}{\omega}$ has been evaluated numerically by Imry et Shiren for a multi-level system using Kubo formula in the context of persistent currents[22]. Its phase dependence is shown at two different temperatures in fig.1.5. A remarkable feature is the emergence of half-periodicity with increasing temperature. In sharp contrast with $\chi''_D(\Phi, \omega, T)$, this conductance peaks at multiples of $\Phi = \frac{\Phi_0}{2}$ at low temperature and has a phase dependence opposite in sign to the one of $\chi''_D(\Phi, \omega, T)$ at high-temperature.

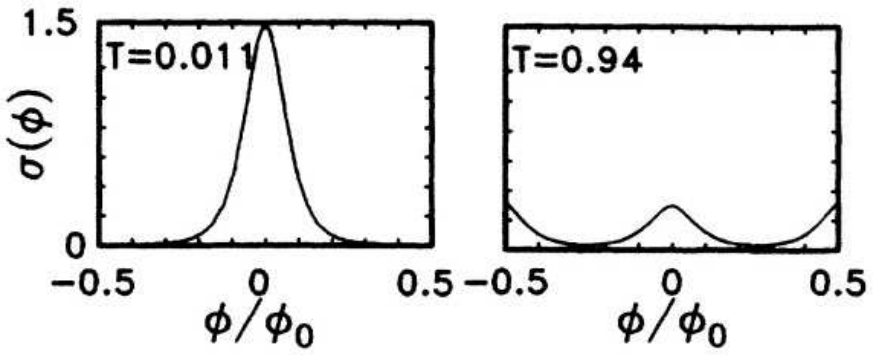

Figure 1.5: AC conductance $\sigma(\Phi, T)$ for two different temperatures (in units of the average level separation) related to the absorption of microwaves. Note the peak at $\Phi = 0$. From [22]

This two-level model contains the main physical mechanisms we will consider all along this dissertation: the relaxation of population driven out-of-equilibrium by a time-dependent phase biasing and microwave-induced transitions within the spectrum[3]. Before deriving these contributions on a more solid ground following an approach developed by Trivedi and Browne in [23] (see chap.3), we compare the predictions of this simple model with our observations.

[3] At the time when [20, 22] were written, it was not clear that both contributions have to be taken into account to calculate the conductance. This was later clarify by Trivedi and Browne in [23].

1.2 From a two-level model to the detection of finite-frequency effects in phase-coherent systems

We showed with a simple model that a system having a phase-dependent spectrum exhibits non-dissipative currents at equilibrium and, correlatively, a frequency dependent ac conductance given by the sum of two distinct contributions: induced transitions and relaxation. In the following we give a brief overview of the technique we used to probe the ac conductance of phase-coherent rings and the results of our latest experiment on hybrid NS rings.

Finite frequency phase biasing using a multimode resonator

To perform finite-frequency phase biasing we use a technique developed in the nineties by H. Bouchiat and B. Reulet [36]. The system is electromagnetically coupled to a superconducting multimode resonator that provides both excitation and detection at its eigenfrequencies (see fig.1.6). One can thus drive the phase at frequencies ranging from a hundred of MHz to a few GHz. Detection relies on the perturbation of the resonator's impedance by the mesoscopic samples. The amplitude of the perturbation is proportional to the current in the samples; therefore the larger the current in the samples, the stronger the signal.

As already mentioned, the minigap imposes its curvature to all energy levels in a SNS junction whereas in a normal ring the sign of single level currents alternates therefore the total current is roughly given by the topmost level. The supercurrent in a SNS junction is therefore greater than the persistent current in a normal ring by a factor g where g is the dimensionless conductance of the normal wire. As a direct consequence, whereas it is necessary to have about 10^5 normal rings to obtain a measurable signal, a single hybrid NS ring yields the same signal.

AC linear response of phase-coherent systems

The ac conductance of normal mesoscopic rings has been measured in the nineties [36, 37, 6]. It was found that the conductance measured in an isolated system is fundamentally different from its value measured in a connected one. In particular, it is dominated by its imaginary non-dissipative component, not measurable with a connected geometry. In contrast with a wire attached to leads where dissipation is mainly brought by the contacts, the intrinsic dissipative components of an isolated sample is due to induced transitions within the spectrum. These experiments however did not reveal any dynamical contribution to the conductance, predicted when the excitation frequency is of the order of the inelastic scattering rate.

These experiments were performed in two opposite limits: the *discrete* spectrum and *continuous* spectrum. In the current work we address the question of the ac conductance of a hybrid NS ring. In contrast with purely normal rings, the spectrum of a NS ring is fundamentally modified by the penetration of superconducting correlations in the normal part with the emergence of a phase dependent gap. When the normal part is a diffusive wire longer than the superconducting coherence length, its maximum amplitude is smaller than the superconducting gap, it is therefore called the minigap. Except for

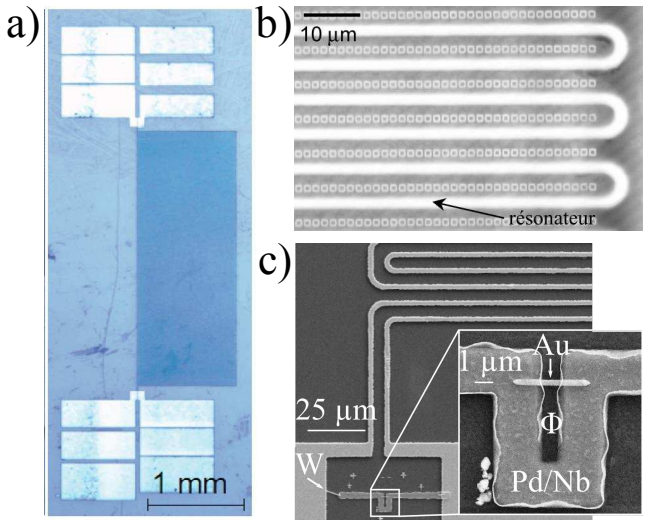

Figure 1.6: Finite frequency phase-biasing setup. **a)** Multimode Nb resonator that provides excitation and detection at its eigenfrequencies. **b)** This resonator can detect the persistent currents of an assembly of normal metal rings deposited onto the resonator (from [6]) it can also be used to probe the properties of a single NS ring, here (**c**) connected to the contact pads of the resonator.

the minigap, the spectrum of a SNS junction is continuous. We expect the ac conductance to be sensitive to the presence of the minigap.

As detailed in chap.3 and 4, we address this question theoretically following a Kubo-formula approach. These works indicates that the minigap is indeed a relevant timescale. It should be possible to perform its spectroscopy by susceptibility measurements. Yet it is not the only relevant timescale, the relaxation time of the populations having also great importance.

In agreement with these theoretical predictions and as briefly introduced in sec.1.1, we found two contributions to the ac conductance. The first one describes the relaxation of populations driven out-of-equilibrium by the excitation and therefore emerges on a scale given by the inelastic scattering time τ_{in}. Its evolution with temperature and frequency revealed a puzzling inelastic scattering time. It also unveiled the existence of an equilibrium supercurrent noise.

The second contribution describes induced transitions across the minigap that emerges on the frequency scale of the minigap. The evolution of its phase dependence with temperature and frequency is determined by the phase-dependent minigap for frequencies larger than the temperature; in the opposite limit, it is related to the phase-dependence of the non-diagonal elements of the current operator. They show an interesting physics since they favor transitions between electron/hole symmetric states, thus acting as selection rules. These findings are introduced in chap.6 after a presentation of the experimental techniques in chap.5.

2

Basic concepts and state of the art

In this chapter we present the basic concepts of mesoscopic physics and superconductivity necessary to understand our experiment on the linear response of a NS ring. We develop on the analogy between persistent currents in normal rings and supercurrents in SNS junctions. We underscore the essential role of phase in such phase-coherent systems and discuss the different ways to carry out phase-biased experiments.

2.1 The mesoscopic scale

Electronic transport in metals at low temperature presents various interesting features due to the interference between the electronic wavefunctions. In particular, Ohm's law is no more verified; even more, the notion of conductance depends on the way it is measured.

The phase coherence length

The phase coherence length L_Φ is the characteristic length for the interferences of the electronic wave functions. It is the typical length on which a wave packet can travel without loosing its phase coherence. L_Φ increases with decreasing temperature and can be much larger than l_e, the elastic mean free path. It is the relevant length scale for mesoscopic physics. L_Φ is limited by all possible physical mechanism susceptible to suppress quantum interference between electronic wavefunctions. In particular it is a measure of the coupling of the interfering electrons with their environment i.e. the heat bath. This environment consists of phonons, electromagnetic fluctuations, other electrons, magnetic impurities among other possible excitations. In most cases L_Φ is related to inelastic collisions like electron-phonon and at lower temperature electron-electron interactions [38]. However phase breaking processes do not necessarily involve energy exchange between the interfering particle and environment degrees of freedom, but at least some modification of the environment state [39]. This is for instance the case of spin-flip scattering against paramagnetic impurities which gives rise to a contribution to L_Φ which is independent of temperature at zero field.

Definitions of conductance

Mesoscopic systems are characterized by their phase coherence, this means electrons go through the sample without interacting much with the thermal

bath. The *conductance* of such a system is a rather paradoxical concept since any physical measurement of conductance involves Joule effect and energy dissipation.
There are two theoretical definitions of the conductance, one developed by Landauer [40, 41, 42, 12], the other one by Kubo and Greenwood [43, 44]. Kubo-Greenwood approach relates the conductance to the absorption of an electromagnetic wave by an isolated sample. It can be used to compute the dc conductance of a connected sample, the system to consider is then the total system: sample plus leads. Within this framework, the conductance of an isolated system, with a discrete spectrum, is expected to show peaks at frequencies equal to the difference of two eigen-energies of the system. The conductance at zero-frequency is expected to be zero. For a connected sample, there is hybridization of eigenstates of the sample and of the leads. The spectrum is then continuous and absorption can occur at any frequency leading to a finite dc conductance.
Within Landauer approach the conductance is defined as the transmission of the electronic waves through the sample. The sample is then analog to a waveguide connected to reservoirs. The reservoirs absorb all incoming electrons and emit them with a random phase. The obstacle is characterized by the transmission probability τ for carriers to traverse the sample. At zero temperature, the conductance of a single channel is

$$G_s = \frac{2e^2}{h}\frac{\tau}{1-\tau} \tag{2.1}$$

where the spin degeneracy has been taken into account. This is different from G_c the conductance measured between the two reservoirs

$$G_c = \frac{2e^2}{h}\tau \tag{2.2}$$

The resistance between the reservoirs is

$$G_c^{-1} = G_s^{-1} + \frac{h}{2e^2} \tag{2.3}$$

that is to say the resistance between the reservoirs is the sum of the sample resistance and the contact resistances. One sees that even for a perfect wire ($\tau = 1$) there is still a contact resistance of $\frac{e^2}{h}$ due to the electrons thermalizing in the baths by inelastic scattering.
Even though Landauer and Kubo formulations of conductance start from radically different point of views, it has been shown [45] that they are equivalent in the macroscopic regime. This is not correct for a mesoscopic sample with a discrete spectrum such as isolated AsGa rings [37]. In a connected geometry the conductance does not measure the energy dissipated inside the sample but rather in the leads where thermalisation of the electrons takes place whereas in an isolated sample it measures power absorption.

2.2 Physics of SNS junctions

The modern description of the Josephson effect rely on the existence of bound states in the weak link, called Andreev bound states. They are *localized* in the

weak-link due to the mirror-like boundary conditions at the superconducting interfaces and therefore have quantized energies [46, 47, 29, 31, 48, 49, 50], smaller than the superconducting gap [24]. However behind this unifying concept there is a hidden complexity related to the ratio between characteristic length scales (the physical length of the weak link L and the elastic mean free path l_e) and the superconducting phase coherence length ξ_s. In a ballistic metal $\xi_S = \frac{\hbar v_F}{\Delta}$ whereas in a diffusive metal $\xi_S = \sqrt{\frac{\hbar D}{\Delta}}$ where v_F is the velocity at Fermi energy and D is the diffusion constant. For the sake of clarity, these different regimes are summed up in table.2.1.

	short	long
ballistic	$L < l_e, \xi_s$	$\xi_s < L < l_e$
diffusive	$\xi_s > L > l_e$	$\xi_s, l_e < L$

Table 2.1: Regimes of a SNS junction. L is the length of the normal part, l_e the elastic scattering length and ξ_s the superconducting coherence length.

Andreev reflection

When connecting a normal metal (N) to a superconductor (S), we would naively expect no current flow because, due to the presence of an energy gap Δ in its density of states, there is no states in the superconductor for an electron at Fermi energy in the normal metal. Yet a non-dissipative current can flow. As depicted in fig.2.1 , an incoming electron can be reflected into a hole at the NS interface and thus transfer a Cooper pair in the superconductor. This process is called an Andreev reflection [51, 52, 53]. Electron and hole are conjugated by time reversal symmetry and form a so-called Andreev pair. A normally incident electron of energy $\epsilon_e = E_F + \epsilon$, wave vector $k_e = k_F + q$ and phase φ_e is reflected into a hole of energy $\epsilon_h = E_F - \epsilon$, wave vector $k_h = -k_F + q$ and phase $\varphi_h = \varphi_e + \varphi - \arccos(\epsilon/\Delta) \sim \varphi_e + \varphi - \frac{\pi}{2}$. Similarly, a hole is coherently reflected as an electron at a NS interface.

As measured with shot noise experiments [54], this process transfers a charge of $2e$. It can be seen as the propagation of superconducting correlations in the normal metal as observed with the diminution of the induced gap away from the interface [55].

Andreev Bound States: from the short & ballistic to the long & diffusive junction

In the case of a SNS junction, Andreev reflections at the interfaces between N and S metals lead to the formation of states confined in the N part called Andreev bound states (ABS). They are determined by solving the Bogoliubov-de Gennes hamiltonian that describes the proximity effect [9]. The spectrum of Andreev bound states depends on the limit the junction is in (long/short, ballistic/diffusive). In the following we derive this spectrum in the clean limit and then look at the effect of an impurity. In the diffusive limit, the exact

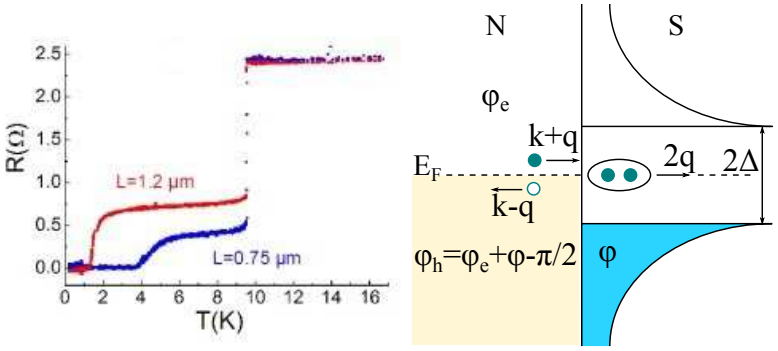

Figure 2.1: **Left:** Vanishing of the resistance of a normal wire of length L connected to two superconducting electrodes. Current is then non-dissipative. This is related to the emergence of phase-dependent states in the normal metal, the Andreev bound states. After [56]. **Right:** Andreev reflection: an incoming electron (hole) is reflected as a hole (electron) at the NS interface.

spectrum depends on the disorder configuration[1]. The density of states in N is determined thanks to Usadel equations that rely on impurity averaging.

Andreev spectrum in the ballistic limit – Scattering by an impurity

Kulik determined the spectrum in the ballistic and zero temperature limit [46] by using the continuity of the wavefunction and its derivative at the interfaces. Following Kulik, we consider a system that consists of a 1D normal wire of length $L = 2d$ connected to two superconducting electrodes of order parameter $\Delta e^{i\varphi_1}$ and $\Delta e^{i\varphi_2}$. First we solve the Bogoliubov-de Gennes equation that reads:

$$\begin{pmatrix} \mathcal{H} & \Delta \\ \Delta^* & -\mathcal{H}^* \end{pmatrix} \psi = E\psi \tag{2.4}$$

with

$$\psi(x) = \begin{pmatrix} u(x) \\ v(x) \end{pmatrix} \tag{2.5}$$

the wavefunction of the system. $u(x)$ describes the electron-like part of this wavefunction while $v(x)$ is the hole-like component. $\mathcal{H} = p^2/2m + V(x) - E_F$ is the one-particle Hamiltonian with energies defined relatively to the Fermi energy. The potential $V(x)$ describes an eventual disorder and is taken as zero in this case. If one considers the bound states of the system ($E_n < \Delta$), the expression of the solutions to this equation in the different part of the junction are:

Left electrode:

$$\psi_L^+(x) = C^+ e^{i\lambda_-(x+d)} \begin{pmatrix} \gamma \\ e^{-i\varphi_1} \end{pmatrix} \tag{2.6}$$

$$\psi_L^-(x) = C^- e^{-i\lambda_+(x+d)} \begin{pmatrix} \gamma^* \\ e^{-i\varphi_1} \end{pmatrix} \tag{2.7}$$

[1] The spectrum can be determined for a given disorder configuration by numerical simulations (see chap.4)

N part:

$$\psi_N^+(x) = A^+ e^{ik_+ x} \begin{pmatrix} 1 \\ 0 \end{pmatrix} + B^+ e^{ik_- x} \begin{pmatrix} 0 \\ 1 \end{pmatrix} \tag{2.8}$$

$$\psi_N^-(x) = A^- e^{-ik_+ x} \begin{pmatrix} 1 \\ 0 \end{pmatrix} + B^- e^{-ik_- x} \begin{pmatrix} 0 \\ 1 \end{pmatrix} \tag{2.9}$$

Right electrode:

$$\psi_R^+(x) = D^+ e^{i\lambda_+(x-d)} \begin{pmatrix} e^{i\varphi_2} \\ \gamma \end{pmatrix} \tag{2.10}$$

$$\psi_R^-(x) = D^- e^{-i\lambda_+(x-d)} \begin{pmatrix} e^{i\varphi_2} \\ \gamma^* \end{pmatrix} \tag{2.11}$$

with

$$\gamma = \frac{\Delta}{E + i\sqrt{\Delta^2 - E^2}} \tag{2.12}$$

$$\frac{\hbar^2 \lambda_\pm^2}{2m} = E_F \pm i\sqrt{\Delta^2 - E^2} \tag{2.13}$$

$$\frac{\hbar^2 k_\pm^2}{2m} = E_F \pm E \tag{2.14}$$

In the N part, the solution denoted with a plus sign corresponds to excitations moving from left to right whereas the minus sign to excitations from right to left. The continuity of the wavefunction and its derivative at the NS interfaces yields the condition of quantification of the energy levels:

$$\gamma^2 e^{2i(k_+ - k_-)d} e^{\pm i\varphi} = 1 \tag{2.15}$$

where $\varphi = \varphi_1 - \varphi_2$. This leads to the quantification relation of energy levels E_n:

$$2\arccos(E_n/\Delta) + \frac{L}{\xi_S}\frac{E_n}{\Delta} \pm \varphi = 2n\pi \tag{2.16}$$

where $\xi_S = \frac{\hbar v_F}{2\Delta}$ is the superconducting coherence length. The term $2\arccos(E_n/\Delta)$ is the phase shift acquired from the evanescent quasiparticle waves penetrating into the superconducting regions. The term $\frac{L}{\xi_S}\frac{E_n}{\Delta}$ is the phase shift acquired from free electron and hole propagation in the normal region. Finally the superconducting phase difference φ enters eq.2.16 because of the additional phase shift between reflected electron and hole acquired during Andreev reflection.

Following [28], we consider the effect of an impurity in an otherwise clean junction in 1D. In the presence of a point impurity potential $V(x) = V_s\delta(x-a)$, eq.2.16 is modified to

$$2\arccos(E_n/\Delta) + \frac{L}{\xi_S}\frac{E_n}{\Delta} \pm \alpha = 2n\pi \tag{2.17}$$

where the phase α is determined from

$$\cos\alpha = \tau\cos\varphi + (1-\tau)\cos\left(\frac{L-2a}{\xi_S}\frac{E}{\Delta}\right) \tag{2.18}$$

Short and clean junction limit

In the short junction limit, $L \ll \xi_S$, we immediately find from eq.2.17 that the Andreev spectrum of a channel of transmission τ is determined as

$$E^{\pm} = \pm\Delta\sqrt{1 - \tau\sin^2(\varphi/2)} \tag{2.19}$$

Beenakker has derived a more general expression in the multichannel case [57]. This result has been previously obtained by Zaitsev by solving the Eilenberger equations [58]. In this case, the spectrum is simply obtained using the transmission τ_n of each independent channel.

This equation calls two comments. First, that disorder drives the amplitude of the supercurrent: since it lifts the degeneracy at $\varphi = \pi$, it imposes the curvature of the Andreev bound state hence the supercurrent $i_n \propto \frac{\partial E_n}{\partial \varphi}$. The size of the gap δ opening at π is

$$\delta = 2\Delta\sqrt{(1 - \tau)} \tag{2.20}$$

The degeneracy is lifted because the impurity, when reflecting quasiparticles, couples the left-going and right-going quasiparticles which pertains to levels symmetric with respect to the Fermi energy. Secondly, it may look surprising that the properties of the Josephson junction are determined by the *normal* state scattering properties of the weak-link. This is because the reflection at the interface that couples the electron and hole states can be separated from the propagation in the weak link that does not couple electrons and holes [57].

This description is well verified experimentally in superconducting atomic contacts where it is possible to determine the set of transmissions [59]. Moreover, the spectroscopy of Andreev Bound States in superconducting atomic contacts has recently been performed [60] and agrees with this picture.

Long and clean junction limit

The case of the long and clean junction has been studied by several authors [46, 47, 29, 28]. The basic picture given before is still qualitatively correct, with the formation of Andreev bound states localized in the weak link. However, when going to the long junction limit it can be noted that, in contrast with short junctions, there are Andreev states whose energies at zero-phase $E_A(\varphi = 0)$ is smaller than the superconducting gap Δ.

Andreev spectrum in the diffusive limit

In the diffusive limit [62], all the transmission coefficients are not independent and one has to consider a number of independent "effective conductive channels" $N_{eff} \sim \frac{Nl_e}{L} \sim g$ where L is the length of the system and l_e the elastic scattering length. $N \sim k_F^2 A$ is, as in the ballistic case, the number of channels given by the quantization of the transverse momentum in a wire of cross section A. g is the dimensionless conductance.

Short and diffusive junction limit

In the short and diffusive junction limit the Andreev spectrum is once again given by

$$E_p^{\pm} = \pm\Delta\sqrt{1 - \tau_p\sin^2(\frac{\varphi}{2})} \tag{2.21}$$

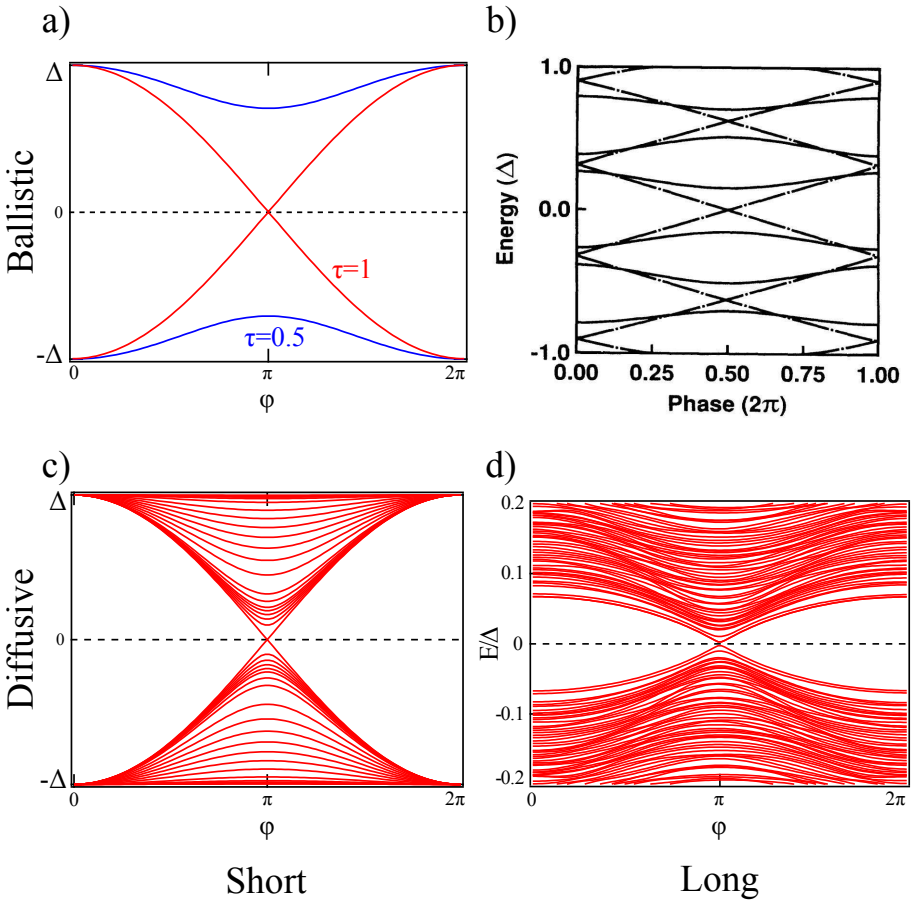

Figure 2.2: Andreev spectra in different limits. Note for all these spectra the electron-hole symmetry. **a.** Andreev levels for transmissions $\tau = 1$ and $\tau = 0.5$ in a short and ballistic junction. The Andreev gap closes at π for transmission 1. **b.**Andreev levels in a long and ballistic junction without (dashed lines) and with (solid lines) an impurity. Note the emergence of states at energies smaller than the superconducting gap (from [28]). **c.** Short and diffusive junction. **d.** In a long and diffusive junction, Andreev bound states leads to the emergence of a phase-dependent minigap. Note that the amplitude of the minigap is much smaller than the superconducting gap Δ. This spectrum has been calculated by numerical simulations (see chap.4 and [61]).

this expression being valid for arbitrary degrees of disorder [57, 63]. Being in the diffusive limit means there are N_{eff} channels, with N_{eff} large. In this case it is easier to use the probability of transmission in the diffusive limit given by [64, 65]

$$P(\tau) = \frac{\pi}{2e^2 R_N} \frac{1}{\tau\sqrt{1-\tau}} \tag{2.22}$$

and to replace the sum over the channels by an integration over the transmission.

Long and diffusive junction limit

In the long and diffusive limit it is more convenient to use the quasiclassical Green formalism than the Landauer approach, since one cannot relate a particular Andreev level to an eigenmode of the transmission matrix like in short junctions. The equivalence between these two approaches is demonstrated in [66]. The density of states in N has been calculated within quasiclassical formalism in [67, 68]. It exhibits a phase-dependent gap $E_g(\varphi) \simeq 3.1E_{Th}\,|\cos(\varphi/2)|$ closing linearly at π. Its amplitude is maximal at $\varphi = 0$ and is given by $E_g(\varphi = 0) \simeq 3.1E_{Th}$. The spectroscopy of the minigap has been done by scanning tunneling microscopy [25] and a good agreement with quasiclassical theory is found.

Amplitude of the critical current

The amplitude of the critical current I_c, the maximum of the supercurrent, depends on the limit the junction is in. The theoretical predictions concerning its value (except for the long and diffusive junction) are reviewed by Likharev in [69]. There are two limiting cases:

- **Short junction** In this case $E_{Th} \gg \Delta$, the amplitude of the critical current is imposed by the superconducting gap Δ. At zero temperature, Kulik and Omelyanchuk predict that:
  - $eR_N I_c = 2.07\Delta$ for a diffusive junction [70]
  - $eR_N I_c = \pi\Delta$ for a ballistic junction [71]
- **Long junction** In this case $E_{Th} \ll \Delta$, the amplitude of the critical current is imposed by the Thouless energy E_{Th}. At zero temperature, it is predicted that:
  - $eR_n I_c = 10.82E_{Th}$ for an infinitely long diffusive junction [72] where $E_{Th} = \frac{\hbar D}{L^2}$ with D the diffusion coefficient and L the length of the junction.
  - $eR_n I_c = E_{Th}$ for a ballistic junction [46] where $E_{Th} = \frac{\hbar v_F}{L}$ with v_F the velocity at Fermi energy and L the length of the junction.

Continuum of states at high energy

At energies greater than the superconducting gap, quasiparticles are no more confined to the weak link and form a continuum of states [46, 29]. It has been shown not to contribute to the supercurrent in point contacts [57], it has however a small contribution in junction of finite length [73].

To summarize, on the one hand one sees that going from the short to the long junction limit allows for states at energies smaller than Δ at $\varphi = 0$. The transition from short to long is addressed in [74, 75] where it is shown that the size of E_g interpolates between a few E_{Th} in the long junction limit to Δ in the short junction limit. On the other hand going from ballistic to diffusive does not qualitatively change the picture, one has just to consider an increasing number of channels when going toward the diffusive limit. At some point, it is easier to use the quasiclassical formalism that averages on the disorder rather than the Landauer formalism to determine quantities of interest.

Current-phase relation in a long and diffusive Josephson junction

Josephson's prediction was that a SIS junction with a phase drop φ across the superconducting electrodes supports a sinusoidal supercurrent $I_J(\varphi)$ of maximal amplitude I_c, the critical current:

$$I_J(\varphi) = I_c \sin(\varphi) \tag{2.23}$$

In the general case the current-phase relation has to be determined from the Andreev spectrum (see [63] for a review). The total supercurrent is the sum of the single level current multiplied by their occupation probability at temperature T which is a fermi distribution $f_n(\varphi, T) = f(E_n(\varphi), T)$ at equilibrium:

$$I_J(\varphi, T) = \sum_n f_n(\varphi, T) i_n(\varphi) \tag{2.24}$$

One sees from eq.2.24 that the supercurrent depends on the spectrum as well as on its occupation; therefore the shape of the current-phase relation can be modified by manipulating the occupation numbers of Andreev bound states, i.e., creating a non-equilibrium distribution function. This has been done in[76, 77] where the current-phase relation has been shifted by a phase of π. From the microscopic point of view, this is simply due to the fact that enough positive energy levels, carrying an opposite current, are occupied. This is possible since, as shown in [78], due to the scarcity of inelastic scattering in mesoscopic wires, electronic distribution can be driven out-of-equilibrium, having a non-Fermi, double-step-like, dependence on energy.

In the following, we describe the current-phase relation of long and diffusive junction since it is the type of Josephson junction we have experimentally studied. The supercurrent of a long and diffusive junction has been determined by Heikkilä *et al.* [79]. It is not purely sinusoidal at zero-temperature:

$$I_s = \sum_n I_{c,n} \sin(n\varphi) \tag{2.25}$$

with

$$I_{c,n} = -(-1)^n \frac{10.82 E_{Th}}{e R_N} \frac{3}{(2n+1)(2n-1)} \tag{2.26}$$

where R_N is the resistance in the normal state. The occurrence of higher harmonics may be interpreted as a correlated transfer of n Cooper pairs through the weak-link due to Andreev pairs undergoing several Andreev reflexions before being transmitted. The current-phase relation however turns sinusoidal at high enough temperature, $T \gtrsim E_g$, as observed experimentally [80]. The temperature dependence of the critical current has been calculated and measured by Dubos *et al.* [72, 5]. At high temperature ($T > 5E_{Th}$) it roughly decreases exponentially with temperature on a scale given by the Thouless energy.

The current-phase relation reflects both the Andreev spectrum and its occupation. One of the goals of this work is to see how the current-phase relation is affected by a finite frequency phase-biasing.

Out-of-equilibrium effects in a voltage biased SNS junction

When a SNS junction is voltage biased several out-of-equilibrium effects arise, they are described in the following.

AC Josephson effect

A dc bias voltage V drives the phase according to:

$$\frac{d\varphi}{dt} = \frac{2eV}{\hbar} \tag{2.27}$$

The phase therefore increases linearly with time with a slope given by the Josephson pulsation:

$$\omega_J = \frac{2eV}{\hbar} \tag{2.28}$$

This is the ac Josephson effect. Following the interpretation of Bloch detailed in the introduction [34], the ac Josephson effect proceeds from the 2π-periodicity of the Andreev spectrum.

Multiple Andreev reflections

Under a voltage bias V, quasiparticles below the superconducting gap can cross the weak link by undergoing $n = \frac{2\Delta}{eV}$ Andreev reflections [81]. This process, called multiple Andreev reflections (MAR), can be described as successive Andreev reflections. At each traversal of the junction, quasiparticles gain an energy eV which allows them to eventually overcome the superconducting gap and escape the weak link.

At low voltage bias and for short and ballistic SNS junctions, this phenomenon can be described in term of coherent Landau-Zener transitions [82]. This theory quantitatively describes the current-voltage IV characteristics in superconducting atomic contacts [59, 83].

The case of long and diffusive junction is more involved with a transition from a coherent regime at low voltage ($eV < E_{Th}$) to an incoherent regime at large voltage ($eV > E_{Th}$) compare to the Thouless energy [84, 85]. On the one hand, the incoherent regime can be well described by the quasi-classical theory [86, 87, 88]. On the other hand, while the current-voltage characteristics can be calculated at zero temperature in the coherent regime [89], the noise has not yet been derived. Recent measurements [90, 84, 85] show that the noise in such junctions is strongly enhanced at low voltage, which is partially described in the framework of coherent MAR. However, this analysis leads to surprisingly large effective charges compared to the expected cutoff of coherent MAR due to inelastic processes. Thus the transport in a voltage biased long SNS junction is not completely understood yet.

Relaxation of populations driven out-of-equilibrium by the ac Josephson effect

The question of the relaxation of populations driven out-of-equilibrium by the ac Josephson effect has been addressed theoretically by several authors [91, 92, 93, 94] within Green functions formalism. Their work mainly consist in approximating Usadel equations in an adiabatic regime when voltage biasing is such that the Josephson frequency ω_J is small compared to the inverse diffusion time τ_D^{-1} :

$$\omega_J \tau_D = \frac{2eV}{\hbar}\tau_D \ll 1 \tag{2.29}$$

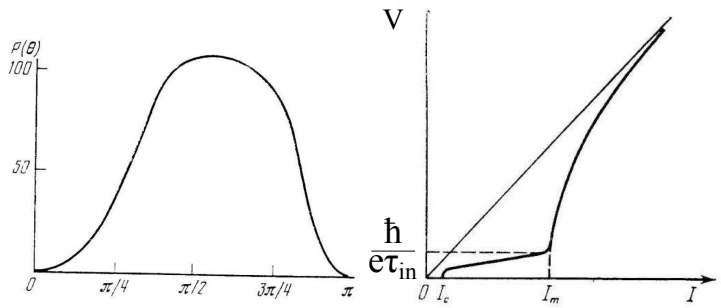

Figure 2.3: **Left:**Phase dependence of the function $P(\theta)$ that determines the non-equilibrium current at low voltages ($\omega_J \tau_D = \frac{2eV}{\hbar}\tau_D \ll 1$). **Right:** Current-voltage characteristic of a SNS junction when relaxation of Andreev pairs is taken into account. After [91]

According to the ac Josephson effect, voltage biasing leads to a phase increasing linearly with time with a slope ω_J. If the phase changes, so does the energy spectrum with its phase-dependent levels $\epsilon_n(\varphi)$ and so does the distribution $f(\epsilon_n(\varphi))$ which depends on the phase via the energy. If the phase evolution is slow compared to the inelastic scattering time[2], the electronic system has time to relax toward an equilibrium distribution. However, as soon as the phase evolution is faster than the inelastic scattering time, populations start being out-of-equilibrium. **Therefore a dc voltage leads to an out-of-equilibrium occupation of energy levels.** S. Lempiskii the first drew an approximated phase dependence of this effect and conclude to the existence of a bend in the current-voltage characteristic. This non-equilibrium effect is embodied in the function $P(\theta)$ that depends on the phase difference θ (see fig.2.3).

The phase dependence in fig.2.3 and 1.4 are actually similar[3]. It is simply because they address the same phenomenon: the relaxation of populations of a phase-dependent system driven out-of-equilibrium by a time-dependent phase. The origin of energy levels oscillation is different in these two theoretical works with one given by the ac Josephson effect whereas the other one is imposed by an oscillating flux. We comment on the difference between these two configurations in the following.

2.3 Comparison between dc voltage biasing and ac phase biasing

Considering the ac Josephson effect, one could naively think that voltage biasing and phase biasing are equivalent. This is not correct and we discuss some of the differences, sketched in fig.2.4, in the following.

[2]for instance, the electron-phonon scattering time

[3]In normal metal ring, the double peak is centered either at zero either at $\Phi_0/2$ depending on where the gap $E_{n+1} - E_n$ is minimal. Moreover, the hand-drawn phase dependence in [91] should display a more pronounced cusp at π

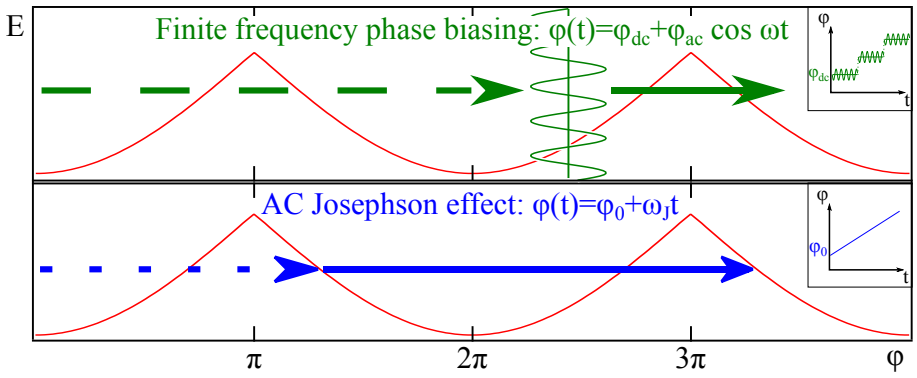

Figure 2.4: The difference between phase biasing and voltage biasing is summarized in this sketch of a phase dependent spectrum. Finite frequency phase biasing corresponds to phase oscillations of controlled amplitude φ_{ac} at frequency ω around a chosen value φ_{dc}. The value of φ_{dc} can be swept all over the spectrum to probe its phase dependence. This is different from what happens when biasing a Josephson junction with a voltage V. Due to the ac Josephson effect the phase starts increasing linearly with time with a slope $\omega_J = \frac{2eV}{\hbar}$. If one only considers the evolution of energy levels with phase, the ac Josephson effect would correspond to an ac phase biasing at frequency ω_J with an amplitude of 2π .

Due to the ac Josephson effect, the phase of a dc voltage biased SNS junction evolves as:

$$\varphi(t) = \varphi(0) + \omega_J t \tag{2.30}$$

where $\omega_J = \frac{2eV}{\hbar}$ is the Josephson frequency. If the Andreev bound states are considered, one sees that, due to their phase dependence, their energy oscillates at a frequency ω_J. However, due to the voltage biasing, it is not possible to probe the *equilibrium* properties of the junction and so to distinguish between out-of-equilibrium and finite-frequency effects.

On the contrary, when performing finite frequency phase-biased experiments by imposing a phase difference the system is probed at *equilibrium* or close to equilibrium in a controlled way. Finite frequency phase-biasing is achieved by imposing a phase difference such as:

$$\varphi(t) = \varphi_{dc} + \varphi_{ac} \cos \omega t \tag{2.31}$$

where the phase φ_{dc} can be unambiguously imposed by a coil and swept to probe the phase-dependent properties of a junction. The amplitude of the oscillation φ_{ac} at frequency ω can be made as small as wanted and so experiments can be carried out in a linear regime. This allows to only probe the effect of a finite frequency phase biasing and access the *dynamics* of a SNS junction.

If one only considers the evolution of energy levels with phase, the ac Josephson effect would correspond to a ac phase biasing at frequency ω_J with an amplitude of 2π, however, in addition to the phase evolution non-linear processes such as multiple Andreev reflections appears. That makes experiments in linear regime impossible to perform. Consequently even though voltage biasing and finite frequency phase biasing both entails finite frequency effects, they are

not equivalent. In particular, **voltage biasing does not allow to probe the equilibrium properties of a Josephson junction, only accessible via phase biasing.**

2.4 Recent works on the AC linear response of a NS ring

AC phase biasing allows to probe the *adiabatic* properties of a SNS junction at *equilibrium*. We briefly review in the following the results of recent works on the dynamical properties of a long and diffusive NS ring.

AC linear response of a NS ring: theoretical predictions

From the theoretical point of view, Usadel formalism successfully accounts for the critical current temperature dependence [18], the density of states of a proximitized normal metal [25] and the current-phase dependence of a NS ring under RF irradiation [80]. The current-voltage characteristics can also be calculated [89] however the noise is not totally described by Usadel formalism: whereas noise at large voltage can be well reproduced at large voltage bias [86, 87, 88], the description of low voltage bias regime ($eV < E_{Th}$) remains incomplete [90, 84, 85]. The ac linear response of diffusive SNS junctions has been developed by Virtanen *et al.* [95]. This work is in qualitative agreement with previous experiments carried out in the group[96] and the agreement is even quantitative with the results of the present work in the low frequency regime (see chap.6). Yet it fails to describe the dissipative response in [96] and more recent results at higher frequencies as it will be detailed in chap.6. That is why we decided to follow another approach based on some earlier works on persistent currents in purely normal rings [23, 97]: calculate the magnetic susceptibility of a ring in a linear regime using a Kubo formula approach (see chap.3).

AC linear response of a NS ring: first experiment

Recent experiments [17, 18, 80] show that non-equilibrium effects strongly modify the physics of SNS junctions compared to the equilibrium case with the emergence of harmonics 2 and 3 in the current-phase relation. The appearance of these harmonics is accounted for by transitions of Andreev pairs across the minigap according to [80]. While providing an explanation to the modification of the current-phase relation, Fueschle *et al.* does not emphasize the role of the timescales (the inelastic scattering time τ_{in} and the diffusion time τ_D) which, according to [98], should play an important role. Moreover, these experiments lack a control over the injected power and are probably in a non-linear regime such that nothing can be said about the equilibrium current-phase relation in a non-adiabatic regime[4].

In contrast to these experiments in non-linear regime, we determine the properties of a NS ring close to equilibrium to understand its dynamics. One way to probe the dynamics of a SNS junction is to measure the a.c. susceptibility of a NS ring in a linear regime. Such an experiment provide two pieces of in-

[4]The equilibrium and adiabatic current-phase relation has been measured in absence of RF irradiation in [80],

formation: the real part of the susceptibility gives the non-dissipative response and therefore the supercurrent while the imaginary part gives the dissipative response and so the conductance. Moreover, according to the fluctuation-dissipation theorem, the dissipative response can be related to the noise in the system.

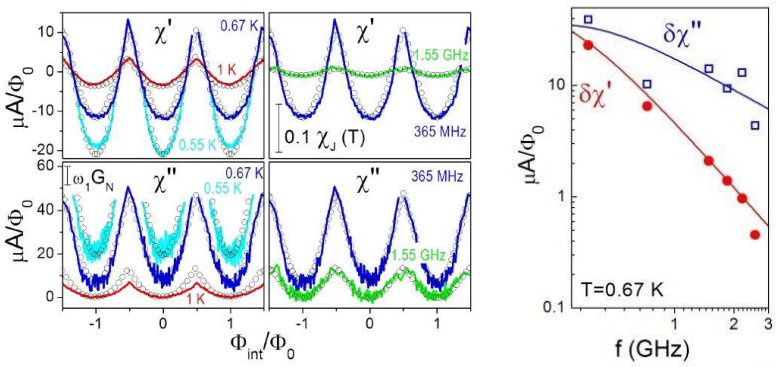

Figure 2.5: **Left:** $\chi'$and χ"for $f_1 = 365MHz$ at T = 0.55 K, T = 0.67 K and T = 1 K and for $f_4 = 1.5GHz$ at T = 0.67 K (lines). Numerical simulations developed by Virtanen *et al.* [95] for $T/E_{Th} = 5, T/E_{Th} = 6$ and $T/E_{Th} = 9$ (circles) with $\tau_A = 7.5\tau_D$. The amplitude of the theoretical simulations for χ'has been rescaled by a factor 0.28, while the amplitude for χ"has been rescaled by a factor 0.36 (see the main text for more details). **Right:** Frequency dependences of $\delta\chi'$ and $\delta\chi''$, the amplitude of respectively $\chi'$and χ", at 670 mK.

A first experiment by F. Chiodi *et al.* [96] found a large dissipative response as well as a non-dissipative one that differed notably from the adiabatic susceptibility, the flux derivative of the ring's Josephson current. These results, shown in fig.2.5, were partially explained by the theory of the proximity effect [95]. Indeed, the amplitude of the non-dissipative response $\chi'$was found to be 10 times smaller than the expected one given by the amplitude of the adiabatic response χ_J. Its phase dependence was however well explained by introducing a finite-frequency effect accounting for the relaxation of ABS populations to their equilibrium value (they are indeed slightly driven out-of-equilibrium by the phase biasing). Besides, the dissipative response remained poorly understood in this experiment, performed in a limited range of temperature and frequency: the frequencies ranged from 365 MHz to 2.6 GHz and temperatures from 550mK to 1K. This corresponds to $6E_{Th} < k_BT < 11Eth$ and $0.2E_{Th} < hf < 1.4Eth$ for E_{Th} estimated to $E_{Th} \equiv 90mK$. The temperature range was limited by the apparition of hysteresis at low temperature (this is a difficulty we did not manage to overcome during my thesis). The use of a dilution fridge without 1K bath set the upper temperature limit to $T \sim 1.2K$. The explored frequency range is given by the resonator's fundamental frequency for the lower limit and by the signal amplitude[5] for the upper limit. Surprisingly a strong frequency dependence (fig.2.5) at frequencies quite small compared

[5]attenuation of the lines increases with frequency

to E_{Th} was observed whereas the amplitude of the response is expected to be close to the one of the zero-frequency regime.

Finally, this first experiment points out the existence of finite-frequency effects that could be qualitatively described by theory. However, the phase dependence of the dissipative response remained poorly understood. In addition, in contrast with theoretical predictions, no evolution of the phase dependence is observed in the limited range of temperature and frequency explored. To get new insights on this problematic, we developed an alternative theoretical framework described in chap.3 and 4 and carried out another experiment presented in chap.5 and 6.

3

AC conductivity of an isolated ring within Kubo formalism

This chapter focuses on determining the ac conductivity of an isolated mesoscopic ring both in the case of a purely normal ring and of a NS ring. We start by introducing the Kubo approach of conductance then, following Trivedi and Browne [23], it is applied to calculate the conductivity of a normal ring and of a NS ring. The differences between these two cases are discussed. After determining an expression for the susceptibility of a NS ring, the temperature, phase and frequency dependences are calculated.

3.1 Linear response: an introduction

A general way to get information from a system is to apply a small perturbation and to analyze the system's response and so study its dynamics when it is slightly out-of-equilibrium[1] (see fig.3.1). Let $f(t)$ be a small perturbation which couples to an observable of the system A. This observable A is correlated to an other one, B, which is measured. The response $\chi_{BA}(t)$ which characterizes the linear response to this perturbation is defined as :

$$\langle B(t)\rangle_f = \langle B\rangle + \int_{-\infty}^{\infty} dt' \chi(t-t') f(t') \tag{3.1}$$

where $\langle B(t)\rangle_f$ and $\langle B\rangle$ are respectively the average in presence and in absence of the perturbation. The aim is then to calculate χ. To this end, we have to determine $\langle B(t)\rangle_f = Tr(\rho(t)B)$ where $\rho(t)$ is the density matrix.

The density matrix is obtained by solving Liouville equation :

$$\frac{\partial \rho}{\partial t} = \frac{i}{\hbar}[\rho(t), H(t)] \tag{3.2}$$

where $H(t) = H_0 + H_{pert}(t)$ is the hamiltonian of the system in presence of the perturbation, H_0 is the hamiltonian in absence of perturbation and $H_{pert}(t) = -f(t).A$ describes how the perturbation couples to the system. To simplify calculations, we define $\tilde{\rho}(t) = e^{\frac{i}{\hbar}H_0 t}\rho(t)e^{-\frac{i}{\hbar}H_0 t}$. Liouville equation then reads :

$$\frac{\partial \tilde{\rho}}{\partial t} = \frac{i}{\hbar}[\tilde{\rho}(t), H_I(t)] \tag{3.3}$$

[1] This introduction to the linear response formalism is strongly inspired by a course by C. Texier [99]

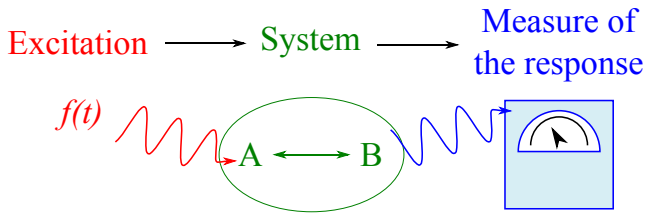

Figure 3.1: Principle of a linear response experiment : a small perturbation $f(t)$ couples to the observable A. The dynamics of the observables A and B are correlated. A measuring device follows the evolution of B.

where $H_I(t) = e^{\frac{i}{\hbar}H_0 t} H_{pert}(t) e^{-\frac{i}{\hbar}H_0 t}$. Let's write ρ in the form $\rho(t) = \rho^0(t) + \rho^1(t) + \dots$ where $\rho^n(t) = O(f^n)$ then we have :

$$\frac{\partial \tilde{\rho}^{(n)}}{\partial t} = \frac{i}{\hbar}[\tilde{\rho}^{(n-1)}(t), H_I(t)] \tag{3.4}$$

Assuming the system is initially at thermodynamical equilibrium : $\rho(-\infty) = \rho_{eq}$, we obtain :

$$\tilde{\rho}^{(n)}(t) = -\frac{i}{\hbar}\int_{-\infty}^{t} dt' f(t')[\tilde{\rho}^{(n-1)}(t'), A(t')] \tag{3.5}$$

Finally, if we just keep the first order in f, we have :

$$\tilde{\rho}(t) = \rho_{eq} - \frac{i}{\hbar}\int_{-\infty}^{t} dt' f(t')[\rho_{eq}(t'), A(t')] + O(f^2) \tag{3.6}$$

which allows to calculate $\langle B(t)\rangle_f = Tr(\rho(t)B) = Tr(\tilde{\rho}(t)B(t))$ where $B(t) = e^{\frac{i}{\hbar}H_0 t} B e^{-\frac{i}{\hbar}H_0 t}$. We finally obtain :

$$\chi(t) = \frac{i}{\hbar}\theta(t)\langle[B(t), A]\rangle \tag{3.7}$$

where $\theta(t)$ is the Heaviside function and is present to ensure the causality. This shows that the dynamical response is related to equilibrium correlations.In Fourier space, it is a complex number:

$$\chi(\omega) = \chi'(\omega) + i\chi"(\omega) \tag{3.8}$$

whose real part describes a non-dissipative response whereas its imaginary part accounts for dissipation.

Kramers-Kronig relations

Due to causality, there are relations between the non-dissipative and the dissipative responses that are called Kramers-Kronig relations. They read:

$$\chi'(\omega) = \frac{1}{\pi}\mathcal{P}\int_{-\infty}^{\infty} d\omega' \frac{\chi"(\omega')}{\omega' - \omega} \tag{3.9}$$

$$\chi"(\omega) = -\frac{1}{\pi}\mathcal{P}\int_{-\infty}^{\infty} d\omega' \frac{\chi'(\omega')}{\omega' - \omega} \tag{3.10}$$

where $\mathcal{P}$ denotes the Cauchy principal value: $\mathcal{P}\int_{-\infty}^{\infty}$ means $\lim_{\epsilon\to 0}\int_{-\infty}^{\omega-\epsilon} + \int_{\omega+\epsilon}^{\infty}$.

3.2 AC Conductivity calculated within linear response

In the following we apply the formalism we have introduced to the case where the perturbation is an electric field $\vec{E}(t)$. The potential is then $\phi(\vec{r}) = -\vec{r}.\vec{E}(t)$ and the perturbation hamiltonian is $H_{pert} = -e\vec{r}.\vec{E}(t)$. If we measure the current density $\hat{j} = \frac{e}{\mathcal{V}}\hat{v}$ where $\hat{v}$ is the velocity operator and $\mathcal{V}$ the volume, we can apply eq.3.7 with $f \to E$, $A \to r_j$ and $B \to \hat{j}_i$ (the indexes i and j denote spatial coordinates). The response, which is the conductivity $\sigma_{ij}(t)$, reads :

$$\sigma_{ij}(t) = \frac{i}{\hbar}\theta(t)\langle[\frac{e}{\mathcal{V}}\hat{v}_i, e\hat{r}_j]\rangle \tag{3.11}$$

If we now apply a sinusoidal electric field at frequency ω such as

$$\vec{E}(t) = -\frac{\partial \vec{A}_{ext}}{\partial t} = E_\omega e^{-i\omega t} \tag{3.12}$$

where $\vec{A}_{ext}$ is the potential vector , the unperturbed hamiltonian is

$$H = \frac{p^2}{2m} + V \tag{3.13}$$

and the perturbation hamiltonian is :

$$H_{pert} = -e\hat{v}A_{ext} \tag{3.14}$$

Here we have considered that the electrical potential is zero. The current density operator has now two contributions :

$$\hat{J} = \frac{e}{\mathcal{V}}(\hat{v} - \frac{e}{m}A_{ext}) = \hat{j} - \frac{e^2}{m\mathcal{V}}A_{ext}(t) \tag{3.15}$$

The response of the velocity operator is given by :

$$\langle\hat{v}(t)\rangle_{A_{ext}} = \langle\hat{v}\rangle + e\int dt' K(t-t')A_{ext}(t') \tag{3.16}$$

where

$$K(t) = \frac{i}{\hbar}\theta(t)\langle[\hat{v}(t), \hat{v}]\rangle \tag{3.17}$$

Doing the average in grand canonical ensemble yields :

$$K(t) = \frac{i}{\hbar}\theta(t)\sum_{\alpha}^{\beta}(f_\alpha - f_\beta)\left|v_{\alpha\beta}\right|^2 e^{i\frac{\epsilon_\alpha - \epsilon_\beta}{\hbar}t} \tag{3.18}$$

where $\{\epsilon_\alpha, |\alpha\rangle\}$ is a set of eigenvalues and eigenvectors of H and $f_\alpha = f(\epsilon_\alpha)$ with f the Fermi-Dirac distribution. Then, taking the Fourier transform with a 0^+ which accounts for an adiabatic switching of the perturbation yields :

$$K(\omega) = -\sum_{\alpha\beta}(f_\alpha - f_\beta)\frac{\left|v_{\alpha\beta}\right|^2}{\hbar\omega + \epsilon_\alpha - \epsilon_\beta + i0^+} \tag{3.19}$$

The conductivity is defined by

$$\langle\hat{J}(t)\rangle = \langle\hat{J}\rangle + \int dt'\sigma(t-t')E(t') \tag{3.20}$$

With $\hat{J}$ given by eq.3.15, one can notice that the last term of eq.3.15 already gives a contribution of first order to $\langle\hat{J}(t)\rangle$ which reads, after averaging in grand canonical ensemble, $-\frac{e^2}{m\mathcal{V}}A_{ext}(t)\sum_\alpha f_\alpha$. Then

$$\langle\hat{J}(t)\rangle = \langle\hat{j}(t)\rangle - \frac{e^2}{m\mathcal{V}}A_{ext}(t)\sum_\alpha f_\alpha \tag{3.21}$$

Using the expression of $\langle\hat{j}(t)\rangle = \frac{e}{\mathcal{V}}\langle\hat{v}(t)\rangle$ given by eq.3.16 we have :

$$\langle\hat{J}(t)\rangle = \langle\hat{j}\rangle + \int dt' \left[-\frac{e^2}{m\mathcal{V}}\sum_\alpha f_\alpha\delta(t-t') + \frac{e^2}{\mathcal{V}}K(t-t')\right]A_{ext}(t') \tag{3.22}$$

taking the Fourier transform yields :

$$\int dt e^{i\omega t}\langle\hat{J}(t)\rangle = 2\pi\delta(\omega) + \frac{e^2}{\mathcal{V}}\left[K(\omega) - \frac{1}{m}\sum_\alpha f_\alpha\right]A_{ext}(\omega) \tag{3.23}$$

Noting that $A_{ext}(\omega) = \frac{E(\omega)}{i\omega}$, we finally obtain the conductivity :

$$\sigma(\omega) = \frac{i}{\omega}\frac{e^2}{\mathcal{V}}\left[\frac{1}{m}\sum_\alpha f_\alpha - K(\omega)\right] \tag{3.24}$$

with $K(\omega)$ given by eq.3.19. It is worth emphasizing that the eigenstates $|\alpha\rangle$ considered here are those of the isolated system. If the sample were connected to leads, we would have to consider the eigenstates of the total system consisting in the sample and the leads which could be very different from the eigenstates of the isolated system. This remark will be of importance when considering adding some thermal bath to provide relaxation (see sec.3.3).

f-sum rule

Using commutation relations, we show that a sum rule holds. On one hand we have :

$$[x, v_x] = \frac{i\hbar}{m} \tag{3.25}$$

so

$$\sum_\beta (x_{\alpha\beta}(v_x)_{\beta\alpha} - (v_x)_{\alpha\beta}x_{\beta\alpha}) = \frac{i\hbar}{m} \tag{3.26}$$

on the other hand we have :

$$v_x = \frac{\partial x}{\partial t} = \frac{i}{\hbar}[H, x] \tag{3.27}$$

so

$$(v_x)_{\alpha\beta} = \frac{i}{\hbar}(\epsilon_\alpha - \epsilon_\beta)x_{\alpha\beta} \tag{3.28}$$

Using eq.3.26 and eq.3.28, we can establish the so-called **f-sum rule:**

$$\sum_\beta \frac{|v_{\alpha\beta}|^2}{\epsilon_\alpha - \epsilon_\beta} = -\frac{1}{2m} \tag{3.29}$$

then, by multiplying by $\sum_\alpha f_\alpha$, we have :

$$\frac{1}{m}\sum_\alpha f_\alpha = -2\sum_{\alpha\beta}\frac{|v_{\alpha\beta}|^2}{\epsilon_\alpha-\epsilon_\beta}f_\alpha = -\sum_{\alpha\beta}\frac{|v_{\alpha\beta}|^2}{\epsilon_\alpha-\epsilon_\beta}(f_\alpha-f_\beta) = K(\omega=0) \quad (3.30)$$

Therefore, the conductivity can be written as:

$$\sigma(\omega) = \frac{ie^2}{\mathcal{V}}\frac{K(0)-K(\omega)}{\omega+i0^+} \quad (3.31)$$

or, writing explicitly the function K:

$$\sigma(\omega) = \frac{ie^2}{\mathcal{V}}\sum_{\alpha,\beta,\alpha\neq\beta}\frac{f_\alpha-f_\beta}{\epsilon_\alpha-\epsilon_\beta}\frac{|v_{\alpha\beta}|^2}{\epsilon_\alpha-\epsilon_\beta+\omega+i0^+} \quad (3.32)$$

The dissipative part of the conductivity then reads:

$$Re(\sigma(\omega)) = -\frac{\pi e^2}{\mathcal{V}}\sum_{\alpha,\beta,\alpha\neq\beta}\frac{f(\epsilon_\alpha+\omega)-f(\epsilon_\alpha)}{\omega}|v_{\alpha\beta}|^2\,\delta(\epsilon_\alpha-\epsilon_\beta+\omega) \quad (3.33)$$

which is the usual expression of the Kubo formula. In the case of a macroscopic sample (or a mesoscopic sample connected to leads), the spectrum is continuous thus there is absorption at any frequency. There is therefore a dc conductivity equal to the Drude expression:

$$\sigma_{Drude}(\omega=0) = \frac{ne^2\tau}{m} \quad (3.34)$$

3.3 Kubo formula in a ring

In the following we show that, due to its multiply connected topology, the expression of the conductivity in a ring is different from the one in a wire.

modified f-sum rule

The f-sum rule (eq.3.29) does not hold anymore in a ring geometry since its derivation relies on the commutation rule $[X,P] = i\hbar$. This commutation rule does not hold in a ring geometry since the operator X is no more single-valued. To derive the modified f-sum rule, one has to consider the change in the Hamiltonian H:

$$H = \frac{(p-eA)^2}{2m} \quad (3.35)$$

by adding a small amount of flux $\delta\Phi$. In a 1D ring of perimeter L, the flux is related to the potential vector A by $A = \Phi/L$. To $O((\delta\Phi)^2)$, the change in the Hamiltonian is

$$\delta H = -\frac{e\delta\Phi}{L}\left(\frac{p-eA}{m}\right) + \frac{1}{2m}\left(\frac{e\delta\Phi}{L}\right)^2 \quad (3.36)$$

The change in the energy of the state $|\alpha\rangle$ caused by δH is evaluated by 2^{nd} order perturbation theory. Using that

$$j = e\frac{p-eA}{m} \quad (3.37)$$

we have

$$\epsilon_\alpha(\Phi+\delta\Phi) = \epsilon_\alpha(\Phi) + \langle\alpha|\, j\, |\alpha\rangle + \sum_{\beta\neq\alpha} \frac{|j_{\alpha\beta}|^2}{\epsilon_\alpha - \epsilon_\beta} \tag{3.38}$$

By comparing terms with the Taylor expansion of the energy

$$\epsilon_\alpha(\Phi+\delta\Phi) = \epsilon_\alpha(\Phi) + \frac{\partial\epsilon_\alpha}{\partial\Phi}\delta\Phi + \frac{1}{2}\frac{\partial^2\epsilon_\alpha}{\partial\Phi^2}(\delta\Phi)^2 \tag{3.39}$$

we obtain, from the first order terms,

$$\frac{\partial\epsilon_\alpha}{\partial\Phi} == -\langle\alpha|\, j\, |\alpha\rangle = -j_\alpha \tag{3.40}$$

This tells us that there is a current flow due to the flux-sensitivity of energy levels. Equalizing the second order terms yields a **modified f-sum rule:**

$$\frac{1}{m} + 2\sum_{\alpha,\beta\neq\alpha} \frac{|j_{\alpha\beta}|^2}{\epsilon_\alpha - \epsilon_\beta} = \frac{L^2}{e^2}\frac{\partial^2\epsilon_\alpha}{\partial\Phi^2} \tag{3.41}$$

Evidence for an incorrect introduction of dissipation

Using the modified f-sum rule for a 1D ring of perimeter L threaded by a flux Φ, the ac conductivity finally reads :

$$\sigma(\omega) = \frac{ie^2}{L}\frac{K(0)-K(\omega)}{i\omega} + \frac{L}{i\omega}\sum_\alpha f_\alpha \frac{\partial j_\alpha}{\partial\Phi} \tag{3.42}$$

Using that

$$f_\alpha\frac{\partial j_\alpha}{\partial\Phi} = \frac{\partial(f_\alpha j_\alpha)}{\partial\Phi} - j_\alpha\frac{\partial f_\alpha}{\partial\Phi} \tag{3.43}$$

and

$$\frac{\partial f_\alpha}{\partial\Phi} = \frac{\partial f_\alpha}{\partial\epsilon_\alpha}\frac{\partial\epsilon_\alpha}{\partial\Phi} = -j_\alpha\frac{\partial f_\alpha}{\partial\epsilon_\alpha} \tag{3.44}$$

eq.3.42 can be rewritten as:

$$\sigma(\omega) = \frac{e^2}{L}\frac{K(0)-K(\omega)}{i\omega} + \frac{L}{i\omega}\frac{\partial I_p}{\partial\Phi} + \frac{L}{i\omega}\sum_\alpha j_\alpha^2\frac{\partial f_\alpha}{\partial\Phi} \tag{3.45}$$

where

$$I_p = \sum_\alpha f_\alpha j_\alpha \tag{3.46}$$

is the persistent current flowing through the ring.

The dissipation, given by $Re(\sigma)$, is just due to the first term in eq.3.45 i.e. the transition term. This disagrees with the simple model we introduced in sec.1.1 where there is a dynamical contribution to the dissipation due to the relaxation of the populations back to equilibrium.

This departure is related to the way dissipation is introduced: if it is done by simply arguing that, as in [22], the Dirac function broadens into a Lorentzian of width $1/\tau_{in}$, where τ_{in} is a relaxation time, one does not obtain the contribution due to the relaxation of populations. The correct way to introduce dissipation is to add a relaxation term in Liouville equation (eq.3.2) that accounts for the coupling of the system with a thermal bath [23].

Correct introduction of dissipation

Since the system is described by a Hamiltonian, it cannot show a resistive behavior. To provide a relaxation mechanism, the electrons must be coupled to a thermal bath. Dissipation is included in the system by modeling the dynamics by a master equation with a relaxation term that phenomenologically accounts for the coupling of the electronic system to an external environment, for instance the phonon bath. This approach is inspired by previous work on the dynamics of persistent currents in normal mesoscopic Aharonov Bohm rings [23, 97].

Liouville equation in presence of relaxation

As in the preceding, we investigate the linear dynamics of a ring excited by an ocillating flux

$$\delta\Phi(t) = \delta\Phi \exp(-i\omega t) \tag{3.47}$$

leading to the time dependent Hamiltonian

$$H(t) = H_0 - \mathbf{J}\delta\Phi(t) \tag{3.48}$$

where $\mathbf{J}$ is the current operator. In contrast with the usual approach (eq.3.2), we use as a starting point the master equation describing the relaxation of the density matrix towards equilibrium:

$$\partial\rho(t)/\partial t = (1/i\hbar)\,[H(t), \rho] - \Gamma[\rho(t) - \rho_{eq}(t)] \tag{3.49}$$

where the equilibrium density matrix $\rho_{eq}(t) = \exp -H(t)/k_BT$ and the phenomenological relaxation tensor Γ describes the coupling of the system to a thermal reservoir. Its diagonal elements $\gamma_{nn} = \gamma_D = \hbar/\tau_{in}$ describe the relaxation of the populations f_n of the Andreev states due to inelastic scattering such as electron-phonon or electron-electron collisions. Non-diagonal elements γ_{nm} describe the relaxation of the coherences $\rho_{nm}(t)$ due to interlevel transitions. This kinetic equation neglects changes in the equilibrium density matrix induced by the coupling to the thermal bath. The above relaxation time approximation can be justified from a microscopic theory when the coupling to the environment is weak.
Following [23, 97], the linear current response $\delta I(t)$ is given by:

$$\delta I(t) = Tr(J\delta\rho(t)) + Tr(\delta J(t)\rho_0) \tag{3.50}$$

where ρ_0 is the unperturbed matrix density:

$$\rho_0 = \sum_n f_n(\Phi_{dc})|n><n| \tag{3.51}$$

The linear current response is expressed via the complex susceptibility $\chi(\omega)$:

$$\chi(\omega) = \delta I(t)/\delta\Phi(t) \tag{3.52}$$

It reads:

$$\begin{aligned}\chi(\omega) = -N\frac{e^2}{2mL^2} - \sum_n \frac{\partial f_n}{\partial\epsilon_n}|J_{nn}|^2\frac{\gamma_D}{\gamma_D - i\omega} \\ - \textstyle\sum_{n,m\neq n}|J_{nm}|^2\dfrac{f_n - f_m}{\epsilon_n - \epsilon_m}\dfrac{i(\epsilon_n - \epsilon_m) + \hbar\gamma_{nm}}{i(\epsilon_n - \epsilon_m) - i\hbar\omega + \hbar\gamma_{nm}}\end{aligned} \tag{3.53}$$

where N is the system's number of electrons, J_{nm} is the matrix element of the current operator between the eigenstates n and m of the unperturbed Hamiltonian H_0 and $J_{nn} = i_n$. Using the sum rule derived from the second order perturbation of H with respect to the perturbation $J\delta\Phi$ [23, 100]:

$$\sum_{m\neq n} \frac{|J_{nm}|^2}{(\epsilon_n - \epsilon_m)} = -\frac{1}{2}\frac{\partial i_n}{\partial \Phi} - \frac{e^2}{2mL^2} \tag{3.54}$$

$\chi(\omega)$ can be expressed as:

$$\begin{aligned}\chi(\omega) = \frac{\partial I_J}{\partial \Phi} - \sum_n i_n^2 \frac{\partial f_n}{\partial \epsilon_n}\frac{i\omega}{\gamma_D - i\omega} - \\ \sum_{n,m\neq n} |J_{nm}|^2 \frac{f_n - f_m}{\epsilon_n - \epsilon_m}\frac{i\hbar\omega}{i(\epsilon_n - \epsilon_m) - i\hbar\omega + \hbar\gamma_{nm}}\end{aligned} \tag{3.55}$$

This second expression clearly yields the zero frequency limit of the susceptibility $\chi(\omega = 0) = \partial I_J/\partial\Phi$. This expression also emphasizes the two relaxation processes that cause frequency dependent effects as discussed in the next sections.

Difference between the Kubo formula in a NS ring and in a normal ring

One of the most remarkable feature of a NS ring is the presence of a phase-dependent minigap in its density of states. This unique property contrasts with purely normal rings. We expect to find signatures of the presence of the minigap in the non-diagonal contribution since it describes induced transitions. One would thus expect an absence of dissipation at frequencies smaller than the minigap. In the following we contrast this naive picture with analytical predictions.

3.4 AC linear response of a NS ring - analytics

We present in this section the phase, temperature and frequency dependences of the different contributions to the susceptibility. They are determined analytically. We will denote from now on the amplitude measured between $\varphi = \pi$ and $\varphi = 0$ as $\delta_{\pi-0}\chi$ and $\delta\chi$ the total amplitude.

Josephson contribution: adiabatic term

In the adiabatic regime ($\omega \to 0$) the susceptibility reduces to the Josephson susceptibility which is just the derivative of the Josephson supercurrent. In long SNS junctions the current-phase relation is not a pure sine at low temperature because of Andreev pairs undergoing several reflections before being transmitted from one electrode to the other (see eqs. 2.25 and 2.26) . However at high enough temperature ($T \gtrsim E_g$) the current-phase relation is just a sine [5, 80]: $I_J = I_c \sin(\varphi)$ and the Josephson susceptibility reads :

$$\chi_J = -\frac{2\pi}{\Phi_0}\frac{\partial I_J}{\partial \varphi} = -\frac{2\pi I_c}{\Phi_0}\cos(\varphi) \tag{3.56}$$

This contribution, just as the supercurrent it measures, stems from the phase-dependence of the ABS and does not depend on the frequency. It is purely non-dissipative. In the following we discuss the extra contributions to susceptibility that emerge with increasing frequency.

Diagonal contribution: relaxation term

We discuss in the following the second term of expression 3.55 that we call diagonal contribution and denote χ_D. It is the finite frequency non-adiabatic contribution due to the thermal relaxation of the populations f_n of the Andreev levels with the characteristic inelastic time τ_{in} [71]. It is proportional to the sum over an energy range k_BT around the Fermi energy of the square of the single level current i_n^2. It reads:

$$\chi_D(\omega) = -\frac{i\omega\tau_{in}}{1-i\omega\tau_{in}} \sum_n i_n^2 \frac{\partial f_n}{\partial \epsilon_n} \tag{3.57}$$

We recast χ_D into a product of a frequency dependent term and a phase dependent one:

$$\chi_D(\omega) = A(\omega, T)F(\varphi, T) \tag{3.58}$$

where the phase dependent terme $F(\varphi, T)$ reads:

$$F(\varphi, T) = -\sum_n i_n^2 \frac{\partial f_n}{\partial \epsilon_n} \tag{3.59}$$

and the frequency dependent one $A(\omega, T)$ reads:

$$A(\omega, T) = \frac{i\omega\tau_{in}(T)}{1-i\omega\tau_{in}(T)} \tag{3.60}$$

This contribution is exactly the same as the one introduced by Buttiker [20] to describe the ac conductance of a mesoscopic normal ring. It is related to the phase-sensitivity of the spectrum and is therefore correlated to the existence of non-dissipative currents at equilibrium.

Phase dependence of the diagonal contribution

In the continuous spectrum limit and for $k_BT \gg E_{Th}$, $F(\varphi, T)$ can be written in terms of the spectral current $J(\epsilon)$ and the density $n(\epsilon)$ of Andreev levels as

$$F(\varphi, T) = \int \frac{J^2(\varphi, \epsilon)}{k_BTn(\epsilon)} d\epsilon \tag{3.61}$$

This function, initially introduced by Lempitskii [91] to describe non equilibrium effects in voltage biased SNS junctions, can be approximated by the analytical expression derived from Usadel equations[2] [95, 96]:

$$F_U(\varphi, T) = 8.9\frac{G_N E_{Th}^2}{T}\left([-\pi + (\pi+\varphi)[2\pi]]\sin(\varphi) - \frac{|\sin(\varphi)|}{\pi}\sin^2(\varphi/2)\right) \tag{3.62}$$

[2]There is a misprint in [95] and the prefactor in F_U indeed reads $\frac{G_N E_{Th}^2}{T}$

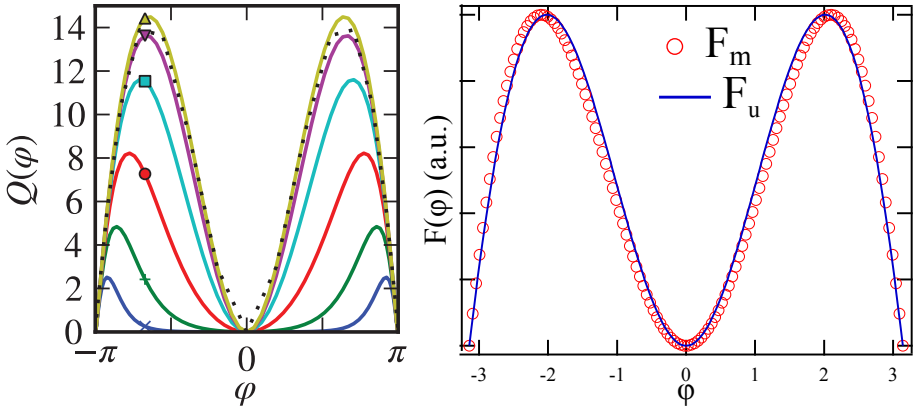

Figure 3.2: **Left:**Function $Q(\varphi, T)$ describing the phase dependence of the diagonal contribution at several temperatures: $T/E_{Th} = 16(\triangle), 8(\triangledown), 4(\square), 2(\circ), 1(+), 0.5(\times)$. The dotted lines represent the analytic high-temperature approximations to which Q tends for $T \gg E_{Th}$. From [95].**Right:** The high temperature analytical approximation F_U is compared to the phase dependence of $F_m = \cos(\varphi) - 2\,|\cos(\varphi/2)|$.

This expression is valid at high temperature ($T \gtrsim 8E_{Th}$). At lower temperature, one has to resort to numerical resolutions of Usadel equations. The results of this numerical simulation is shown in fig.3.2 where the function $Q(\varphi, T)$ is defined as:

$$Q(\varphi, T) = \frac{T}{G_N E_{Th}^2} F(\varphi) \tag{3.63}$$

This function shows sharp cusps at odd multiples of π when the minigap closes. It is dominated by its second harmonic because its phase dependence is given by the square of single level currents. Its amplitude between $\varphi = \pi$ and $\varphi = 0$, $\delta_{\pi-0}\chi_D = \chi_D(\pi) - \chi_D(0)$, vanishes since single level currents are zero at these values where the energy is extremal. It can be noticed that the position of the maximum is slightly changing with temperature.

It is remarkable that a similar phase dependence is obtained by subtracting the minigap's phase dependence to the one of the Josephson susceptibility:

$$F_m = \cos(\varphi) - 2\,|\cos(\varphi/2)| \tag{3.64}$$

However, this may be accidental and we do not have any strong evidence to support this expression. It might rely on the fact that we did not consider the impact of the minigap on the electron number: one might have to modify the first term in eq.3.53 by using a density of states n_g that takes the minigap into account. Then we have:

$$N\frac{e^2}{2mL^2} \to \frac{e^2}{2mL^2}\int d\epsilon n_g(\epsilon) \tag{3.65}$$

where

$$n_g = n_0\left[\theta(\epsilon - E_g(\varphi)) + \theta(-\epsilon - E_g(\varphi))\right] \tag{3.66}$$

with n_0 a constant and θ the Heaviside function. We however did now develop this approach further.

Temperature dependence of the diagonal contribution

The evolution with temperature of χ_D has two distinct origins :

- The temperature dependence of the F function that is due to the temperature dependence of Fermi distributions. Thus the amplitude of F decreases as $1/T$ at high temperature compared to the minigap.
- The temperature dependence of the inelastic scattering time τ_{in}. This depends on the specific mechanism at the origin of inelastic scattering.

Finally, the amplitude of χ_D decreases as a power law of T at high temperature compared to the minigap, in contrast with the amplitude of $\chi_J$which exponentially decreases with temperature. The exact power depends on the mechanism at the origin of the relaxation.

Frequency dependence of the diagonal contribution

The frequency dependence of the diagonal contribution stems from the term

$$A(\omega) = \frac{i\omega\tau_{in}}{1 - i\omega\tau_{in}} \tag{3.67}$$

The real part of this term saturates at high frequencies compared to $1/\tau_{in}$ whereas its imaginary part is peaked at $1/\tau_{in}$ and decreases to zero when $\omega\tau_{in} \gg 1$ (see fig.3.3). Explicitly written, $\chi'_D$and χ''_Dreads:

$$\chi'_D = \frac{\omega^2\tau_{in}^2}{1 + \omega^2\tau_{in}^2} F(\varphi, \omega, T) \tag{3.68}$$

and

$$\chi''_D = -\frac{\omega\tau_{in}}{1 + \omega^2\tau_{in}^2} F(\varphi, \omega, T) \tag{3.69}$$

It is important to note that:

$$\chi''_D = -\frac{\chi'_D}{\omega\tau_{in}} \tag{3.70}$$

since this relation will be used to interpret our data.

Non-diagonal contribution: absorption term

We now consider the contribution involving the non-diagonal elements of the current operator which describe the physics of microwave induced transitions within the Andreev spectrum:

$$\chi_{ND} = -\sum_{n,m\neq n} |J_{nm}|^2 \frac{f_n - f_m}{\epsilon_n - \epsilon_m} \frac{i\hbar\omega}{\gamma_{nm} + i(\epsilon_n - \epsilon_m - \hbar\omega)} \tag{3.71}$$

One difficulty to evaluate this contribution stems from the fact that $|n\rangle$, $|m\rangle$ are not eigenvectors of the current operator, it is therefore difficult to predict the phase dependence of $|J_{nm}|^2$ analytically. We will therefore consider them as phase independent in a first approximation. For the sake of simplicity, we

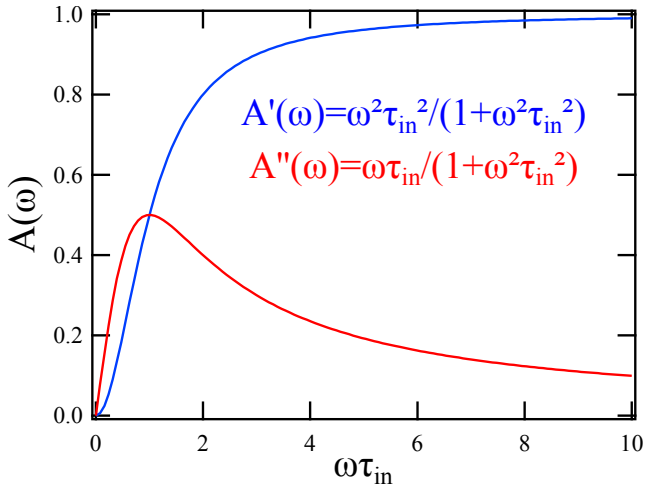

Figure 3.3: Frequency dependence of the diagonal contribution.

also assume that all γ_{nm} are identical given by a single γ_{ND} that is taken as phase, temperature and energy independent. χ_{ND}then reads :

$$\chi_{ND} = -\sum_{n,m\neq n} |J_{nm}|^2 \frac{f_n - f_m}{\epsilon_n - \epsilon_m} \frac{i\hbar\omega}{i(\epsilon_n - \epsilon_m) - i\hbar\omega + \hbar\gamma_{ND}} \tag{3.72}$$

Contrary to χ_D, χ_{ND}can not be recast into a product of a frequency dependent and a phase dependent term. This complicates the understanding of this contribution, in the following we introduce some approximations to have a rough idea of its behavior.

Origin of the phase dependence of χ_{ND}

We can distinguish two origins of the phase dependence of χ_{ND}. The first one is related to the transitions within the spectrum given by the terms:

$$\frac{f_n - f_m}{\epsilon_n - \epsilon_m} \frac{i\hbar\omega}{i(\epsilon_n - \epsilon_m) - i\hbar\omega + \hbar\gamma_{ND}} \tag{3.73}$$

whereas the second one is related to the phase dependence of the non-diagonal elements of the current operator $J_{nm}(\varphi)$. To have a better idea of the interplay between these two phase dependences, we will consider first that the $J_{nm}(\varphi)$ can be replaced by a constant J, independent of phase and energy. Then we will try to evaluate the phase dependence of $J_{nm}(\varphi)$.

Approximation of constant J^2 : low temperature and high frequency regime

We consider the continuous spectrum limit since this is the limit in which the experiment is carried out[3]. We do the following transformation:

$$\epsilon_n \to \epsilon; \epsilon_m \to \epsilon'$$

[3]At the highest temperature explored, the inelastic scattering time is of the order of the diffusion time. In terms of energy, it means that the level broadness is about the Thouless energy, much larger than the average level spacing

$$J_{nm} \to J(\epsilon, \epsilon')$$

In the continuous spectrum limit, the average level spacing δ_N is much smaller than the energy scales γ_{ND}, k_BT and $\hbar\omega$, so that one can write:

$$\chi_{ND} = -\int_{-E_M}^{E_M} |J_{\epsilon,\epsilon'}|^2 \frac{f(\epsilon) - f(\epsilon')}{\epsilon - \epsilon'} \frac{i\hbar\omega}{i(\epsilon - \epsilon') - i\hbar\omega + \gamma_{ND}} n(\epsilon) n(\epsilon') d\epsilon d\epsilon' \tag{3.74}$$

where E_M is a high energy cutoff of the order of the bandwidth from now on arbitrarily taken as unity, and $n(\epsilon)$ is the density of states at energy ϵ. In the long junction limit the induced minigap is very small compared to the superconducting gap Δ so that the density of states can be approximated as a constant above $E_g(\varphi)$:

$$n(\epsilon, \varphi) = n_0 \left[\theta(\epsilon - E_g(\varphi)) + \theta(-\epsilon - E_g(\varphi))\right] \tag{3.75}$$

with $\theta(x)$ the Heaviside function. In the following we approximate $|J_{\epsilon,\epsilon'}|^2$ by a constant J^2. We will see in chap.4 that this approximation is valid when $k_BT \ll E_g < \hbar\omega$ where the dominant contribution comes from matrix elements nearly independent of φ. This leads to:

$$\chi_{ND} = -n_0^2 \int\int_{|\epsilon|,|\epsilon'| \geq E_g(\varphi)} d\epsilon d\epsilon' \left[|J|^2 \frac{f(\epsilon) - f(\epsilon')}{\epsilon - \epsilon'} \frac{i\hbar\omega}{i(\epsilon - \epsilon') - i\hbar\omega + \gamma_{ND}} \right] \tag{3.76}$$

frequency dependence of χ_{ND}

We define $\delta\chi'_{ND} = \chi'_{ND}(\pi) - \chi'_{ND}(0)$ and $\delta\chi''_{ND} = \chi''_{ND}(\pi) - \chi''_{ND}(0)$ as the amplitudes of the flux dependent components of the real and imaginary parts of $\chi(\Phi, \omega)$. The frequency dependence of these quantities are depicted in Fig.3.4 for several values of the minigap larger than the temperature. We find that:

- $\delta\chi'_{ND}$ is negative and decreases slowly at low frequency with an inflexion point at $\omega = E_g(0)/\hbar$. That means that the amplitude of the non-dissipative response barely changes with frequency up to $\omega_g = \frac{E_g(\varphi=0)}{\hbar}$. At frequencies larger than ω_g, the non-dissipative response quickly diminishes.
- $\delta\chi''_{ND}$ is positive and increases linearly with frequency up to ω_g and is independent of frequency at larger values.

These results, in agreement with Kramers Kronig relations, show that the minigap is the fundamental frequency scale for $\chi_{ND}(\varphi)$.

phase dependence of χ''_{ND}

In the limit where $\gamma_{ND} \ll \omega$ and $\gamma_{ND} \ll k_BT$, the term

$$\delta_\gamma = \frac{\gamma_{ND}}{(\epsilon - \epsilon' - \hbar\omega)^2 + \gamma_{ND}^2} \tag{3.77}$$

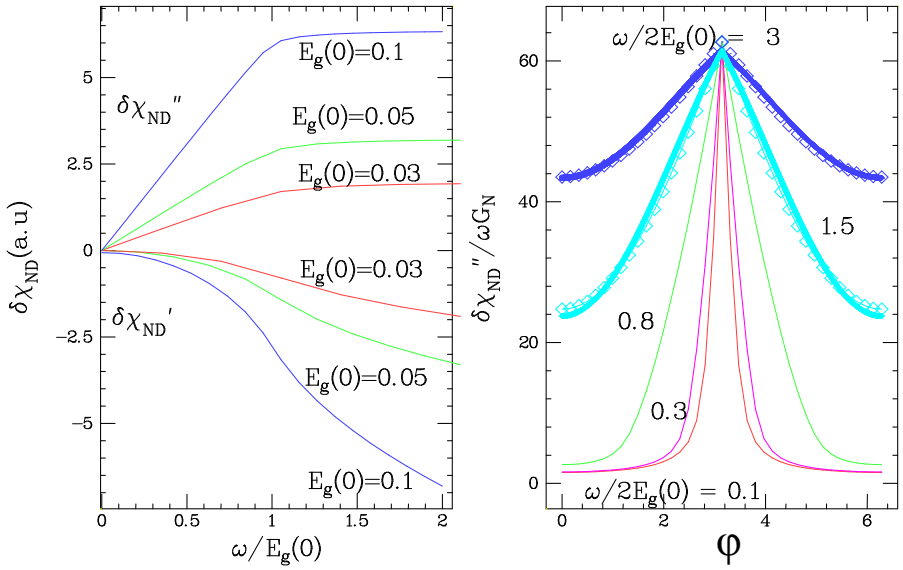

Figure 3.4: Non diagonal susceptibility calculated assuming no phase dependence for the non diagonal matrix elements of the current operator. The temperatures and frequencies investigated correspond to $T \ll \hbar\omega$. The values of γ_{ND} and k_BT were both taken equal to 0.01 i.e. much smaller than the minigap $2E_g(0)$. **Left:** frequency dependence of $\delta\chi''_{ND}$ and $\delta\chi'_{ND}$ dissipative and non-dissipative responses for different values of the minigap in units of E_M, the high energy cutoff we used (see main text). **Right:** phase dependence of χ''_{ND} for different frequencies. The thick continuous lines corresponds to a fit with a $-|\cos(\varphi/2)| \propto -E_g(\varphi)$ dependence.

entering in χ'' deduced from Eq.3.76 can be approximated by the delta function:

$$\delta_\gamma \sim \delta(\epsilon - \epsilon' - \hbar\omega) \tag{3.78}$$

It is then possible to express simply $\chi''_{ND}(\omega, \varphi)$ analytically as:

$$\chi''_{ND} = n_0^2 |J|^2 \int_{|\epsilon| \geq E_g(\varphi)} [f(\epsilon) - f(\epsilon + \hbar\omega)]\, d\epsilon \tag{3.79}$$

In the high frequency and low temperature limit $\omega \geq 2E_g(\varphi) \gg k_BT$, $\chi"_{ND}(\varphi)$ mimics the minigap (with a minus sign). This is due to the fact that the variation in φ is only contained in the integration limits. It reads:

$$\chi''_{ND}(\varphi, \omega) = (\omega - \frac{2E_g(\varphi)}{\hbar}) G_N \tag{3.80}$$

where the normal state conductance G_N is given by the value of the non-diagonal contribution where the minigap closes:

$$G_N = \chi''_{ND}(\pi)/\omega \tag{3.81}$$

and can be expressed as

$$G_N = |J|^2 n_0^2 \tag{3.82}$$

Eq.3.79 describes induced transitions across the minigap, then there is no transition possible while $\omega < E_g(\varphi)$ at a given excitation frequency ω. As a result when $\omega \ll E_g(0)$ the flux dependent absorption exhibit sharp peaks at odd multiples of π which amplitude scales linearly with ω as shown on Fig.3.4. In the limit

$$k_B T \ll \omega \lesssim E_g \tag{3.83}$$

it can be shown that:

$$\frac{\delta\chi''_{ND}}{\delta\chi'} \propto \frac{\hbar\omega}{E_g} \tag{3.84}$$

There is however no simple analytical expression for the complete phase and frequency dependences of $\chi'(\omega,\varphi)$ owing to the fact that, according to Eq.3.76, it explicitly depends logarithmically on the energy cutoff E_M.

Estimation of the phase dependence of J_{nm} : low frequency and high temperature regime

In the opposite limit of high temperature

$$T \gg E_g \gtrsim \hbar\omega \tag{3.85}$$

we can find from Eq.3.74, under the assumption that $|J(E,E')|^2$ does not depend much on energy on a range $k_B T$, that

$$\frac{\delta\chi''_{ND}}{\delta\chi'} \propto \frac{\hbar\omega}{k_B T} \tag{3.86}$$

It is however not possible to use Eq.3.79 to deduce the phase dependence of χ''_{ND}. This equation relies on a crude approximation neglecting the phase dependence of the non diagonal matrix elements of the current operator. We will show in chap.4 devoted to numerical calculations, that this approximation is only reasonable at low temperature and large frequency. In this regime, only a small number of matrix elements $|J_{\epsilon,\epsilon'}|^2$ contribute to χ''_{ND}. These matrix elements , coupling negative energy levels close to the minigap to positive energy levels much larger than E_g, have indeed only a very small phase dependence. On the other hand, at high temperature, $k_B T \gg E_g$, a large number of matrix elements $|J_{\epsilon,\epsilon'}|^2$ contribute to the integral in ϵ' in Eq. 3.74. We can then estimate their contribution to the phase dependence of χ''_{ND} using that

$$Tr(J^2) = \sum_n |J_{nn}|^2 + \sum_{n,m\neq n} |J_{nm}|^2 \sim constant_{|\varphi} \tag{3.87}$$

does not depend on the Aharonov-Bohm phase like

$$Tr(\mathcal{H}) = Tr(J^2) + Tr(V) \tag{3.88}$$

where V is the (phase-independent) disorder potential. The phase independence of $Tr(\mathcal{H})$ is related to the fact that a full band does not display orbital magnetism. It also means that the Aharonov-Bohm phase only affects non-diagonal matrix elements of $\mathcal{H}$.

The sum of all non-diagonal matrix elements $|J_{nm}(\varphi)|^2$ with $m \neq n$ is thus opposite in sign to the variation of $F(\varphi) \propto \sum_n |J_{nn}|^2$ at large T:

$$\sum_{n,m\neq n} |J_{nm}|^2(\varphi) \sim -F(\varphi) \tag{3.89}$$

Therefore, in the limit of high temperature

$$T \gg \hbar\omega \simeq E_g(0) \tag{3.90}$$

where the sum of a large number of non diagonal matrix elements $|J_{nm}(\varphi)|^2$ with $m \neq n$ contribute to the phase dependence of χ''_{ND}, the phase dependence of χ''_D and χ''_{ND} are thus expected to be reversed from one another:

$$\chi"_{ND}(\varphi) \sim -\chi''_D(\varphi) \tag{3.91}$$

Results of numerical simulations presented in chap.4 agree with this qualitative prediction.

3.5 Summary

The linear ac response of a diffusive SNS junction has been addressed theoretically by Virtanen *et al.* [95]. This work reproduces well the experimental non-dissipative response; yet it disagrees with the dissipative one. To understand this puzzling dissipation, we developed an alternative approach. Following previous work on the dynamics of persistent currents in normal mesoscopic Aharonov Bohm rings [23, 97] we developed a Kubo formula approach. In this approach, χ splits naturally into three parts, $\chi = \chi_J + \chi_D + \chi_{ND}$, with :

$$\chi_J(\varphi, T) = -\frac{2\pi}{\Phi_0}\frac{\partial I_J}{\partial \varphi} \tag{3.92}$$

$$\chi_D(\omega, \varphi, T) = -\frac{i\omega}{\gamma_D - i\omega}\sum_n i_n^2 \frac{\partial f_n}{\partial \epsilon_n} \tag{3.93}$$

$$\chi_{ND}(\omega, \varphi, T) = -\sum_{n,m\neq n} |J_{nm}|^2 \frac{f_n - f_m}{\epsilon_n - \epsilon_m}\frac{i\hbar\omega}{i(\epsilon_n - \epsilon_m) - i\hbar\omega + \hbar\gamma_{nm}} \tag{3.94}$$

where $I_J(\varphi)$ is the phase dependent Josephson supercurrent at equilibrium, ϵ_n the energy of the n^{th} ABS, f_n its thermal occupation factor, J_{nm} the current operator taken between states n and m with $J_{nn} = i_n = -\frac{2\pi}{\Phi_0}\frac{\partial \epsilon_n}{\partial \varphi}$. γ_D and γ_{nm} are relaxation rates which accounts for the finite lifetime of the states.

As sketched in fig.3.5, these three contributions describe (a) the Josephson susceptibility χ_Ji.e. the adiabatic response of the supercurrent, (b) the diagonal susceptibility χ_D due to the effect of the dynamic variation of Andreev states population, (c) the non-diagonal susceptibility χ_{ND} due to microwave induced transitions between levels. The frequency dependence of these contributions is schematically represented in fig.3.5. There are three different regimes for χ':

- the adiabatic regime when $\omega\tau_{in} \ll 1$
- the low frequency regime when $\hbar\omega/E_g \lesssim 1$ where the non-diagonal contribution is negligible

- the high frequency regime when $\hbar\omega/E_g \gtrsim 1$ where the non-diagonal contribution is not negligible

There are two different regimes for χ":

- the regime where χ''_D dominates when $\omega\tau_{in} \sim 1$
- the regime where χ''_{ND}dominates when $\omega E_g/\hbar \gtrsim 1$

These three contributions and the way they are extracted from data are described in more details in chap.6 where we show the complex evolution we observe is well accounted for in this framework.

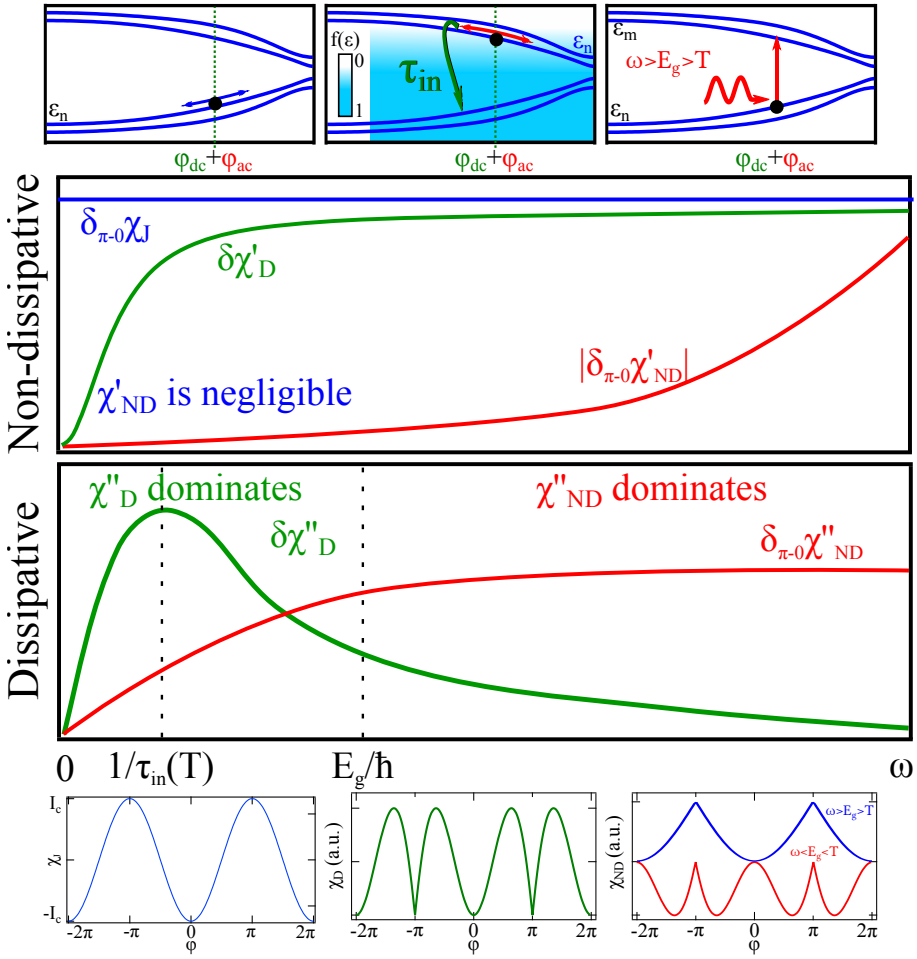

Figure 3.5: **Top:** Sketch of the physical mechanisms at the origin of the finite-frequency response: (Left:) the adiabatic response χ_J; (Middle:) the relaxation of populations driven out-of-equilibrium by the finite-frequency phase-biasing, denoted χ_D; (Right:) the microwave induced transitions among the spectrum, denoted χ_{ND}. **Middle:** Schematic frequency dependence of each contribution for the non-dissipative (Top) and dissipative (Bottom) responses. At low frequency, $\chi'_{ND}$is negligible and χ"can be dominated by $\chi''_D$for $\omega\tau_{in} \sim 1$. At high frequency χ"is dominated by χ''_{ND}. **Bottom:** Phase dependence of each contribution. χ_J is a cosine when the equilibrium current-phase relation is purely sinusoidal, $\chi_D$has almost half the periodicity of χ_J. The phase dependence of χ_{ND}depends on the temperature and frequency. At low temperature and high frequency, χ_{ND}mimics the minigap whereas at low frequency and high temperature χ_{ND}has a phase dependence opposite to the one of χ_D.

4

Susceptibility of a NS ring from Bogoliubov-de Gennes hamiltonian diagonalization

This numerical work has been mainly motivated by our lack of understanding of χ"and particularly χ''_{ND}but also to find an alternative approach to numerical simulations of Usadel equations. The main programming work has been done by Meydi Ferrier. It has progressed hand in hand with our experimental understanding. This model however does not aim at giving quantitative predictions and comparisons with experiments but rather at providing some insights on the role of the phase dependence of the non-diagonal elements of the current operator.

4.1 Bogoliubov-de Gennes equation

The formation of pairs is described in the BCS theory by the exchange of virtual phonons [4] but it can be equivalently formulated as an interaction between quasiparticles conjugated by time-reversal symmetry, without specifying the nature of the coupling. In this point of view, the electron and hole are coupled by the pairing hamiltonian $\Delta = \begin{pmatrix} 0 & \Delta \\ \Delta^* & 0 \end{pmatrix}$ Thus, the eigenstates of the system no longer correspond to electron or hole-like quasiparticles but to a superposition of them called Bogoliubons following [101]. The two corresponding amplitudes $u(\vec{r})$ and $v(\vec{r})$ obey the Bogoliubov-de Gennes (BdG) equation [9] :

$$\begin{pmatrix} H & \Delta \\ \Delta^* & -H^* \end{pmatrix} \begin{pmatrix} u(\vec{r}) \\ v(\vec{r}) \end{pmatrix} = \epsilon \begin{pmatrix} u(\vec{r}) \\ v(\vec{r}) \end{pmatrix} \tag{4.1}$$

where H is the usual electronic Hamiltonian containing the kinetic and potential terms and Δ is the pair potential, to be determined self-consistently.

It can be shown [102] that the BdG equation can be viewed as a "one-particle" wave equation whose eigenstates can be filled up systematically to describe the superconducting state, in the same way that one fills the eigenstates of the Schrödinger equation to describe normal conductors. The only difference with the normal case is that one needs to start from a special vacuum $|V\rangle$, consisting of a full band of down-spin electrons, instead of the usual vacuum devoid of all particles. Any quantity of interest, A (such as the charge density or the current density), can be interpreted as the sum of a "vacuum contribution" A_{VAC} due to the vacuum $|V\rangle$ and a one-particle contribution A_{BdG} due to the filled eigenstates of the BdG equation. This one-particle is what we called a bogoliubon and is a superposition of an up-spin electron and

a down-spin hole. New creation and annihilation fermionic operators can be defined as follow:

- $\gamma^{\dagger}_{k\pm}$ creates a bogoliubon at energy $E_{k\pm} = \pm\sqrt{\Delta^2 + \xi_k^2}$
- $\gamma_{k\pm}$ annihilates a bogoliubon at energy $E_{k\pm} = \pm\sqrt{\Delta^2 + \xi_k^2}$

where ξ_k is the kinetic energy measured from the Fermi energy.

The ground state $|G\rangle$ is obtained by filling up all the eigenstates of the BdG equation having energy smaller than the Fermi energy (i.e. the E_{k-} states) starting from this special vacuum $|V\rangle$:

$$|G\rangle = \prod_k \gamma^{\dagger}_{k-} |V\rangle \tag{4.2}$$

At finite temperature, the appropriate many-body state is obtained by filling up the eigenstates of the BdG equation according to the Fermi function at that temperature.

This description is well-adapted for photon absorption since an induced transition corresponds to applying $\gamma^{\dagger}_{k+}\gamma_{k-}$ to the ground state, that is destroy a particle from the lower band to create one in the upper band.

4.2 Tight binding model

We implement the Bogoliubov-de Gennes Hamiltonian described by the 4 blocks matrices,

$$\mathcal{H} = \begin{pmatrix} H - E_F & \Delta \\ \Delta & E_F - H^* \end{pmatrix} \tag{4.3}$$

where H and $-H^*$ are $N \times N$ matrices which describe respectively the electronic and hole wave function components of a hybrid NS ring within a tight binding 2D Anderson model.

$$H = \sum_{i=1}^{N} \epsilon_i |i><i| + \sum_{i \neq j} t_{ij} |i><j| \tag{4.4}$$

The ring has N $= N^N + N^S = N_x \times N_y$ sites on a square lattice of period a, with a normal portion of $N^N = N_x^N \times N_y$ sites in contact with a superconducting one of $N^S = N_x^S \times N_y$ sites. The on-site random energies ϵ_i of zero average and variance W^2 describe the disorder in the ring. The hopping matrix element between nearest neighbors reads

$$t_{ij} = t \exp i\varphi_{ij} \tag{4.5}$$

where the phase factor is related to the superconducting phase difference through the normal junction via:

$$\varphi_{ij} = (\pi/2\Phi_0) \int \vec{A}\vec{dl} = (x_i - x_j)\varphi/N_x^N \tag{4.6}$$

describes the effect of an Aharonov Bohm flux $\Phi = AN_x^N a = \Phi_0\varphi/2\pi$ and $\Phi_0 = h/2e$ is the superconducting flux quantum. For sites in the S part $\phi_{ij} = 0$.

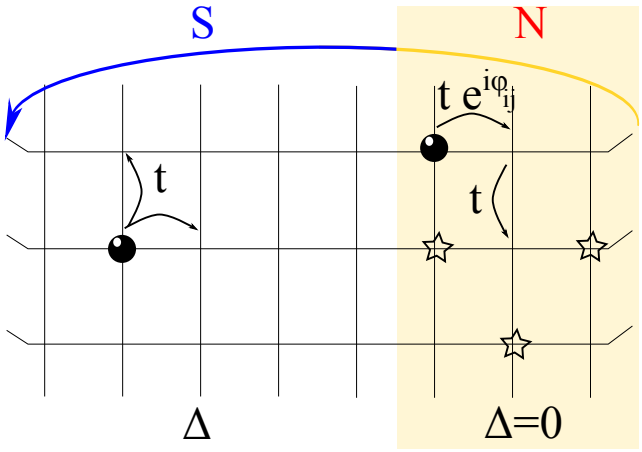

Figure 4.1: Sketch summarizing our model : in the superconducting region S, there is a coupling energy Δ between e^- and holes on site i and a purely real hopping term of amplitude t. In the normal region N, $\Delta = 0$ but quasiparticles acquire a phase φ_{ij} at each hop. Stars symbolize on-site disorder and the hopping amplitude is non-zero between the last N site and the first S site.

spectrum	N_x^N	N_x^S	N_y	t	Δ	W	$\frac{\Delta}{E_{Th}}$
fig.4.2 a	20	20	100	4	1	6	40
fig.4.2 b	60	50	24	4	1	6	75

Table 4.1: Typical parameters used for simulations

The $N \times N$ BCS diagonal matrix $\mathbf{\Delta}$ couples electron and hole states exclusively in the S part: $\Delta_{i,i} = \Delta$ for $N_N + 1 \leq i \leq N$ and is zero otherwise. We have chosen the amplitude of the superconducting gap $\Delta = t/4$ such that the S coherence length $\xi_s = at/\Delta \ll N_N$ in order to avoid the reduction of the superconducting correlations in the S region by the inverse proximity effect. The number of transverse channels and the disorder amplitude W correspond to the diffusive regime where the length $N_x^N a$ of the normal region is longer than the elastic mean free path

$$l_e \simeq a15(t/W)^2 \tag{4.7}$$

in 2D [100] and shorter than the localization length Ml_e, where M is the number of channel. We checked that the results do not depend of the position of the Fermi energy, typically chosen at filling 1/4. Hereafter, all energies are taken relatively to E_F. Typical parameters used for simulations are gathered in table.4.1.

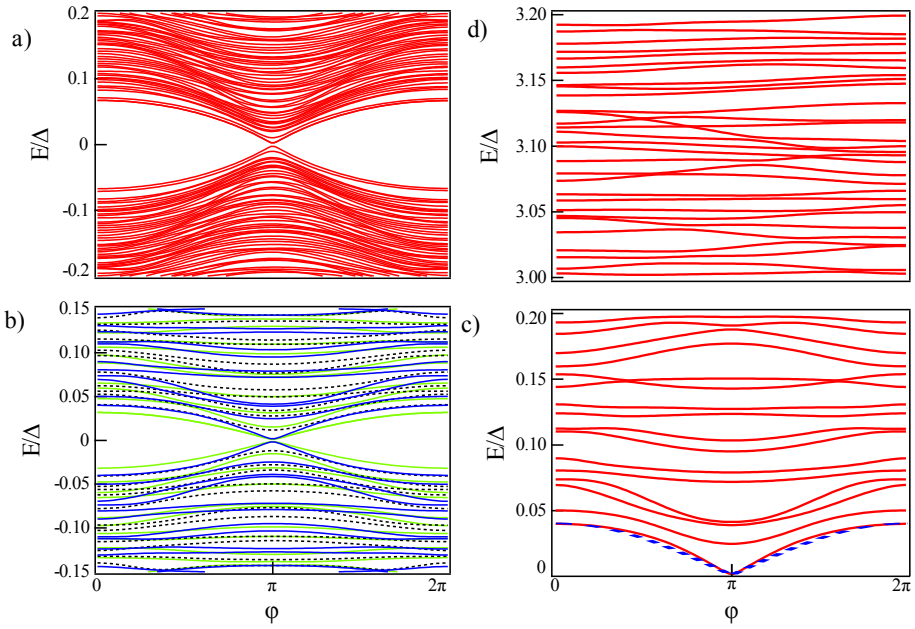

Figure 4.2: Phase dependent spectrum of Andreev levels for NS rings of different sizes. In the following, spectrum **a.** will be referred to as the "large minigap spectrum" whereas spectrum **b.** as the "small minigap spectrum". **a.**diffusive ring with a larger number of transverse channels $N^N = N_x^N \times N_y = 20 \times 100$ normal sites for a single disorder configuration of amplitude $W/t = 1.5$ with $t = 4\Delta$. The number of S sites is $N^S = 20 \times 100$. **b.** diffusive ring with $N^N = N_x^N \times N_y = 60 \times 24$ and $N^S = 50 \times 24$ for 3 different disorder configurations (different colors) of amplitude $W/t = 1.5$ with $t = 4\Delta$. Note the symmetry of the spectra in **a** and **b** with respect to the Fermi level at zero energy as well as the opening of the phase dependent minigap which amplitude scales with the Thouless energy, $E_{Th} = \delta_N N_y l_e / N^N a$ where δ_N is the energy level spacing in the normal region. **c.** Close-up view of low energies for a spectrum of **b**. Note the 2π-periodicity which corresponds to quasiparticles of charge $2e$ localized in the weak link. Dashed line is the analytical expression $E_g(\varphi) \propto |\cos(\varphi/2)|$. **d.** In contrast, the periodicity changes at energies greater than the superconducting gap Δ. It is 4π-periodic, that corresponds to quasiparticles of charge e delocalized all over the ring as for a normal ring.

4.3 Spectrum of a NS ring

Spectrum

Typical flux dependent spectra obtained upon diagonalization of the hamiltonian $\mathcal{H}$ (4.3) are shown in Fig.4.2. Note that due to spin degeneracy, each levels of the spectra are doubly-degenerated.

Emergence of a minigap

The most striking feature in the spectrum is the emergence of a phase-dependent gap in the normal metal's density of states. It closes linearly at odd multi-

ples of π in the limit of a very dense spectrum and can be well described by $E_g(\varphi) = E_g(0)|\cos(\varphi/2)|$ as predicted in[67] (Fig.4.2 c). This closing of the gap at $\varphi = \pi$ is directly related to the existence of conductance channels of transmission one in a large diffusive system [65, 64]. We define the Thouless energy E_{Th} in the following from:

$$E_g(0) = 3.1E_{Th} \tag{4.8}$$

Evolution of periodicity and level spacing with energy

At energies well below the superconducting gap, energy levels exhibit a mean level spacing

$$\delta_N = E_F/N^N \tag{4.9}$$

characteristic of the normal part to which the Andreev bound states are confined and a $\Phi_0 = h/2e$ periodicity (see fig.4.2c). These constitute the Andreev spectrum. A denser spectrum is observed above the superconducting gap with the periodicity $\frac{h}{e}$ as expected for a normal ring, see Fig.4.2d. By construction the spectrum is perfectly symmetric with respect to the Fermi energy. We observe disorder dependent fluctuations (Fig.4.2b) of the position of the energy levels in the spectrum. At low energy, the amplitude of these fluctuations is of the order of the mean level spacing δ_N.

4.4 Susceptibility of a NS ring from its spectrum and wavefunctions

Knowing the set of $\{\epsilon_n, |\Psi_n\rangle\}$ given by numerical diagonalisation of the hamiltonian, the different contributions to the susceptibility can be computed.

Josephson contribution

The Josephson current I_J is given by:

$$I_J = \sum_n f_n \epsilon_n \tag{4.10}$$

and the Josephson susceptibility by:

$$\chi_J = -\frac{2\pi}{\Phi_0}\frac{\partial I_J}{\partial \varphi} \tag{4.11}$$

I_J is calculated using the eigenenergies determined by the numerical diagonalization of the Bogoliubov-de Gennes hamiltonian. The occupation distributions are Fermi distributions:

$$f_n = \frac{1}{1 + \exp(\frac{\epsilon_n}{k_B T})} \tag{4.12}$$

I_J and χ_J are calculated at several temperatures for the small minigap spectrum, the result after filtering is shown in fig.4.3.

Phase dependence of χ_J

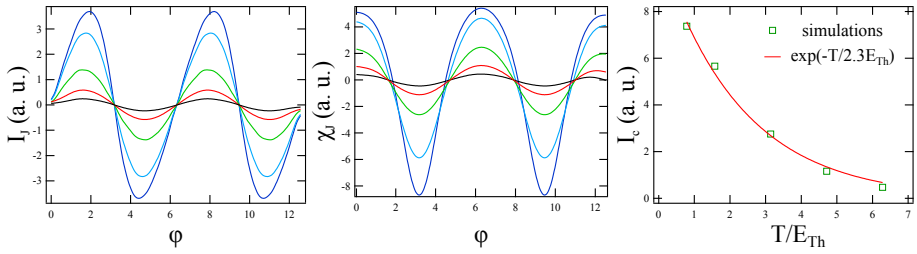

Figure 4.3: Phase dependent Josephson current (**Left**) and susceptibility (**Middle**) calculated from the Andreev spectrum shown in Fig.4.2b. The temperatures correspond to 0.01,0.02,0.04,0.06 and 0.08 in the units of the superconducting gap Δ. The amplitude of the minigap is 0.04 Δ, therefore $\Delta/E_{Th} = 75$. The anharmonicity is best revealed on the derivative $\frac{dI_J}{d\varphi}$. **Right** Temperature dependence of the critical current calculated from the bottom left spectrum of fig.4.2. The data points are for the same temperatures as in left and middle panels.

As shown in fig.4.3, the flux dependence of the Josephson current $I_J(\varphi)$ and its flux derivative at low temperature are sensitive to the anharmonicity of the flux dependence of low energy levels and exhibit a slight skewness. $I_J(\varphi)$ becomes sinusoidal at temperatures larger than the Thouless energy of the order of 0.04Δ according to [79]. We will see in the following that the ac current response is much more sensitive than the Josephson current to the strong anharmonicity of the flux dependent minigap, and exhibits strong cusps at π which survive at temperatures larger than the Thouless energy.

Temperature dependence of χ_J

As shown in fig.4.3, the critical current and therefore the amplitude of $\chi_J$decreases roughly like an exponential at high temperature. This is in qualitative agreement with quasiclassical theory in long and diffusive junction [5].

Evolution of the diagonal contribution

We discuss in the following the second term of expression 3.55 that we call χ_D and is the finite frequency non-adiabatic contribution due to the thermal relaxation of the populations f_n of the Andreev levels with the characteristic inelastic time τ_{in} [103, 20, 91, 95]. It reads:

$$\chi_D(\omega) = \frac{i\omega\tau_{\rm in}}{1 - i\omega\tau_{\rm in}} F(\varphi, T) \tag{4.13}$$

where

$$F(\varphi, T) = -\sum_n i_n^2 \frac{\partial f_n}{\partial \epsilon_n} \tag{4.14}$$

contains the phase dependence of χ_D.

Phase dependence of χ_D

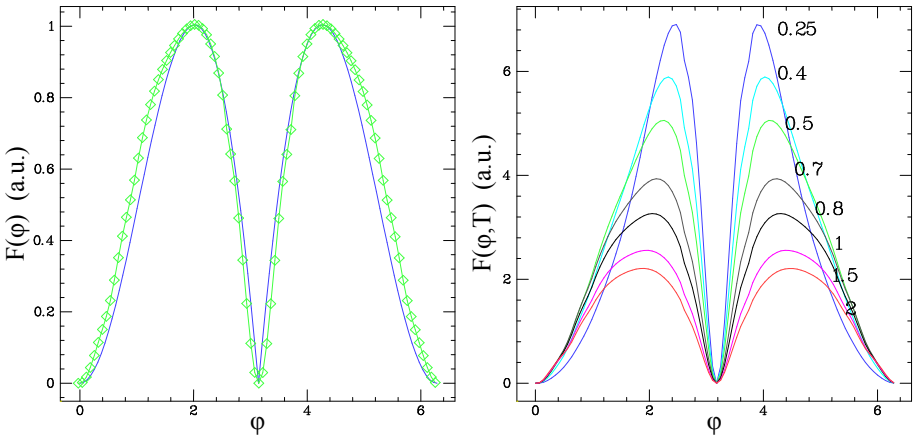

Figure 4.4: **Left.** comparison of the numerical results (connected diamonds) with the analytical expression 4.15 (continuous line) at a temperature equal to the minigap 0.08Δ.**Right.**phase dependence of the function F computed for different temperatures increasing from the top to the bottom curves in units of the total minigap $2E_g$.

We have numerically evaluated this function deriving i_n from the phase derivative of each eigenenergy pictured in Fig.4.2. $F(\varphi)$ is shown for different temperatures in Fig.4.4. Due to its dependence on the square of the single level currents, $F(\varphi)$ has a strong second harmonics component and exhibits sharp cusps at odd multiples of π for which the minigap closes. It has been determined analytically solving the Usadel equations by Virtanen *et al.* in the low frequency limit ($\omega \ll E_g$). Its high temperature ($T > 8E_{Th}$) limit $F_U(\varphi)$ is well approximated by:

$$F_U(\varphi) = [-\pi + (\pi + \varphi)[2\pi]]\sin(\varphi) - \frac{|\sin(\varphi)|}{\pi}\sin^2(\varphi/2) \tag{4.15}$$

As shown on Fig.4.4 this analytical form describes well the phase dependence of the numerical results at temperatures larger than $E_g(0)$.

Temperature dependence of χ_D

We find that our numerical simulations are in qualitative agreement with the one of Virtanen *et al.* [95] (see fig.4.9) which consist in solving Usadel equations: they have similar temperature dependences (see fig.4.5) and both show a change of the position of the maximum with temperature; at low temperature the first maximum for positive values of φ is closer to π than at high temperature. Moreover, it is worth noting that at high temperature ($T \gtrsim 8E_{Th}$), the diagonal contribution decreases as $1/T$.

Evolution of the non-diagonal contribution

The non-diagonal contribution describes microwaves induced transitions within the spectrum. It reads:

$$\chi_{ND} = -\sum_{n,m\neq n} |J_{nm}|^2 \frac{f_n - f_m}{\epsilon_n - \epsilon_m} \frac{i\hbar\omega}{i(\epsilon_n - \epsilon_m) - i\hbar\omega + \hbar\gamma_{ND}} \tag{4.16}$$

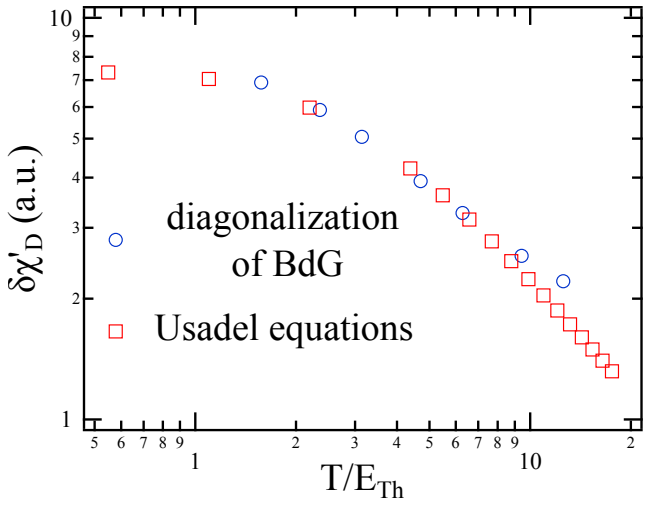

Figure 4.5: Temperature dependence of the diagonal contribution from numerical diagonalization of Bogoliubov-de Gennes hamiltonian (circles) and from numerical simulations of Usadel equations done by Virtanen *et al.* (boxes).

In the preceding chapter (sec.3.4), we made a rough approximation based on neglecting the phase dependence of the current elements to analytically determine the evolution of χ''_{ND}. We are now able to compute these terms. In the following we show that $|J_{nm}(\varphi)|^2$ has a non-trivial evolution with n and m.

Phase dependence of the non-diagonal elements of the current operator

The non-diagonal matrix elements of the current operator

$$\vec{J} = \frac{-i\hbar\vec{\nabla} - q\vec{A}}{m} \tag{4.17}$$

along the ring are calculated from the eigen wavefunctions according to:

$$\begin{aligned} J_{nm} = \frac{\hbar}{im}\sum_j \Psi_n^{e*}(x_j,y_j)(\Psi_m^e(x_j+1,y_j) - \Psi_m^e(x_j,y_j) + eA(x_j)\Psi_m^{e*}(x_j,y_j)) \\ +\Psi_n^{h*}(x_j,y_j)(\Psi_m^h(x_j+1,y_j) - \Psi_m^h(x_j,y_j) - eA(x_j)\Psi_m^{h*}(x_j,y_j)) \end{aligned} \tag{4.18}$$

where $\Psi_m^e(x_j,y_j)$ and $\Psi_m^h(x_j,y_j)$ correspond respectively to the electron and hole components of the wave function at point j of coordinates x_j, y_j in units of a.

Phase dependence

The phase dependence of the square modulus of these matrix elements is shown in Fig.4.6 for various values of indexes n and m on the same side or on opposite sides of the minigap. The index n and m are taken respectively positive above and negative below the minigap. Whereas $|J_{-1,1}(\varphi)|^2$ exhibits a strong peak at $\varphi = \pi$ the amplitude of $|J_{-1n}(\varphi)|^2$ is much smaller at $n > 1$. On

from / to	n
n	dip at $\varphi = \pi$, amplitude decreases very fast ($\delta \left\|J_1\right\|^2 = 5\delta \left\|J_2\right\|^2$)
-n	peak at $\varphi = \pi$, amplitude decreases slowly ($\delta \left\|J_{-1,1}\right\|^2 = 3\delta \left\|J_{-9,9}\right\|^2$)
$m \neq n, -n$	small amplitude compared to $\left\|J_{-nn}\right\|^2$

Table 4.2: Evolution of $\left\|J_{nm}\right\|^2$ with n and m. The slow decay with energy of the $\left\|J_{n,-n}\right\|^2$ terms indicates the existence of selection rules.

the other hand matrix elements $|J_{-nn}(\varphi)|^2$ corresponding to states symmetric with respect to the minigap, i.e. electron hole symmetric states, keep a phase dependence peaked at π similar but reversed in sign compared to $|J_{1,1}(\varphi)|^2$. Their amplitude decreases only slowly with n in contrast to the fast amplitude decrease of the diagonal matrix elements J_{nn}. This difference between the phase dependence of $|J_{-nn}(\varphi)|^2$ compared to $|J_{-1n}(\varphi)|^2$ can qualitatively explain the evolution of the shape of $\chi_{ND}(\varphi)$ we derived analytically in sec.3.4:

- in the limit $\omega > E_g \gg k_B T$ the main contribution stems from matrix elements $|J_{-1n}(\varphi)|^2$ where $n \gg 1$ with a very small phase dependence. χ''_{ND}thus performs the minigap spectroscopy.

- In the opposite limit $\omega < E_g \ll k_B T$ a much larger number of matrix elements contribute to χ_{ND} including the electron-hole symmetrical ones $|J_{-nn}(\varphi)|^2$ that strongly depends on the phase. Their phase dependence is opposite to the one of i_n^2, leading to a $\chi"_{ND}$ with a phase dependence opposite to the one of χ'_D.

Evolution of the non-diagonal contribution including the phase dependence of the non-diagonal elements of the current operator

$\chi_{ND}(\varphi)$ is computed from these matrix elements and the related energy spectrum following Eq.4.16. We took $\gamma_{ND} = \delta_N$ in order to reproduce the continuous spectrum limit. The results concerning the imaginary component $\chi''_{ND}(\varphi)$ are shown in Fig.4.7. We find that:

- for $\hbar\omega > k_B T$, we find good qualitative agreement with our analytical findings neglecting the flux dependence of the $|J_{nm}|^2$. In particular $\chi''_{ND}(\varphi)$ is peaked at π and its amplitude increases linearly with frequency up to $\hbar\omega = 2E_g$

- for $\hbar\omega < k_B T$, the shape of $\chi''_{ND}(\varphi)$ is very similar to the opposite of the function $F(\varphi)$, with a characteristic bump at $\varphi = 0$.

A similar behavior is found for $\chi'_{ND}(\varphi)$.

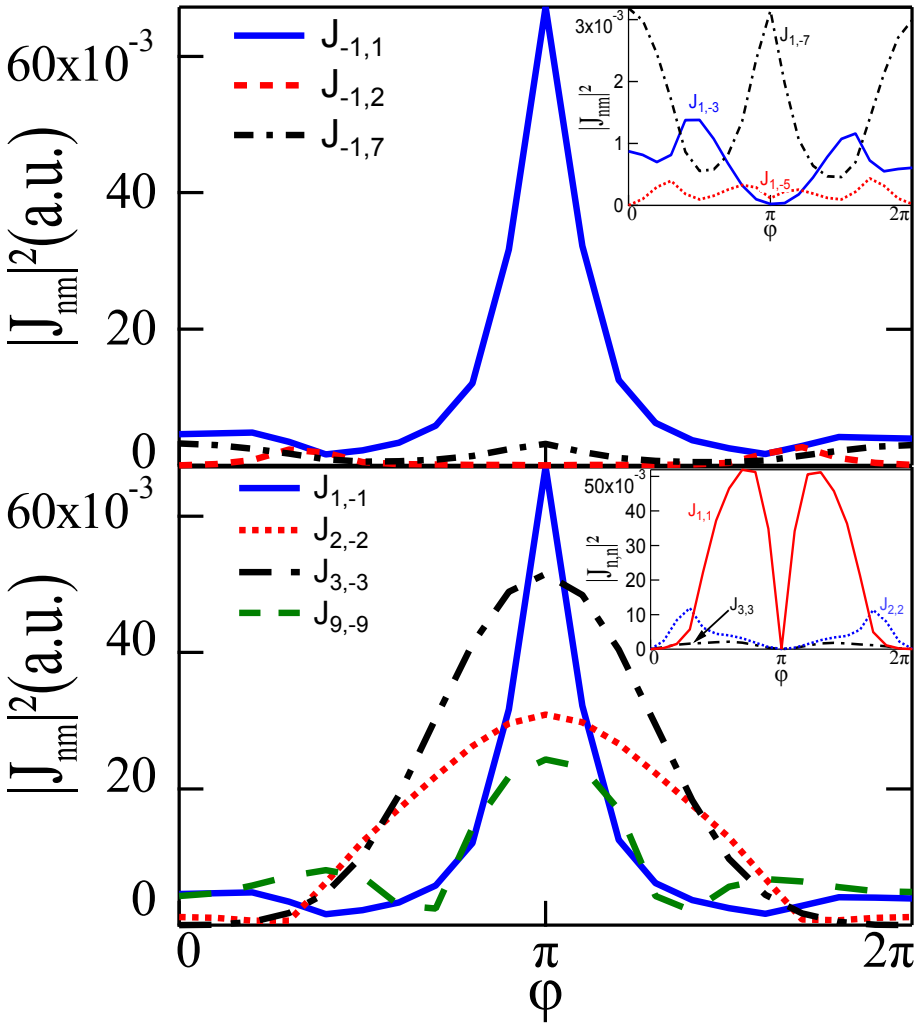

Figure 4.6: Phase dependence of the non-diagonal current matrix elements obtained from the exact diagonalization of the spectrum of a NS ring whose normal region size is 90×30 and $W/t = 2$. The minigap amplitude is $2E_g(0) = 8\delta_N$. **Top:** Phase dependence of the non diagonal current matrix elements $|J_{-1,n}|^2$ coupling the highest level below the minigap to levels above the minigap. Inset: zoom on $|J_{-1,n}|^2$ with $n > 1$ which have a very small phase dependence compared to $|J_{-1,1}|^2$. **Bottom:** Phase dependence of the electron-hole symmetrical non-diagonal matrix elements compared to the diagonal ones (Inset).

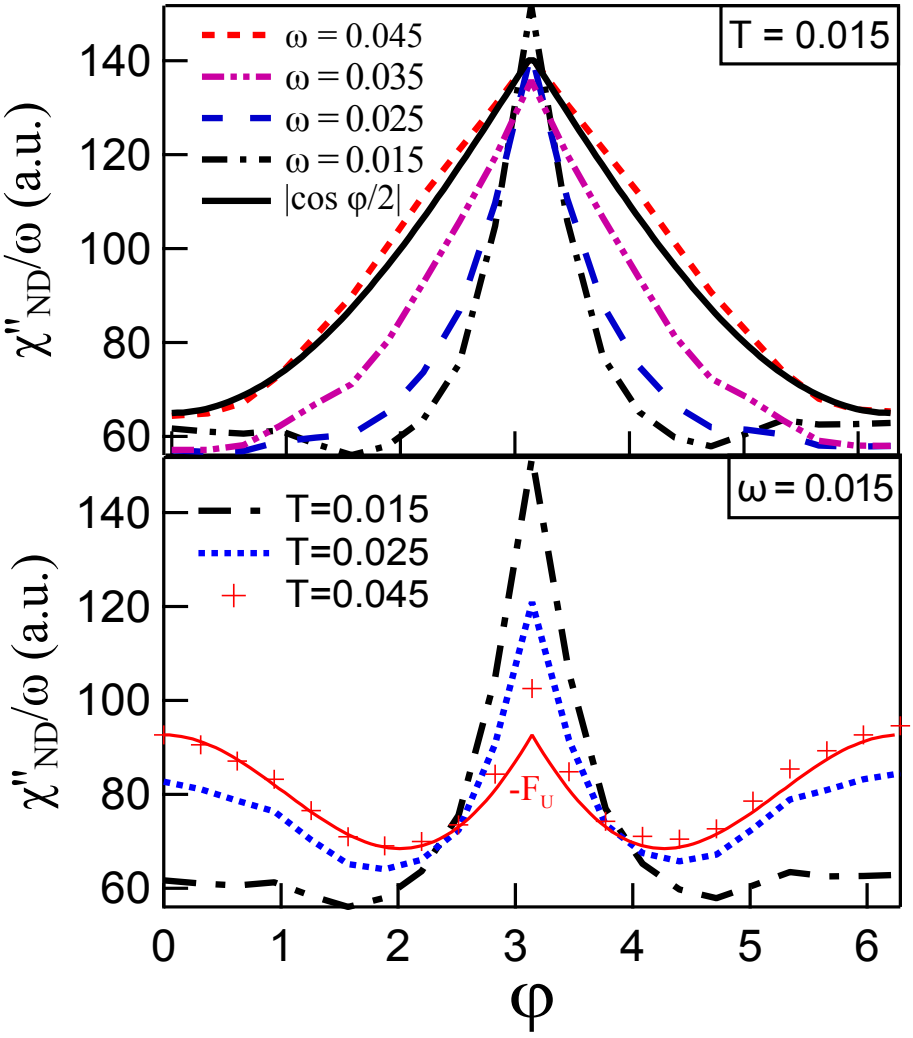

Figure 4.7: Evolution of the phase dependence of $G_{ND} = \chi''_{ND}/\omega$ obtained from the exact diagonalisation of the spectrum of an NS ring (size 90×30) $W/t = 2$ using Eq.4.16 $\gamma_{ND} = 2\delta_N$ **Top:** $k_BT = 2\delta_N$ and different frequencies $\hbar\omega > k_BT$ below and of the order of the minigap, note the good agreement with the data obtained fig.3.4, neglecting the phase dependence of the current matrix elements. **Bottom:** $\hbar\omega = 2\delta_N$ and different temperatures $k_BT > \hbar\omega$ below and of the order of the minigap. For the largest temperature the phase dependence observed is close to the opposite of the function $F_U(\varphi)$, continuous line.

Non-diagonal elements of current operator as selection rules

We see from this numerical simulations that the non-diagonal elements of the current operator act as phase-dependent selection rules: at $\varphi = 0[2\pi]$, all the transitions have a similar probability since all the $|J_{nm}|^2$ have a similar amplitude. In contrast, at odd multiples of π, the transitions between electron-hole symmetrical states are greatly enhanced compared to the others with $|J_{-n,n}|^2$ orders of magnitude larger than the others $|J_{nm}|^2$.

4.5 Comparison between numerical resolution of Usadel equations and diagonalization of Bogoliubov-de Gennes hamiltonian

The results of numerical simulations are consistent with analytical predictions within a Kubo-formula approach (sec.3.4). We found two contributions to the dissipation. The first contribution, χ''_D, is related to the relaxation of Andreev states populations driven out-of-equilibrium by the finite-frequency phase driving. It displays a phase dependence with almost half the periodicity of the Josephson contribution (see fig.4.4). The second contribution, χ''_{ND}, is related to induced transitions within the spectrum. We found two limiting behaviors for χ''_{ND}:

- in the limit of low temperature and high frequency, the phase dependence of $\chi''_{ND}$is due to microwave induced transitions and is reminiscent of the minigap's
- in the opposite limit of low frequency and high temperature, the phase dependence of $\chi''_{ND}$is dominated by the one of $|J_{nm}|^2$. It is similar to the one of χ''_Dbut reversed in sign.

As shown in fig.4.8 and detailed in chap.6, this picture is in agreement with our experimental findings.

In [95], Virtanen *et al.* determined the linear ac response of diffusive SNS junctions by solving Usadel equations. They show the admittance $Y = \chi/i\omega$ can be split into three parts:

$$Y = Y_{sc} + Y_{dy} + Y_{qp} \tag{4.19}$$

that describe:

- for Y_{sc}, the supercurrent
- for Y_{dy}, the effect of the dynamic variation of the populations of the Andreev levels
- for Y_{qp}, the quasiparticle current driven directly by the field

As detailed previously, the dynamical contribution Y_{dy} corresponds to what we called diagonal contribution $\chi_D = i\omega Y_{dy}$. This term contributes the dissipation on the timescale of the inelastic scattering time. Another contribution to dissipation originates from Y_{qp} and Y_{sc}. The phase dependent part of this

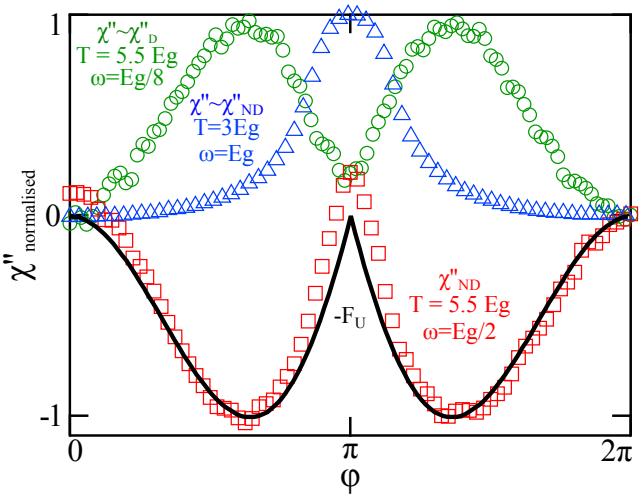

Figure 4.8: Typical experimental phase dependences of χ"(symbols). At frequencies close to τ_{in} ($\omega\tau_{in} \sim 1$) and high temperature ($T > E_g$), χ"can be dominated by its diagonal contribution χ''_D. At high frequency ($\omega \gtrsim E_g$) , the phase dependence of χ"is almost the minigap's. At low frequency and high temperature, χ''_{ND}phase dependence is almost the opposite of the one of the diagonal contribution (solid black line). In this regime $\chi''_{ND}$and χ''_Dnearly cancel each other.

contribution has to be compared with what we called the non-diagonal contribution χ''_{ND}. According to that mapping, we should have at low frequency ($\omega < E_g$):

$$\chi''_D = \frac{\omega\tau_{in}}{1+\omega^2\tau_{in}^2}\frac{G_N E_{Th}^2}{T}Q(\varphi,T) \tag{4.20}$$

and

$$\frac{\chi"_{ND}}{\omega} = \frac{G_N E_{Th}^2}{T}P(\varphi,T) \tag{4.21}$$

with G_N the normal state conductance and $P(\varphi,T)$ and $Q(\varphi,T)$ shown in fig.4.9. Although P and χ''_{ND}both have a phase dependence reminiscent of the minigap's at low temperature, their high temperature phase dependences differ. In particular, P does not display a phase dependence opposite to the one of Q. This is in disagreement with our numerical and experimental findings.

In [104] the linear response of a short SNS junction is addressed. Kos *et al.* considered two Andreev bound states (the ground and the excited states) plus the continuum. As in our work, the response is split into several contributions. In addition to the adiabatic response and the transition between electron-hole symmetric states, Kos *et al.* considered (a) transitions from bottom to top continuum bands, (b) transitions within the continuum, (c) transitions from the excited Andreev bound state to the continuum and a last one (d) that creates one quasiparticle in the excited bound state and one in the band. These contributions are analogous to what we called the non-diagonal susceptibility. The distinction between continuum and Andreev bound states is however not so clear in the case of a long and diffusive junction, one rather observe an evolution from strongly phase-dependent levels close to the Fermi energy to almost

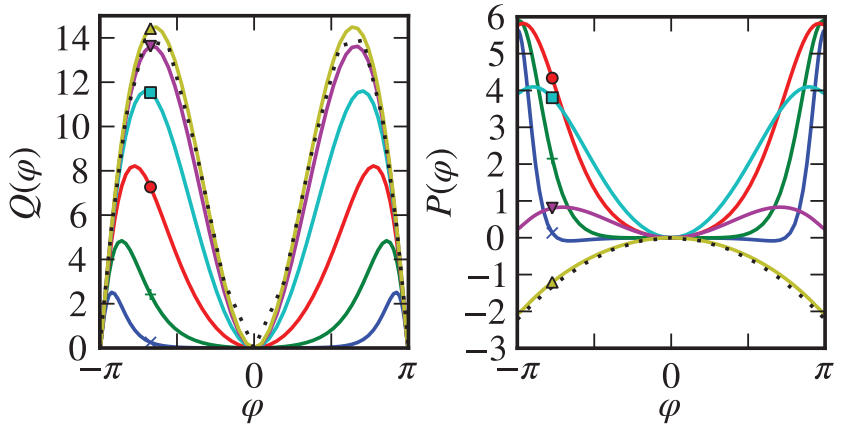

Figure 4.9: Phase dependence of the dissipative parts of the response at several temperatures: $T/E_{Th} = 16(\triangle), 8(\triangledown), 4(\square), 2(\circ), 1(+), 0.5(\times)$. The dotted lines represent the analytic high-temperature approximations to which Q and P tend for $T \gg E_{Th}$. **Left:**Function $Q(\varphi, T)$ describing the phase-dependent dynamic contribution to the response.**Right:** Function $P(\varphi, T)$ describing the phase dependence of the dissipative part of the admittance at low frequencies. After [95]

phase-independent levels at energies larger than Δ. They finally conclude that dissipation is dominated by transitions from the ground Andreev bound state to the excited one at frequencies smaller than the gap. In contrast with our work, Kos *et al.* did not consider the relaxation of Andreev states populations. Moreover, the latest contribution they describe (d) has been observed recently in the context of superconducting atomic contacts [60].

5

Experimental setup & physical quantities measured

The experiment aims at measuring the evolution with phase, temperature and frequency of the magnetic susceptibility of a NS ring in a linear regime. In-phase susceptibility accounts for the non-dissipative response while the out-of-phase part yields the dissipative response, we are thus interested in detecting both. This is done by using a technique developed in the nineties to detect the ac conductivity of an assembly of normal rings involving a multimode resonator[36, 105, 37]. In the following, we start by detailing this technique, then we describe the sample fabrication. Lastly we detail how the susceptibility is obtained and how the out-of-phase signal is calibrated.

5.1 Experimental setup: a hybrid ring coupled to a multimode resonator

The principle of the experiment, sketched in fig.5.1, is to couple a NS ring to a resonator and to follow the modification of the eigenmodes of the resonator when a magnetic field is applied. Indeed, the resonator basically can be considered as a LC circuit and the NS ring to a flux-dependent inductance that modifies the resonator's eigenmodes. The phase-dependent response, obtained by scanning the magnetic field from 0 to a value equivalent to a phase change of 2π, depends on the temperature and on the excitation frequency i.e. the eigenfrequency of the resonator.

The experimental set-up is shown in Fig.5.2 and consists of a NS ring embedded into a resonator. The resonator provides excitation and detection of the NS ring's ac linear response. Experiments can be carried out at the resonator's eigenfrequencies. The resonator consists of a double meander line etched out of a 1 micron thick niobium film sputtered onto a sapphire substrate. A weak capacitive coupling to the microwave generator preserves the high quality factor of the resonances, which can reach $5\,10^4$ up to 14 GHz. The resonator is enclosed in a copper box, shielding it from electromagnetic noise, and cooled down to mK temperature. In addition, it is possible to measure control samples by dc techniques using a second sample holder (see fig. 5.3).

The NS ring fabrication process evolved during my thesis in order to broaden the experimentally accessible range of temperature. The normal part however did not change much and is made of Au fabricated using electron beam lithography techniques. Following the work of F. Chiodi *et al.* [106], we started using Focused ion beam(FIB)-deposited tungsten wires as a superconductor. We

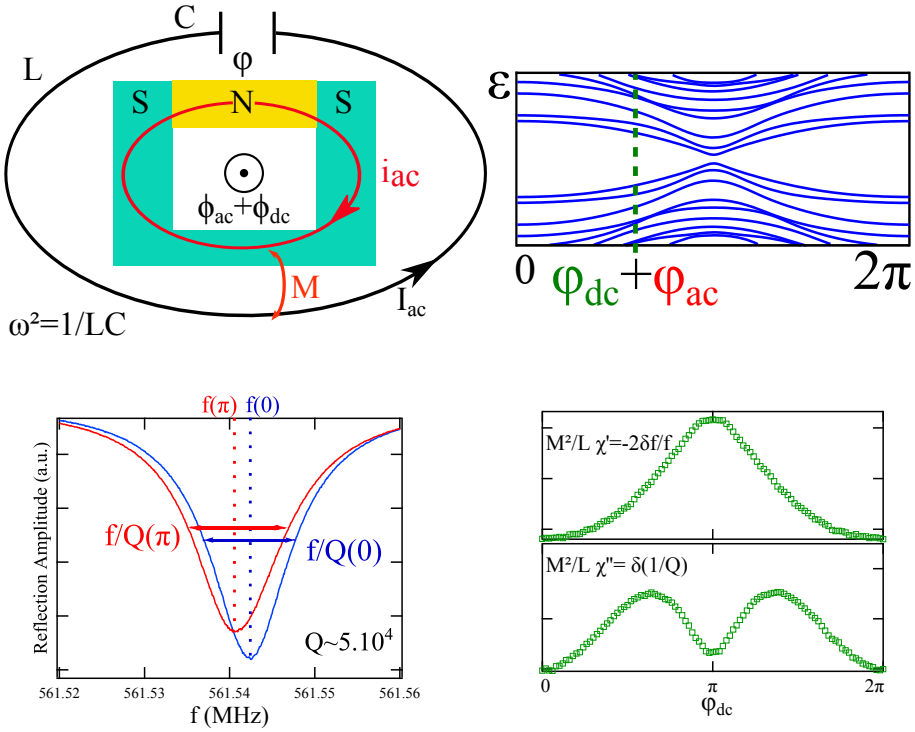

Figure 5.1: Principle of the experiment. **Top left:** A LC resonator is coupled to a NS ring threaded by a dc flux Φ_{dc}. The current in the resonator oscillates at frequency ω that creates an ac flux Φ_{ac} in the loop. The induced ac current in the loop in turn modifies the resonance of the resonator. **Top right:** A dc phase value φ_{dc} is set with a coil (dashed line). Modulation of amplitude φ_{ac} around this value is provided by the resonator at its eigenfrequencies. φ_{dc} is scanned from 0 to 2π to probe the whole spectrum. **Bottom left:** Reflection amplitude at $\varphi_{dc} = 0$ and $\varphi_{dc} = \pi$. Note that the resonance frequency and the quality factor change when phase is varied. Measuring these changes yields the ring's complex susceptibility $\chi = \chi' + i\chi''$. **Bottom right:** The real part of the susceptibility χ' is related to the frequency shift by $\chi' = -2\frac{L}{M^2}\frac{\delta f}{f}$ and the imaginary part χ'' to a change of the inverse quality factor $\chi'' = \frac{L}{M^2}\delta\left(\frac{1}{Q}\right)$. Here L is the inductance of the resonator and M is the coupling inductance between the ring and the resonator. The phase dependence of the susceptibility is thus measured.

measured one sample, named WAu2, made following this process. We finally abandoned this technique in favor of electron-beam lithography and sputtering of a PdNb bilayer.

In earlier experiments, the NS ring was placed between the lines of the resonator. To avoid frequency dependent calibration difficulties, we decided to place the NS ring in between the resonator coupling capacitances. It connects the two lines at one end of the resonator, turning it into a $\lambda/4$ line with a fundamental frequency of 190 MHz, and harmonics 380 MHz apart.

To summarize, three samples have been investigated:

- WAu1: made of FIB-deposited W, placed between the resonator's lines. Response measured at multiples of $360MHz$ [106].
- WAu2: made of FIB-deposited W, placed between the resonator's contact pads. Response measured at odd multiples of $190MHz$.
- PdNbAu: made of sputtered PdNb, placed between the resonator's contact pads. Response measured at odd multiples of $190MHz$.

We detail in the following the different fabrication steps and the reasons why we changed materials.

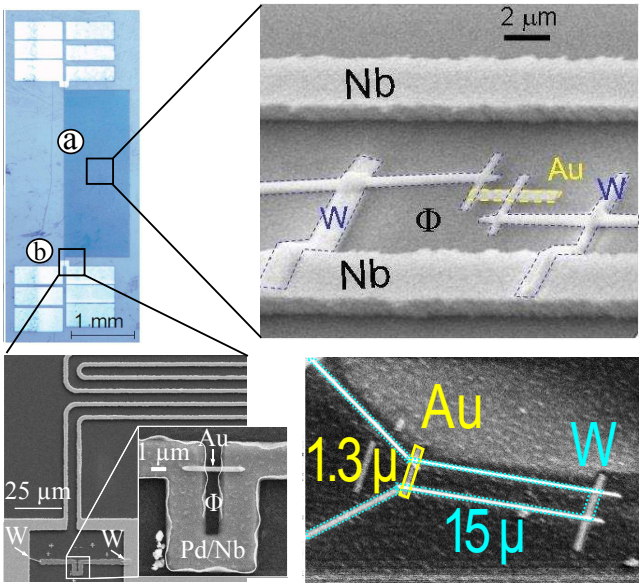

Figure 5.2: Setup used to explore the dynamics of Andreev states. **Top left:** Overview of the resonator in which is embedded a hybrid NS ring. It is possible to place the ring either between the lines (position a) or at the end of the lines (position b). **Top right:** e-beam micrograph of WAu1 sample. The superconducting part of the ring consist of FIB-deposited W wires and a part of the resonator line in Nb. **Bottom left:** Close-up of the area where the ring PdNbAu is located. Note the W wires used to connect the ring. **Bottom right:** sample WAu2. It is similar to WAu1 but connected to the resonator's contact pads, as PdNbAu sample. Picture's quality is bad because of charging effects.

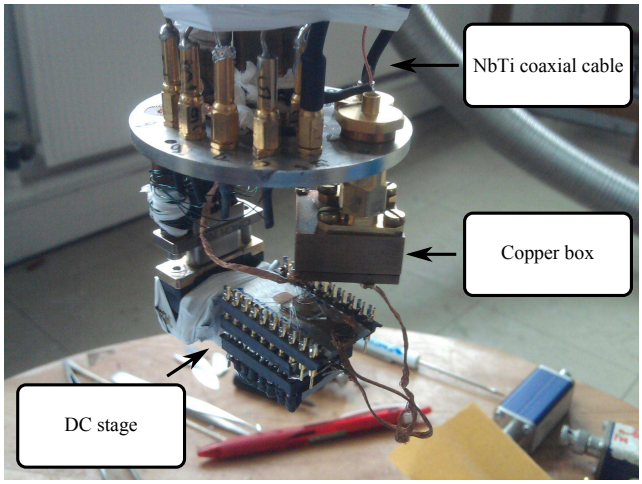

Figure 5.3: A copper box connected by NbTi coaxial cables (only one pad is connected on the picture) is used to shield the resonator from electromagnetic noise. Below, there is a second sample holder that allows to carry out dc experiments. It is thus possible to characterize a control sample with similar characteristics as the NS ring used in the high frequency experiment.

5.2 Sample fabrication

Samples are made in several steps: in a first step, about 30 resonators are deposited on a sapphire 2" substrate, then, after the selection of a resonator to work with, a gold wire is deposited by e-beam lithography and evaporation. In a subsequent step, the S material is deposited, either W by FIB or PdNb by e-beam lithography and sputtering.

Resonator

Resonators are made by UV lithography in the Laboratoire de Photonique et Nanostructures since they require ultra-clean facilities. To deposit the Nb wires thick enough, one can't use standard evaporation/lift-off method. Instead, we deposit by sputtering a Nb film $1\mu m$ thick over the substrate [1]. By optical lithography, we expose the resonator pattern, in which, after developing the resist, we evaporate a 50 nm Al film. The Al film acting as a mask, we etch all the non-protected Nb with a SF_6 Reactive Ion Etching (Nb being more reactive than Al to the fluorine). Finally, we dissolve the remaining Al in a KOH solution.

[1] The film is made thick enough to reduce the magnetic field dependence of the resonance frequency (see [97] for more details). This thickness can be reduced in future experiment where a smaller magnetic field is applied.

Superconducting material: FIB-deposited W

FIB-deposited W looks like an ideal candidate to contact Au with : due to its amorphous nature[2] the superconducting critical temperature of FIB-deposited W is $T_c = 4K$. This technique yields very **clean interface** between the normal and the superconducting metals since there is etching due to Ga^+ ions prior to deposition. This proves useful to contact a NS ring to a resonator since resonators are $1\mu m$ thick and covered by an oxide layer. It has however many drawbacks:

- because of the insulating sapphire substrate, resonator has to be grounded before deposition. If the resonator is not well grounded, the deposited W wires are not well defined (see appendix). Our first attempts were made using tips to ground the resonator but this was not enough. The solution we found was to bond every coupling capacitances of the resonator to a copper plate.
- it is not so easy to obtain reproducible results, the quality of the deposited wire depending on deposition conditions such as nozzle's position (see fig.5.4).
- it is quite time-consuming to implement because of numerous alignment steps: it takes almost a day to make a couple of rings such as the one shown in fig.5.2.
- there is a conducting contamination area of about 200 nm around the deposited wire. The SNS junction can thus be shunted by contamination.
- As detailed in the appendix, it appeared that W has a large kinetic inductance because it is a strongly disordered superconductor with a rather low carrier density. That greatly reduces its interest for making NS ring since a great inductance favors a hysteretical behavior. This last point finally made us abandon that technique to connect gold wires[3].

Superconducting material: PdNb bilayer

As detailed later on, hysteresis appears when $\beta = \frac{2\pi L_l I_c}{\Phi_0} > 1$ with L_l the ring's inductance and $I_c(T)$ its critical current. Because of W's high inductance, it seemed difficult to make NS ring with W without having hysteresis at low temperature so we decided to change material and therefore technique. Nb was a good candidate however the interface between Nb and Au is poor when the two metals are not evaporated in the same vacuum[4] but is greatly improved by a thin (few nm) interlayer of Pd deposited just before Nb. We were inspired in this by contacts on carbon nanotubes or graphene. The interface transparency is however unknown. It may be improved doing the lithography of PdNb and Au in a single step using angle-deposition technique or by doing Ion Beam

[2] to deposit W, a vapor of tungsten hexacarbonyl is decomposed by a focused Ga^+ ion beam. The wire produced is composed by W, C, Ga and O.

[3] This technique is however still useful when the wire to connect is oxidized as Bi nanowires currently measured in the group.

[4] we measured $I_c(T = 0)$ as low as $2\mu A$ for a wire roughly $0.7\mu m$ long, $300nm$ wide and $50nm$ thick

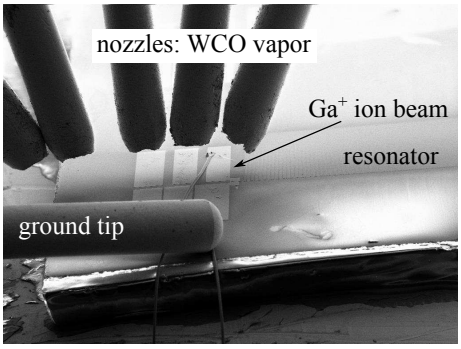

Figure 5.4: Overview of the focused ion beam fabrication process: a vapor of tungsten hexacarbonyl emitted by a nozzle is decomposed by a focused Ga^+ ion beam and produced a wire composed of W, C, Ga and O. To avoid charging effects due to the insulating nature of the sapphire substrate, the sample has to be grounded by connecting the resonator's contact pads to a copper plate but also by using a tip. We finally found that the best way to ground the sample is to connect every contact pads of the resonator to the copper plate and stick the substrate to the copper plate with conducting carbon tape.

Etching prior to PdNb deposition. Finally, because of the thickness of the resonator ($1\mu m$) and the oxide layer on its surface, it is necessary to connect the ring to the resonator using FIB-deposited W.

The main advantage of this technique is the ease of use[5] of e-beam lithography and its reproducibility.

Characteristics of the measured ring

The Au wire (4 micron long, 0.3 micron wide and 50 nm thick) is first deposited by e-beam deposition of 99.999% pure gold (Au 5.9) . The S part is deposited in a second alignment step by sputtering of a Pd/Nb bilayer (6 nm Pd, 100 nm Nb). The resulting uncovered length of the Au wire is $1\mu m$. The ring is connected to the Nb resonator in a subsequent step, using ion-beam assisted deposition of a tungsten wire in a focused ion beam (FIB) microscope. This process creates a good superconducting contact between the resonator and the Pd/Nb part of the ring. The 6 nm-thick Pd buffer layer ensures a good transparency at the NS interface, as demonstrated by the amplitude of the critical current measured with dc transport measurements on control SNS junctions fabricated simultaneously (it is about $50\mu A$ for wires roughly $1.5\mu m$ long, $300nm$ wide and $50nm$ thick ; see chap.6).

Optimization of the coupling between the ring and the resonator

In first experiments, the ring was placed in-between the resonator's meanders but it was soon realized this placement has many drawbacks : the amplitude of

[5]Sapphire is an insulating substrate, we get rid of charging effects using a conducting espacer (espacer 300Z from Showa Denko Europe GmbH) over the usual PMMA/MAA resist.

the signal is small and depends on the order of the harmonic of the resonance because the amplitude of the current does (see fig.5.5). There is also a large contribution of the magnetic field dependence of the resonator itself. We

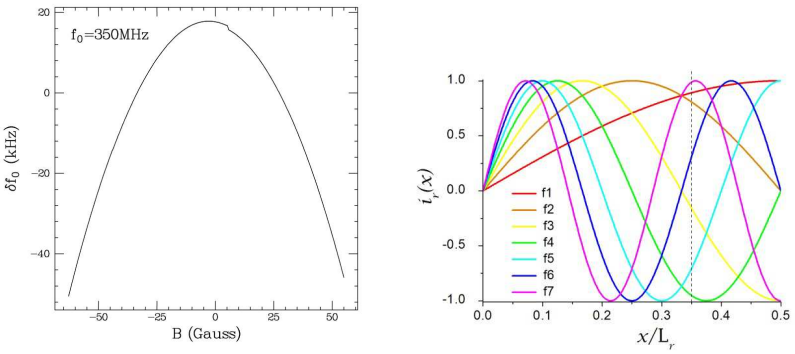

Figure 5.5: **Left:** Magnetic field dependence of the fundamental resonance frequency of the resonator at T=50 mK. After [36]. **Right:** Amplitude of the current of the resonator as a function of the position inside the resonator for several harmonics. Dashed line represent the position of WAu1 sample. From [96]

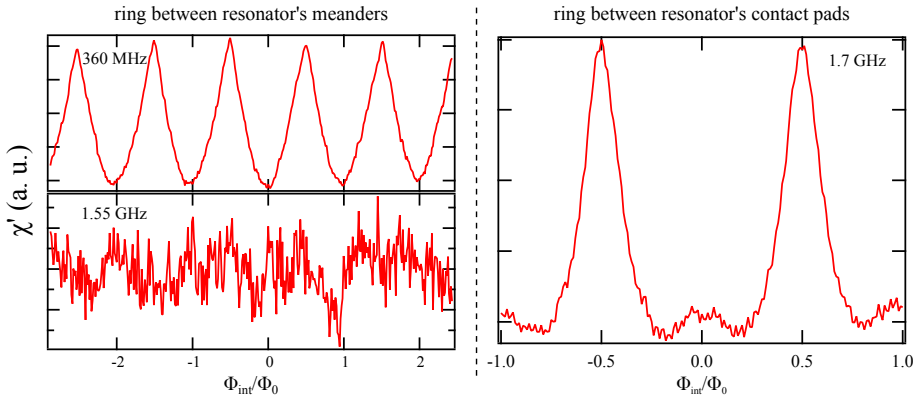

Figure 5.6: Comparison between signals of WAu1 and PdNbAu at T=1K. Signal is at f=360 MHz (top left panel) and f=1.55 GHz (bottom left panel) for WAu1 sample. The signal to noise ratio decreases with increasing frequency. The signal to noise ratio at high frequency is greatly improved when the ring is placed between contact pads, for instance at f=1.7 GHz for PdNbAu (right panel).

finally decided to connect the ring between the coupling capacitances at the end of the lines. This placement has many advantages :

- it is possible to characterize the sample with dc experiments such as differential resistance measurements. It however requires to cut the superconducting wire in parallel with the normal one.

- there is magnetic field focusing between the large Nb pads constituting the coupling capacitances (see fig.5.2): the field experienced by the ring is about five time larger than the applied field. In practice, a field variation of less than 2 G is applied. As shown in fig.5.5, close to zero field the resonance frequency of the resonator does not change much on this field scale. Therefore, the resonator's field dependence does not have to be taken into account.
- The position of the ring corresponds to a maximum of the current through the resonator for all harmonics; there is therefore no frequency dependent effects on the response.

This choice, in addition to the use of NbTi superconducting coaxial wires that do not attenuate the signal over a wide frequency range, lead to an important improvement of the signal to noise ratio : where it was necessary to average 30 to 100 curves to get a signal, a single measurement is enough in this configuration (see fig.5.6).

5.3 Model of the resonator close to a resonance

Around resonance, the properties of the resonator can be well approximated by those of a parallel *RLC* oscillator. In the following we discuss the importance of the coupling between the resonator and the generator. Then we determine its reflection coefficient at resonance. Finally we describe how we obtain a physically meaningful quantity, the susceptibility, from this coefficient.

Different resonator/generator coupling regimes

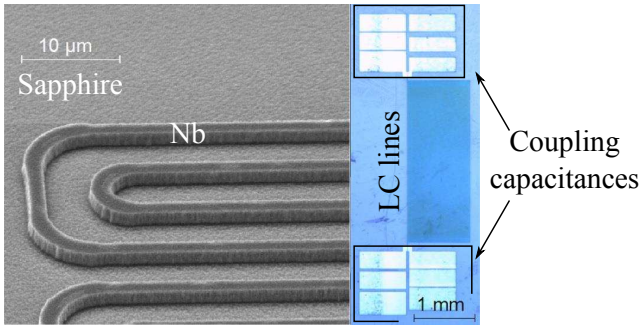

Figure 5.7: **Left:** Close-up view of the Nb lines which are a distributed LC circuit. **Right:** Overview of the resonator with its coupling capacitance. There are three contact pads at each end of the lines to choose the coupling strength.

If the resonator were directly connected to the generator, its quality factor would be greatly reduced since the losses of the circuit would be no more due to the one of the resonator alone but also to the one of the generator [107]. To preserve the quality factor of the resonator, a coupling capacitance C_K is inserted between the resonator and the generator. Its value is small compared to the resonator's capacitance: $C_K \ll C$. This coupling however slightly modifies the resonator's intrinsic resonance as shown in the following.

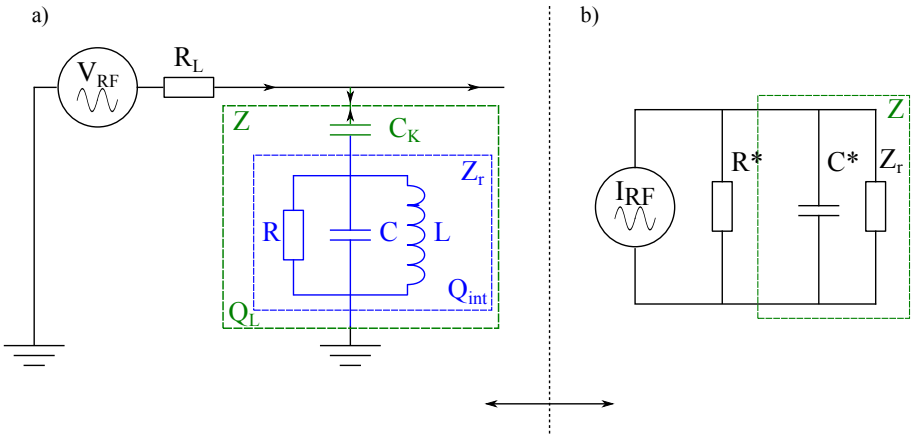

Figure 5.8: Circuit equivalent to the resonator using **a)** Thévenin convention and **b)** Norton convention.

The resonator can be described as a parallel RLC circuit of impedance Z_r connected to a high-frequency generator via a coupling capacitor C_K (see fig.5.8). The impedance of the resonator Z_r reads :

$$Z_r = \frac{RL^2\omega^2 + iR^2L\omega(1 - LC\omega^2)}{L^2\omega^2 + R^2(1 - LC\omega^2)} \tag{5.1}$$

At resonance, $Im(Z_r) = 0$, thus the resonance frequency is :

$$\omega_n = \frac{1}{\sqrt{LC}} \tag{5.2}$$

and the quality factor is

$$Q_{int} = R\sqrt{\frac{C}{L}} = RC\omega_n \gg 1 \tag{5.3}$$

Close to the resonance, the real part of the resonator's impedance has a lorentzian shape:

$$Re(Z_r) = \frac{R}{1 + 4Q_{int}^2(\frac{\omega-\omega_n}{\omega_n})^2} \tag{5.4}$$

Taking into account the coupling capacitance, the impedance is :

$$Z = \frac{1}{iC_K\omega} + Z_r \tag{5.5}$$

Using Norton convention, it can be shown that, for $Q_{int} \gg 1$, the resonance frequency and the quality factor become :

$$\omega_n^* = \frac{1}{\sqrt{L(C + C^*)}} \simeq \omega_n \tag{5.6}$$

and

$$Q_L = \frac{\omega_n C}{\frac{1}{R} + \frac{1}{R^*}} \tag{5.7}$$

where

$$R^* = \frac{1+\omega_n^2 C_K^2 R_L^2}{\omega_n^2 C_K^2 R_L} \tag{5.8}$$

$$C^* = \frac{C_K}{1+\omega_n^2 C_K^2 R_L^2} \tag{5.9}$$

The quality factor of the connected circuit Q_L thus depends on the coupling

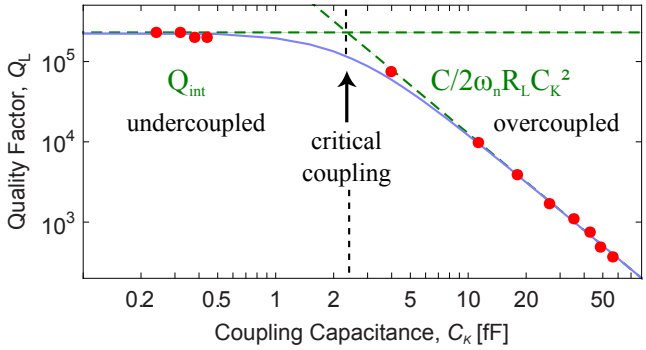

Figure 5.9: Dependence of the connected resonator quality factor Q_L on the coupling capacitance C_K. Data points are measured quality factors. These values are compared to predictions by a RLC model (solid). Dashed line in the over-coupled regime is $C/2\omega_n R_L C_K^2$, in the under-coupled regime it is $RC\omega_n$. After [108].

capacitance C_K. Defining $Q_{ext} = R^* C \omega_n$ as the quality factor of the environment, we have:

$$\frac{1}{Q_L} = \frac{1}{Q_{int}} + \frac{1}{Q_{ext}} \tag{5.10}$$

As shown in fig.5.9, the quality factor of the connected resonator is governed by the intrinsic quality factor for small coupling up to a critical coupling given by:

$$R R_L \omega_n^2 C_K^2 = 1 \tag{5.11}$$

At larger coupling, the quality factor is dominated by the one of the external circuit. On the contrary, we often prefer to work in the under-coupled regime to preserve the quality factor of the resonator. We therefore drop the subscripts in the following and denote the quality factor of the connected resonator Q which is equal to the intrinsic quality factor. We measure quality factors of the order of $Q \sim 5\,10^4$.

Quantities measured: frequency shift and inverse quality factor change

The physical quantity of interest, the magnetic susceptibility χ, can be seen as a phase-dependent inverse complex inductance. What is its impact on the resonator?

The total inductance of the system made of the resonator and the NS ring is $L_T = L_r + L$. As shown in fig.5.10, we define L_r as the inductance of the

resonator, L_c is the coupling inductance (i.e. the part of the ring in parallel with the SNS junction), $\chi(\varphi) = 1/L_{sns}(\varphi)$ is the phase-dependent inverse complex inductance of the SNS junction and L_N its geometric inductance. The phase-dependent inductance of the loop L is given by

$$\frac{1}{L} = \frac{1}{L_c} + \frac{1}{L_N + 1/\chi} \tag{5.12}$$

where χ is the only phase-dependent variable.

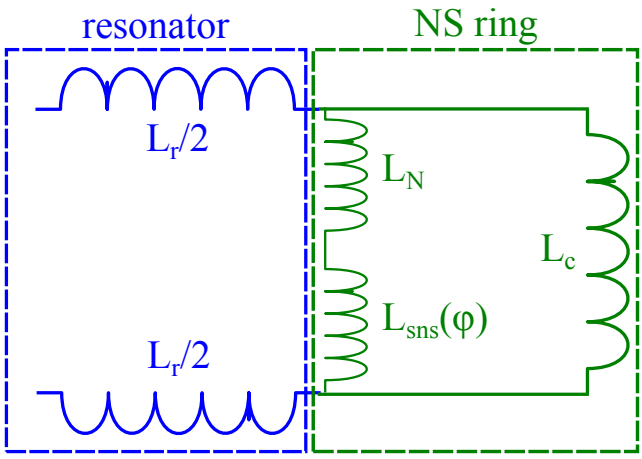

Figure 5.10: Circuit used to calculate the inductance change with the phase.

The relative variation of inductance with the phase δL is due to the branch including the SNS junction:

$$\delta L = L_T - (L_r + L_c) \tag{5.13}$$

since $L_r + L_c$ is the inductance of the circuit when the SNS junction is absent. This yields

$$\delta L = -\frac{L_c^2 \chi}{1 + L_l \chi} \tag{5.14}$$

where $L_l = L_N + L_c$ is the geometric inductance of the isolated loop. δL reads, writing explicitly $\chi = \chi' + i\chi"$ as a complex number,

$$\frac{\delta L}{L_c^2} = \frac{\chi' - L_l(\chi'^2 + \chi"^2)}{(1 - L_l\chi")^2 + (L_l\chi")^2} + i\frac{\chi"}{(1 - L_l\chi")^2 + (L_l\chi")^2} \tag{5.15}$$

In the case where $L_l\chi \ll 1$, eq.5.15 reduces to $\frac{\delta L}{L_c^2} = \chi' + i\chi"$. As shown in the following, in-phase $\delta L'$ and out-of-phase $\delta L''$ variations of L are related to characteristics of the resonance : its quality factor Q and resonance frequency ω_n. Measuring them thus yields χ.

The modification of the resonance by the ring is easier to describe with a resonator modeled by a RLC circuit where the losses are described by a small resistance r in series with the inductance. The resonance frequency of the circuit is $\omega_n = 1/\sqrt{L_r C}$ and its quality factor is $Q = \frac{L_r \omega_n}{r}$. An in-phase

variation of inductance $\delta L'$ amounts to a resonance frequency change $\delta\omega_n$ such that :

$$\frac{\delta L'}{L_r} = -2\frac{\delta\omega_n}{\omega_n} \tag{5.16}$$

while an out-of-phase variation of inductance $\delta L''$ amounts to adding a resistance $\delta r = \omega_n \delta L''$ in series. The variation of the inverse quality factor is:

$$\delta(\frac{1}{Q}) = \frac{\delta r}{L_r\omega_n} - \frac{r\delta L'}{L_r^2\omega_n} - \frac{r\delta\omega_n}{L_r\omega_n^2} \tag{5.17}$$

Using that $\omega_n = 1/\sqrt{L_r C}$ and $Q = \frac{L_r\omega_n}{r}$ we find:

$$\delta(\frac{1}{Q}) = \frac{\delta L''}{L_r} - \frac{1}{2Q}\frac{\delta L'}{L_r} \tag{5.18}$$

The last term of this equation can be neglected since $Q \sim 10^4$ and $\delta L'' \sim \delta L'$. Finally, the variations of the inverse of the quality factor can be related to an out-of-phase variation of the inductance:

$$\delta(\frac{1}{Q}) = \frac{\delta L''}{L_r} \tag{5.19}$$

To sum up, we have shown that in-phase $\chi'$and out-of-phase χ"variations of the susceptibility are related to variations of the resonator's eigenmodes by:

$$-2\frac{\delta f}{f} = \frac{\delta L'}{L_r} = \frac{L_c^2}{L_r}\frac{\chi' - L_c(\chi'^2 + \chi"^2)}{(1 - L_c\chi")^2 + (L_c\chi")^2} \tag{5.20}$$

$$\delta(\frac{1}{Q}) = \frac{\delta L''}{L_r} = \frac{L_c^2}{L_r}\frac{\chi"}{(1 - L_c\chi")^2 + (L_c\chi")^2} \tag{5.21}$$

which simplify to:

$$-2\frac{\delta f}{f} = \frac{L_c^2}{L_r}\chi' \tag{5.22}$$

$$\delta(\frac{1}{Q}) = \frac{L_c^2}{L_r}\chi" \tag{5.23}$$

when $L_l\chi \ll 1$.

These equations show that the susceptibility can be accessed by measuring the variations of resonance frequency and quality factor. Left the question of how to measure these variations.

Resonance frequency detection

As previously described, the resonance is a Lorentzian whose resonance frequency ω_n and quality factor Q depends on the applied magnetic flux. Measuring these variations yields the in-phase $\chi'$and out-of-phase χ"susceptibility.

In this section we describe the setup used to detect the variations of the eigenmodes of the resonator due to the dc flux threading the loop embedded in the resonator. It is sketched in fig.5.11. The signal reflected by the resonator

is measured while keeping the excitation frequency equal to the resonance frequency thanks to a feedback loop. A high frequency generator provides excitation V_g at frequency $\frac{\omega_n}{2\pi}$ modulated at frequency $\frac{\omega_f}{2\pi}$ with an amplitude $\frac{\omega_m}{2\pi}$:

$$V_g = Ve^{i\left[\omega_n t + \frac{\omega_m}{\omega_f}\sin(\omega_f t)\right]} \tag{5.24}$$

ω_n is set at the resonance frequency of the resonator. Excitation is split such as half the power is sent toward the resonator whereas the other half is sent toward a phase shifter. Before entering the resonator, the signal's amplitude is reduced so that experiment is carried in a linear regime. Reflected signal is then amplified and finally multiplied by the reference signal which has been phase-shifted to cancel the phase difference between the two signals. The first two harmonics of the resulting signal are measured by lock-ins working at modulation frequency ω_f and twice the modulation frequency. First harmonic signal is zero at resonance and changes sign when crossing the resonance. This allows to implement a feedback loop with a proportional-integrator-derivative system which lock the generator to the resonance frequency. Measuring the correction voltage thus yields the deviation from resonance δf. Second harmonic signal roughly amounts to measuring the curvature of the resonance which is proportional to the square of the quality factor. However the amplitude of the signal depends on the ratio between the resonance width and the modulation amplitude $\frac{\omega_m Q}{\omega_n}$ and so calibration is necessary as detailed in the following.

Calibration of the dissipative response

We first introduce the principle of the measurement in the ideal case of an infinitely small modulation then we detail the way we have calibrated the dissipative response in the case of a finite amplitude modulation.

Principle of the measurement: ideal case of an infinitely small modulation

We detail in the following the principle of the experiment by considering the effect of a frequency modulation of amplitude much smaller than the width of the resonance. We write the expression of the voltage after: a) reflection by the resonator coupled to the circuit by a capacitance, b)after the phase shifter and c)after the mixer. Finally the signal is written in d).

a) Reflected voltage

The voltage reflected by the resonator is

$$V_r(t) = V\Gamma(\omega)e^{i\left[\omega_n t + \frac{\omega_m}{\omega_f}\sin(\omega_f t)\right]} \tag{5.25}$$

where $\Gamma(\omega)$ is the reflexion coefficient. It is defined by:

$$\Gamma(\omega) = \frac{Z(\omega) - R_L}{Z(\omega) + R_L} \tag{5.26}$$

with Z the impedance of the resonator and the coupling capacitance and $R_L = 50\Omega$ is the characteristic impedance of the coaxial cables. When the coupling between the resonator and the generator is optimum there is no reflected power

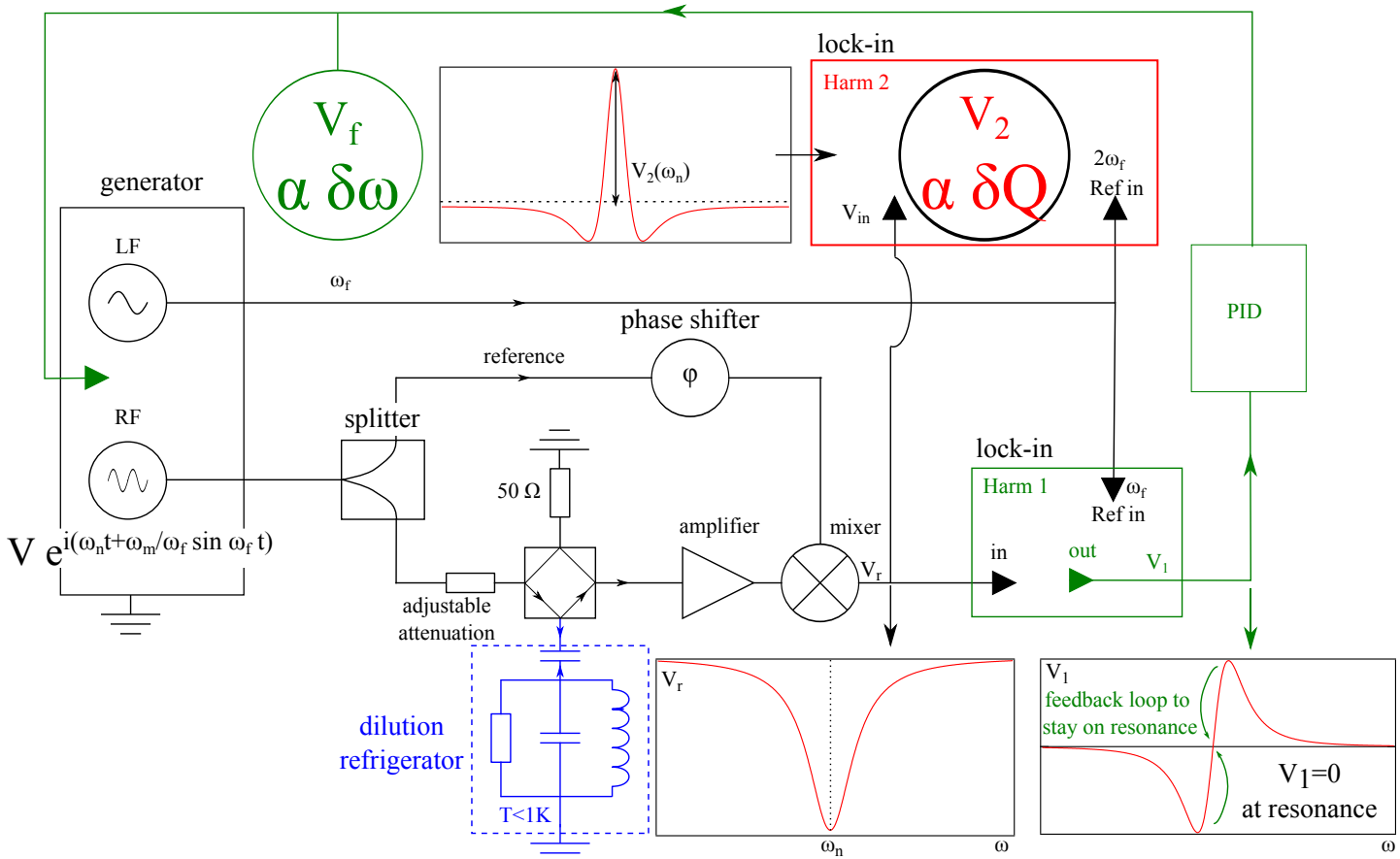

Figure 5.11: Detection setup: A microwave signal locked to the resonance frequency of the sample is split in two half, one half being a reference signal, the other half is sent toward the sample at low temperature (blue). After amplification at room temperature, the signal reflected by the sample is mixed with the reference signal with the phase difference between the reference and the reflected signal corrected thanks to a phase shifter. The reflected signal has a lorentzian shape. Its first harmonic, V_1, is measured by a first lock-in (green) while the second harmonic,V_2, is detected by another lock-in (red). Since V_1 is zero only at resonance, it is used to implement a feedback loop to lock the microwave generator at resonance frequency. The correction signal, V_f, is measured by a voltmeter. V_2 measures a voltage proportional to the quality factor. This setup thus allows to detect the variations of the eigenmodes a resonator.

and then $Z = 50\Omega$. We however often work in the under-coupled limit to preserve the quality factor of the resonator. In this limit we have

$$RR_L C_K^2 \omega^2 \ll 1 \tag{5.27}$$

and

$$Re(Z(\omega)) \gg R_L \tag{5.28}$$

Then the reflexion coefficient is equal to unity far from the resonance and has a lorentzian shape close to the resonance. Close to the resonance it reads:

$$\Gamma \sim 1 - R_L/Z \tag{5.29}$$

and its amplitude at resonance is proportional to the quality factor Q of the resonator. At resonance the reflection coefficient reads:

$$\Gamma(\omega_n^*) = 1 - 2\frac{C_K^2 \omega_n^*}{C} Q \tag{5.30}$$

where ω_n^* is the resonance frequency, C_K the coupling capacitance and C the capacitance as defined in the parallel RLC model described in sec.5.3.

b) Reference voltage

As just described, half of the excitation is sent toward the sample while the second half is sent toward a phase shifter. This part of the excitation is used as a reference signal.

c) Voltage at the output of the mixer

The mixer realizes the product of the reflected signal by the reference. If we write the reference voltage as $V_0 e^{i\omega t+\delta}$ and the reflected voltage as $V_1 e^{i\omega t+\delta'}$, with $V_1 = V_1' + iV_1''$ complex, their product reads:

$$V_m = Re(V_0 e^{i\omega t+\delta})\, Re(V_1 e^{i\omega t+\delta'}) \tag{5.31}$$

$$\begin{aligned} V_m = &\frac{1}{2} V_0 V_1' \left(\cos(2\omega t + \delta + \delta') + \cos(\delta - \delta')\right) \\ &-\frac{1}{2} V_0 V_1'' \left(\sin(2\omega t + \delta + \delta') - \sin(\delta - \delta')\right) \end{aligned} \tag{5.32}$$

The phase of the reference, δ, is then adjusted manually such as the dc output is maximized i.e. when the reference and the reflected signal are in-phase ($\delta = \delta'$). The high frequency part of the output is subsequently filtered using a low-pass filter.

d) Signal

After high frequency filtering at the output of the mixer, the signal reads

$$V_m = \frac{1}{2} V^2 \Gamma'(\omega) \tag{5.33}$$

where $\Gamma'(\omega) = Re(\Gamma(\omega))$ is modulated at frequency ω_f with a small amplitude ω_m. The signal can be expanded into

$$V_m = V^2 \left[\Gamma'(\omega_n) + \frac{\partial \Gamma'(\omega_n)}{\partial \omega} \omega_m \cos\omega_f t + \frac{\partial^2 \Gamma'(\omega_n)}{\partial \omega^2} (\omega_m \cos\omega_f t)^2\right] \tag{5.34}$$

for small amplitudes of modulation. In the ideal case of an infinitely small amplitude of modulation, the second harmonic voltage at resonance $V_2(\omega_n)$ is proportional to the cube of the quality factor and thus the change of the inverse quality factor $\delta(1/Q) = -\delta Q/Q^2$ can be accessed by measuring $V_2 = V_2(\varphi = 0)$ at resonance and its phase dependent change $\delta V_2(\varphi) = V_2(\varphi) - V_2$. The relation between these two quantities reads:

$$\frac{\delta V_2(\varphi)}{V_2} = -3Q\ \delta(\frac{1}{Q(\varphi)}) \tag{5.35}$$

which is related to the dissipative response by eq.5.23. The dissipative response is then accessed by measuring the second harmonic voltage of the reflection coefficient of the resonator. The relation between V_2 and $\delta 1/Q$ is however not as simple as eq.5.35 in the case of a frequency modulation of finite amplitude. A hand-waving explanation would be the following: the second-harmonic voltage is equivalent to the second-derivative with respect to the frequency of the resonance but with a finite frequency step. Therefore, the larger the step, the more different from the exact differentiation. Fig.5.12 shows that when the amplitude of modulation is increased, the measured second-harmonic voltage at resonance decreases.

Real case: modulation amplitude of the order of the resonance's width

Close to the resonance, the amplitude of the reflected signal $A(\omega, \varphi, t)$ after multiplication by the reference in the mixer and for $\omega_f \ll \omega_n/Q$ reads:

$$A(\omega, \varphi, t) \propto \frac{Q(\varphi)}{1 + (Q(\varphi)\frac{\omega_m}{\omega_n}\cos\omega_f t)^2} \tag{5.36}$$

where $\omega = \omega_n + \omega_m \cos\omega_f t$ is the instantaneous frequency. It is a Lorentzian with an amplitude proportional to Q and a width given by $\frac{Q\omega_m}{\omega_n}$. The LI used to measure Q is working at $2\omega_f$; it thus measures the second harmonic, A_2, of $A(\omega, \varphi)$. A_2 depends on the ratio $\frac{Q\omega_m}{\omega_n}$; therefore, when φ varies, Q changes and so does $A_2(\omega, \varphi)$. To calibrate this effect, we recast A_2 as:

$$A_2(\varphi, Q) \propto Q(\varphi) H_2(Q(\varphi)\frac{\omega_m}{\omega_n}) \tag{5.37}$$

where $H_2(Q(\varphi)\frac{\omega_m}{\omega_n})$ accounts for the dependence on the modulation amplitude. To determine the variation of H_2 with $\frac{\omega_m Q}{\omega_n}$, the second harmonic voltage of a resonator has been measured at 4 K with varying $\frac{\omega_m Q}{\omega_n}$ for several frequencies. More precisely, it is the modulation amplitude ω_m which is varied, ω_n and Q being fixed and measured separately. As shown in fig.5.12, it is independent of frequency when normalized to its maximum. From this second harmonic voltage one can precisely measure the function H_2 and therefore the modulation dependent exponent β defined as:

$$\beta = \frac{d \ln H_2}{dQ} \tag{5.38}$$

If now we consider phase biased experiments, the quality factor changes the measured voltage in two ways: first, by the amplitude of the resonance that

is directly proportional to the quality factor; secondly by the amplitude of H_2 that depends on the ratio $\frac{\omega_m Q}{\omega_n}$. We found that $\alpha = \beta + 1$ decreases between 3 at small $\frac{\omega_m Q}{\omega_n}$ to 1 when $\frac{\omega_m Q}{\omega_n} = 1$. Its dependence is plotted in fig.5.12.

Finally, the relation between the voltage of the second harmonic $V_2(\varphi)$ and $\delta(\frac{1}{Q})$ reads:

$$\delta(\frac{1}{Q(\varphi)}) = -\frac{1}{\alpha(\omega_m Q/\omega_n)}\frac{1}{Q}\frac{V_2(\varphi) - V_2(\varphi = 0)}{V_2(\varphi = 0)} \tag{5.39}$$

It can be seen from eq.5.39 that we need to independently measure Q at $\varphi = 0$ with a network analyzer to determine the phase dependence of $\delta(\frac{1}{Q(\varphi)})$.

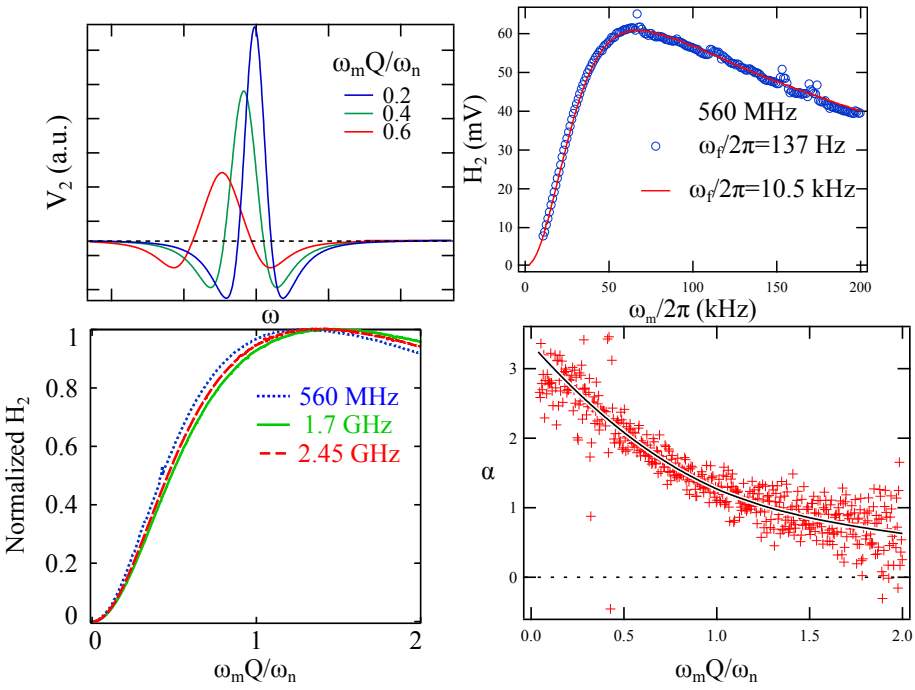

Figure 5.12: **Top left:** Numerical second-derivative of the resonance for several amplitude of modulation.**Top right:** H_2 for $\frac{\omega_f}{2\pi} = 137Hz$ (circles) and $\frac{\omega_f}{2\pi} = 10.5kHz$ (solid line) at $560MHz$. **Bottom left:** Normalized H_2 vs $\frac{\omega_m Q}{\omega_n}$ at $T = 4K$ for three different frequencies. **Bottom right:** the power α relating the measured voltage and the quality factor depends on the amplitude of modulation.

5.4 Data treatment

Before analyzing the evolution of the susceptibility with phase, temperature and frequency, a translation from the measured voltages into quantities that have a physical meaning is necessary.

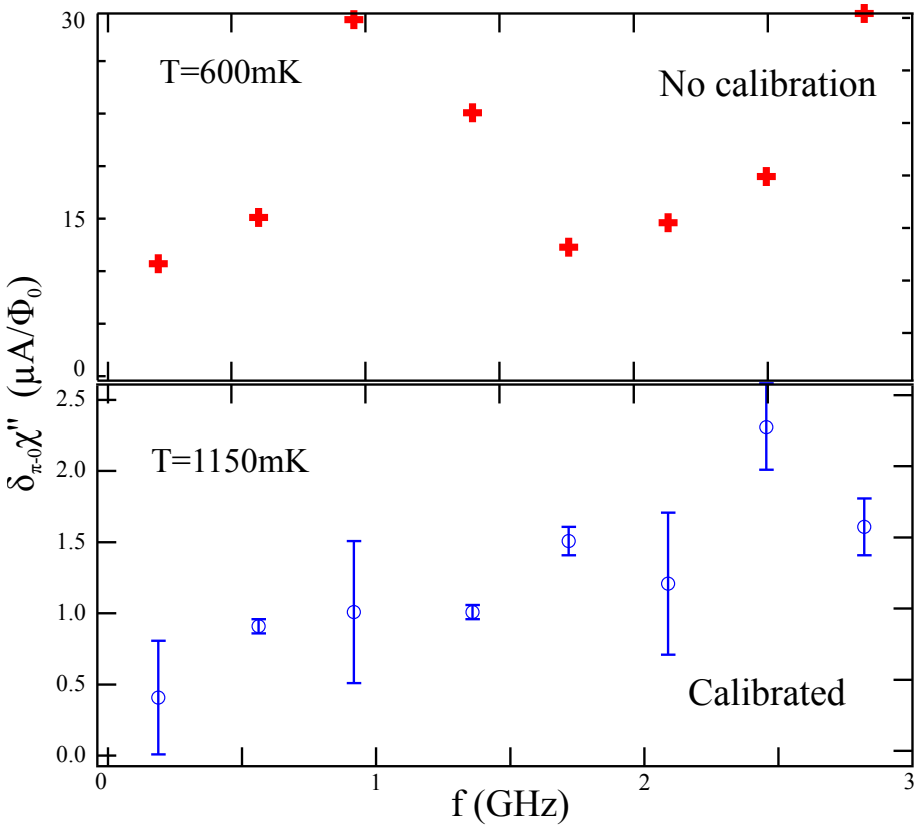

Figure 5.13: **Top:** If the effect of finite frequency modulation is not taken into account, signal amplitude depends on the ratio $\frac{\omega_m Q}{\omega_n}$ and the frequency dependence of χ"is non monotonous whereas a linear dependence is expected. This is the case taking calibration into account (**Bottom**)

From δf and $\delta(Q^{-1})$ to χ' and χ''

In the general case, we have established in eqs. 5.20 and 5.21 relations between δf, $\delta(Q^{-1})$, $\chi'$and χ". Defining F_v and Q_v as :

$$F_v = -2\frac{\delta f}{f}\frac{L_r}{L_c^2} \tag{5.40}$$

$$Q_v = \delta(\frac{1}{Q})\frac{L_r}{L_c^2} \tag{5.41}$$

eqs. 5.20 and 5.21 can be inverted into :

$$\chi' = \frac{F_v + L_l(F_v^2 + Q_v^2)}{(1 + L_l F_v)^2 + (L_l Q_v)^2} \tag{5.42}$$

$$\chi'' = \frac{Q_v}{(1 + L_l F_v)^2 + (L_l Q_v)^2} \tag{5.43}$$

To determine F_v and Q_v and so $\chi'$and χ"it is necessary to determine the coupling inductance. It is given by the inductance of the superconducting

wire in parallel with the normal wire. Its geometrical value is calculated using the following formula, describing the self-inductance of a rectangular ring with sides a and b of wire radius r[109]:

$$L_c = \frac{\mu_0}{2\pi}\left[2a\ln(\frac{2a}{r}) + 2b\ln(\frac{2b}{r}) - 4(a+b) + 4\sqrt{a^2+b^2} - 2a\sinh^{-1}(\frac{a}{b}) - 2b\sinh^{-1}(\frac{b}{a})\right] \tag{5.44}$$

For instance, an inductance of

$$L_c = 9pH \tag{5.45}$$

is found for the sample labeled PdNbAu with $a = 4\mu m$, $b = 5\mu m$, $r = 0.3\mu m$. The normal wire's inductance is negligible and we have considered that the loop's inductance is equal to the coupling inductance: $L_l \simeq L_c$.

Choice of the offset position

The error signal and the amplitude of the 2^{nd} harmonic have to be translated into respectively a frequency shift and a quality factor change. These signals are only relative phase-dependent variations and not absolute so there is an offset to be determined. To do so, we assume that the frequency shift is such that its integral between 0 and 2π vanishes since the current-phase relation is centered around 0. Indeed in the adiabatic regime χ'measures the phase derivative of the supercurrent. We also assume that

$$\delta Q^{-1}(\varphi = 0) = 0 \tag{5.46}$$

because we estimated that dissipation should be the smallest at $\varphi = 0$ when the amplitude of the minigap if the largest in the regime $\hbar\omega, k_BT \ll E_g(\varphi = 0)$, the dissipation has to be zero at $\varphi = 0$).

This choice of the offset position is important only when the condition $L_l\chi \ll 1$ is not met and there is mixing between the in-phase and out-of-phase signals. This mainly happens at low temperature and we have chosen to exploit the data only where these corrections remain small.

Flux rescaling due to flux screening

Lastly, the screening of the magnetic field by the ring has to be taken into account : the effective flux experienced by the ring Φ_{int} is different from the applied flux Φ_{ext}. The relation between the two reads :

$$\Phi_{int} = \Phi_{ext} + L_l I_J(\Phi_{int}) \tag{5.47}$$

where L_l is the loop's inductance and I_J its supercurrent. When the current-phase relation is sinusoidal, $I_J = -I_c \sin\frac{2\pi\Phi_{int}}{\Phi_0}$, eq.5.47 becomes :

$$\Phi_{ext} = \Phi_{int} + L_l I_c \sin(\frac{2\pi\Phi_{int}}{\Phi_0}) \tag{5.48}$$

This leads to a rescaling of the phase. It is important only at low temperature when the term

$$\beta = \frac{2\pi L_l I_c}{\Phi_0} \tag{5.49}$$

grows closer to 1 i.e. once the Josephson inductance is greater than the geometrical inductance, a hysteretic behavior appears. As shown in fig.5.14, when $\beta \geq 1$ the function $\Phi_{int}(\Phi_{ext})$ is no more single valued for Φ_{ext} close to odd multiples of Φ_0 and hysteresis appears. For the PdNbAu loop studied, hysteresis showed up at $T \lesssim T_H = 390mK$. At this temperature the critical current is about $35\mu A$ which is consistent with the geometrical value of the inductance $L_l = 9pH$.

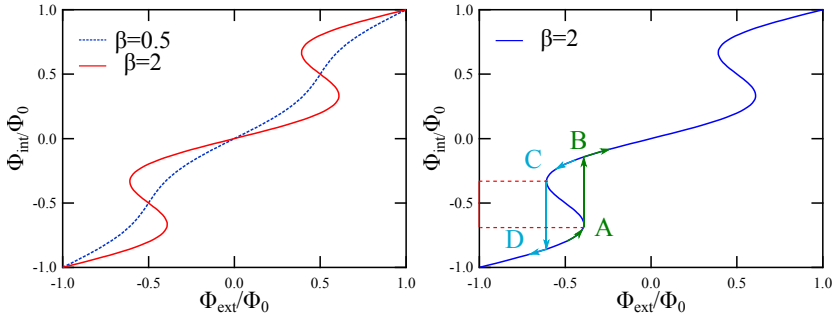

Figure 5.14: **Left:** Dependence of the internal flux on the external flux for $\beta = 0.5$ and $\beta = 2$. Hysteresis appears when the internal flux is not uniquely defined at a given value of the external flux. **Right:** Internal flux vs. external flux for $\beta = 2$. When increasing the external flux, the internal flux follows up to A, where it jumps to B. Decreasing the external flux, the internal flux only jumps back to D in C, creating an hysteresis cycle. The red lines mark the internal flux range not accessible.

At larger temperature, flux screening leads to a rescaling of our data. To take it into account, one has to determine the critical current temperature dependence and the inductance of the NS ring. We determined the temperature dependence of the critical current by making a control sample consisting of a SNS junction with similar characteristics and done in the same batch as the NS ring. This is detailed in the following. An alternative would be to perform

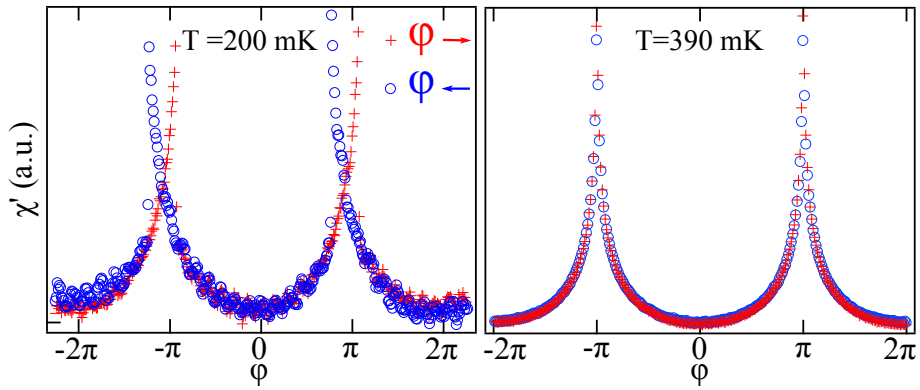

Figure 5.15: **Left:** Response at f=1.7 GHz and T=200 mK. At this temperature the critical current is so large that a hysteretic behavior is observed. **Right:** Hysteresis disappears at temperature larger than $390mK$.

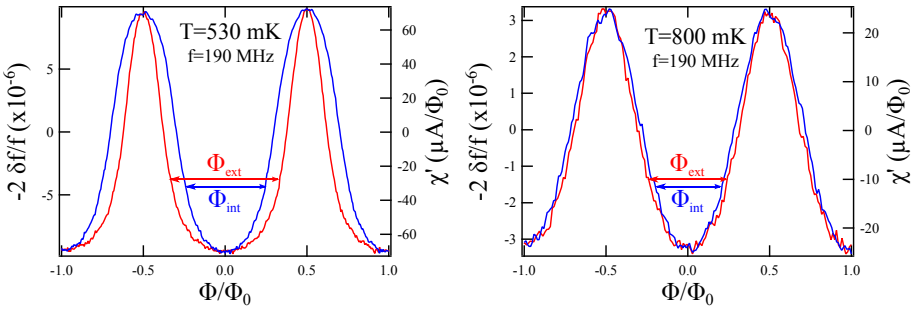

Figure 5.16: Non-dissipative response vs. the applied flux Φ_{ext} (red) and the internal flux Φ_{int} (blue) at $f = 190MHz$ and **Left:** T=530mK and **Right:** T=800 mK

a first set of experiments in a junction geometry and subsequently transform it into a loop so that phase-biased experiment are possible. Lastly, we confirmed experimentally that the amplitude of χ' in the adiabatic regime is $4\pi I_c/\Phi_0$ (see chap. 6), therefore if one is confident enough in the calibration of the amplitude of χ', it could be used to determine the rescaling of the flux.

To determine the inductance of the loop, one can first consider its geometric inductance which is of the order of $1\mu H/\mu m$ for such wires. If the ring displays a hysteretic behavior below a temperature T_H and the value of the critical current at this temperature is known, the inductance can be determined using:

$$\beta(T_H) = \frac{2\pi L_l I_c(T_H)}{\Phi_0} = 1 \tag{5.50}$$

Lastly, it is important to note that screening is negligible only at temperature large compare to the one where hysteresis appears; close to the hysteresis the internal flux notably differs from the applied one. As a consequence, the phase dependence of χ' seems more peaked around π when the screening of the flux is not taken into account, as shown, for instance, in fig. 5.16 for sample PdNbAu.

5.5 Characterization of the setup

In this section we introduce the various preliminary results that are necessary to analyze the signal measured in the ac experiment introduced in chap. 6.

Quality factor measurement

The reflexion coefficient of each resonance is measured thanks to a network analyzer. The quality factor is obtained by fitting the resonance with a Lorentzian curve (see fig.5.17). It is about 50000 at low frequency and 10000 at high frequency.

Verification of the linearity

It is crucial to check that experiments are carried out in a linear regime. To do so, we check as in fig.5.18 that the signal does not depends on the applied

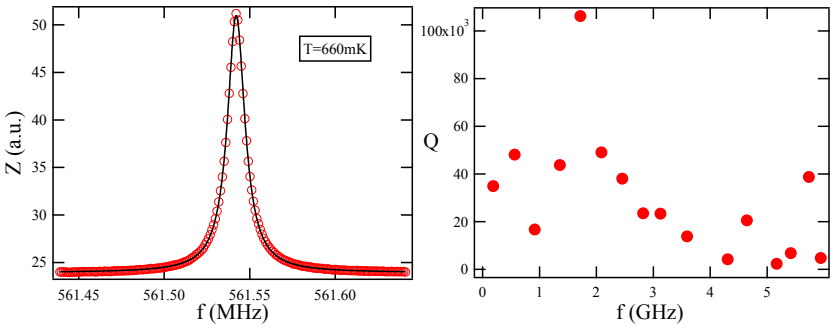

Figure 5.17: **Left:** Resonance close to 560 MHz at 660 mK with P=-90dBm (symbols). The resonance's width and so its quality factor is given by a lorentzian fit (solid line). **Right:** Quality factor for frequencies up to 6 GHz (upper limit of the network analyser).

power. The typical power applied to the resonator is $P = 5pW$, the amplitude

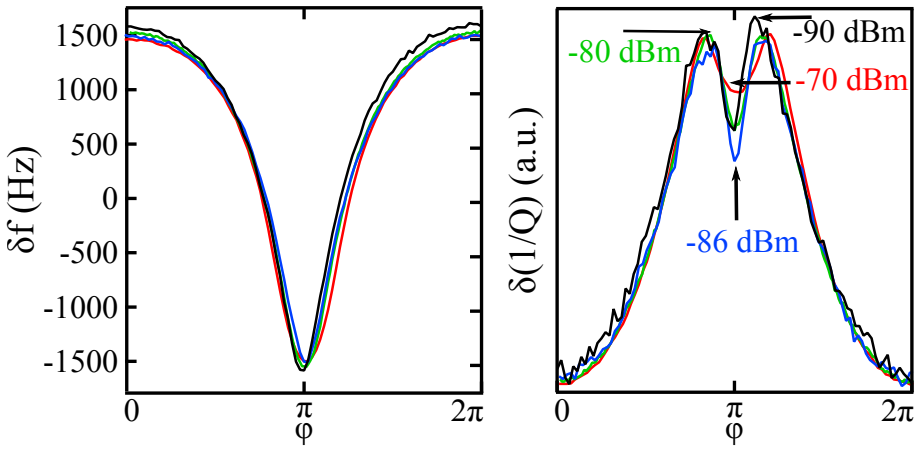

Figure 5.18: Signal at T=700 mK , $f = 560\ MHz$ and several probe powers. In linear regime, response does not depend on power at a given T and ω. The indicated powers do not take into account possible attenuation by the lines.

of the flux modulation $\delta\Phi$ can be estimated by calculating the current in the resonator I_r since $\delta\Phi = L_c I_r$, where L_c is the coupling inductance. I_r can be estimated thanks to the quality factor definition : Q is the ratio between the stored energy $L_r I_r^2$ and P/ω, the energy dissipated in a time $1/\omega$. Assuming there is a perfect coupling between the resonator and the generator (it is not the case since we prefer to be under-coupled to preserve the quality factor), this yields :

$$I_r = \sqrt{\frac{PQ}{L_r \omega}} \sim 10^{-5} A \tag{5.51}$$

and so, with $Q = 5.10^4$, $L_r = 1.5.10^{-7} H$ and $L_c \sim 10pH$, we find $\delta\Phi = 10^{-2}\Phi_0$ which is consistent with the fact that we are doing experiments in the linear regime.

The power dissipated in the ring can also be estimated: a small variation δQ of the quality factor correspond to a dissipated power δP such as :

$$\delta P = L_r I_r^2 \omega \frac{\delta Q}{Q^2} \tag{5.52}$$

Using $I_r \sim 10\mu A$, $L_r \sim 10^{-7}H$, $\omega \sim 10^{-10} rad.s^{-1}$ and that the variation of the inverse of the quality factor $\delta Q/Q^2$ is typically $\delta Q/Q^2 \sim 10^{-7}$, we find that the power dissipated in the ring is of the order of:

$$\delta P \sim 10 fW \tag{5.53}$$

DC characterization of PdNb/Au junctions

In order to characterize SNS junctions made of PdNb and Au, the temperature and magnetic field dependence of the critical current have been performed. The presence of fractional Shapiro steps have also been observed.

Critical current's magnetic field dependence

When a magnetic field is applied perpendicular to the plane of a SNS junction, a decrease of the critical current is observed. The magnetic field dependence

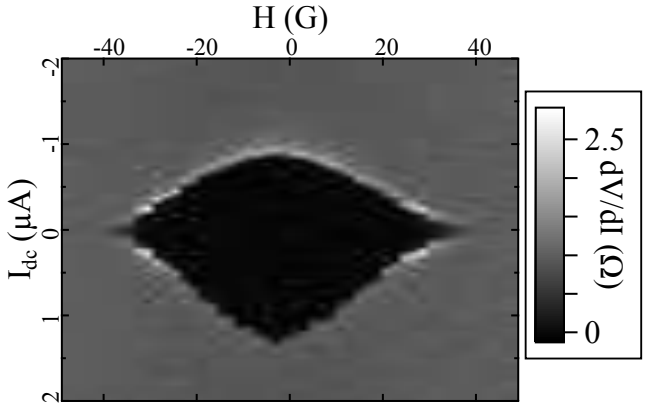

Figure 5.19: Magnetic field dependence of the differential resistance at $T = 60mK$ for sample NL2. A flux quantum through the wire amounts to a field $H_0 = 70G$

depends on the geometry of the junction : if it is 2D, a Fraunhoffer pattern is observed whereas it is a gaussian decay in 1D. This drop of the critical current is related to the pair-breaking effect of the magnetic field and can be accounted for analytically in 1D junction[110] and numerically for a junction of arbitrary shape[111]. In a 1D junction, the critical current vanishes for a flux of about $4\Phi_0$ through the N part of the junction.

In the experimental field dependence of sample NL2 shown in fig.5.19, the critical current decreases very quickly, for fields apparently smaller than Φ_0. This is due to flux focusing by the huge Nb contacts between which the junction is inserted. The magnetic field experienced by the junction is in fact about 7 times larger than the applied field.

Microwave irradiation of a PdNb/Au junction

Sharp dips are observed in the differential resistance characteristic of a junction irradiated by microwaves (see fig.5.20). They correspond to steps in the current-voltage characteristic called Shapiro steps [112]. They are due to beatings of the irradiation at frequency ω_r with the ac current oscillating at frequency $\omega_J = \frac{2eV}{\hbar}$ when the junction is biased with a voltage V. They reflect the harmonic contents of the current-phase relation, albeit out-of-equilibrium: for the harmonic n of the current-phase relation, there is a Shapiro step at voltage $V = \frac{1}{n}\frac{\hbar\omega_r}{2e}$. Fractional Shapiro steps have been observed in SNS junctions [17, 18], at temperatures where the current-phase relation is purely sinusoidal. It has been shown in [113] that this higher harmonic contents does not stem from multiple Andreev reflections. The fractional Shapiro steps can be interpreted by out-of-equilibrium effects; it has been shown indeed that microwave irradiation modifies the harmonic contents of the current-phase relation [80].

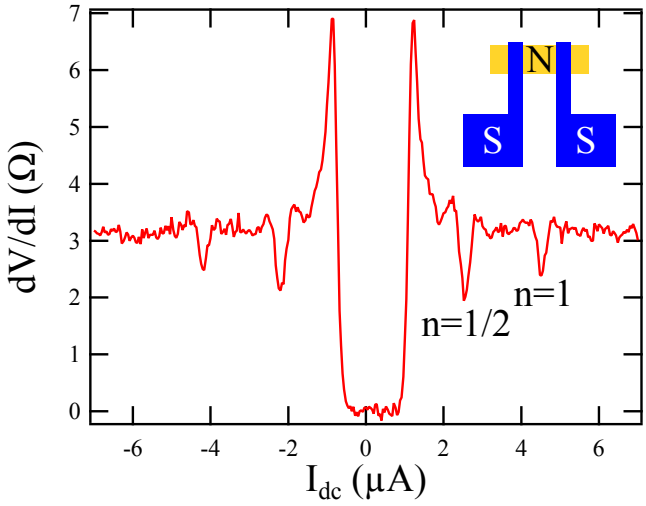

Figure 5.20: Differential resistance of sample NL2 at $T = 60mK$ under microwave irradiation at $f = 6.2GHz$, $P = 35dB$. Note the presence of a fractional dip (n=1/2) larger than the integer one (n=1).

We also observed fractional Shapiro steps (fraction n=1/2) in a test junction made of a 6nm/100nm thick Pd/Nb bilayer connecting a gold wire (see fig.5.20). Interestingly, the $n = 1/2$ dip is deeper than the $n = 1$ dip, indicating an out-of-equilibrium current-phase relation dominated by its second harmonic.

Critical current's temperature dependence

Before doing ac experiments, differential resistance experiments have been carried out to measure the temperature dependence of the critical current and so the Thouless energy of PdNb/Au junctions of given length, width and thickness. These experiments have been done for two batches. The first batch (samples d2 and g3) served as a benchmark to determine the reproducibility of the amplitude of the critical current and of the Thouless energy of PdNb-Au junctions. The second batch (sample 1f) has been co-evaporated with the NS

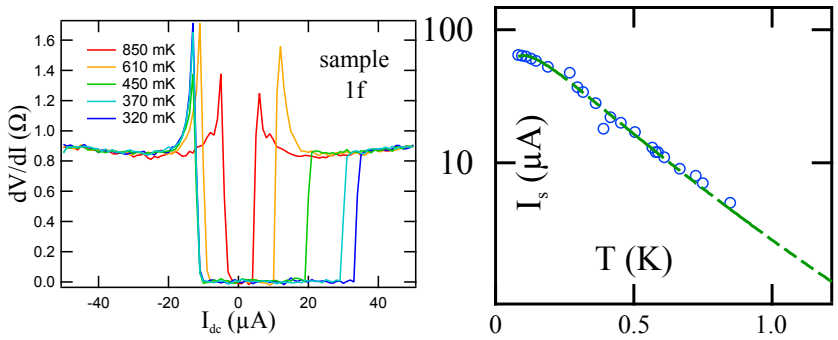

Figure 5.21: **Left:** Differential resistance of the test sample labeled 1f (see table 5.1) at several temperatures. **Right:** Temperature dependence in semi-log scale of the control sample (circles) along with its fit according to the Usadel theory [72].

ring (PdNbAu sample) and served as a control sample. The characteristics of these different samples are summarized in table 5.1.

sample	NL2	d2	g3	1f	NS ring
total normal length (μm)	6	6	6	4	4
normal length (μm)	1.6	1.4	1.4	1.4	1.4
normal thickness (nm)	50	50	50	50	50
normal width (nm)	200	200	200	300	300
R_d (Ω)	3	1.1	1.5	0.9	?
R_N (Ω)	not determined	1	1.1	0.7	0.7
$I_c(0)$ (μA)	1.5	29	25	65	?
E_{Th} (mK)	not determined	57	41	70	71

Table 5.1: Characteristics of PdNb/Au junctions (NL2,d2,g3,1f) and PdNb/Au ring (denoted NS ring). The total normal length is the length of the normal wire whereas the normal length is defined as the length of the normal wire which is not covered by PdNb. The normal thickness and width are the thickness and width of the normal wire. R_d is the resistance found by fitting the temperature dependence of the critical current by theoretical predictions [18] whereas R_N is the normal state resistance, the differential resistance of the junction after switching from the non-dissipative to the dissipative state. $I_c(0)$ is the extrapolated value of the critical current at $T = 0$. E_{Th} is the Thouless energy of the junction. The double bars distinguish between the co-evaporated samples. Co-evaporated samples have similar characteristics but there are important batch-to-batch variations due to changes in the fabrication process.

The control sample (labeled 1f) has a normal-state differential resistance $R_d = 0.9\Omega$ slightly larger than the value determined by the high temperature fit $R_N = 0.7\Omega$. We use the latter value since there could be a small contribution of the electrodes, heated by the normal wire, to the resistance or also from the non-perfect interfaces. The estimated critical current at zero temperature is $I_c(T = 0) \simeq 70\mu A$ and the high temperature fit gives $E_{Th} = 70mK$. This

yields

$$\frac{eR_N I_c}{E_{Th}} \simeq 8 \tag{5.54}$$

This value, to be compared with a value of 10.8 for a perfect interface, indicates that the interfaces are not perfectly transparent but are though quite good. Following [79], a value $\frac{eR_N I_c}{E_{Th}} \simeq 8$ is computed for an interface resistance equal to $R_I = 0.2R_N$. This value reduces the Thouless energy by 14%. The amplitude of the critical current also shows that Pd does not have a dramatic influence on the critical current, even though it is a metal close to a ferromagnetic transition and therefore hosts magnetic excitations [114, 115]. Due to the difficulty to theoretically describe the case of interfaces of intermediate transparency, we will not consider the effect of non-perfect interfaces in the following.

In agreement with findings by Dubos *et al.* [5], we do not observe a drop in the differential resistance in the resistive branch at low voltage bias for junctions having a narrow N wire. Indeed, Dubos *et al.* emphasize that it is necessary to measure the differential resistance of junctions with a large conductance (i.e. a large section) for this drop to be observed. According to Dubos *et al.*, this resistance drop is due to the relaxation of Andreev pairs to equilibrium. In agreement with this analysis, our work (see sec.6) shows that the relaxation term dominates the conductance only when $\omega_J \tau_{in} \sim 1$. Therefore for a given $V_{in} = \frac{\hbar}{2e\tau_{in}}$, if G_N is small the relaxation term is dominant at a bias current $I_{in} = G_N V_{in}$ that is smaller than the critical current and no drop in the differential conductance is observed; if G_N is large enough, the relaxation term can be dominant at bias currents larger than the critical current and a drop in the differential resistance is observed.

5.6 Summary

The experimental setup consists of a NS ring inserted into a Nb multimode resonator to measure the ring's susceptibility χ at the resonator's eigenfrequencies. The in-phase part of the susceptibility $\chi'$is related to a frequency shift δf and the out-of-phase part χ"to a change in the inverse of the quality factor $\delta(1/Q)$ of the resonator. δf and $\delta(1/Q)$ are obtained by measuring the reflexion coefficient of the resonator while magnetic field is swept and detection setup being locked at resonance thanks to a feedback loop. As compared to the previous experiment by F. Chiodi *et al.*, we improved the setup by using 50Ω NbTi superconducting coaxial wires, optimizing the ring's position inside the resonator, changing the superconducting material and calibrating the out-of-phase signal. This calibration was necessary to quantitatively measure the dissipative response χ".

In addition, several corrections have to be taken into account to obtain the exact value of $\chi'$and χ". However these corrections are important only at low temperature and are negligible at $T \sim 1K$ when $\frac{2\pi L_l I_c}{\Phi_0} \ll 1$. In this case, the relation between$\chi'$and δf and χ"and δQ^{-1} simply reads :

$$-2\frac{\delta f}{f} = \frac{L_c^2}{L}\chi' \tag{5.55}$$

$$\delta(\frac{1}{Q}) = \frac{L_c^2}{L}\chi" \tag{5.56}$$

Finally the parameters necessary to analyze the data have been determined by doing preliminar experiments. In particular, the quality factor of each eigenfrequencies of the resonator have been measured using a network analyzer and the temperature dependence of a control sample, which has characteristic similar to the ones of the PdNbAu ring, have been determined.

The next chapter is devoted to the presentation and the analysis of the linear response of a long and diffusive NS ring within the Kubo formula approach we developed in chap. 3 and 4.

6

Measurement of the linear response of a NS ring

The experimental evolution of the susceptibility of a PdNb/Au ring with phase, temperature and frequency is introduced in this chapter. This evolution is deduced from the variations of the eigenmodes of a multimode resonator at temperatures ranging from 400 mK to 1.2 K and frequencies from 190 MHz up to 14 GHz. In a first place, the characterization of the ring is described, then the evolution of susceptibility is introduced and analyzed. Though several samples (WAu1,WAu2 and PdNbAu) have been measured, we focus on the results from the PdNbAu ring which are clearer.

We explored the response of a PdNbAu ring at frequencies ranging from 190 MHz up to 14 GHz. We however observed a qualitative change in the in-phase susceptibility at frequencies higher than 3 GHz, with the emergence of a sharp dip at $\varphi = \pi$ in its phase dependence. We thus focus on the low frequency regime in the following. The response at high frequency is more exploratory and is introduced in sec.6.4.

As shown in fig.6.1 and 6.2 we find a rich evolution of χ with temperature and frequency. At our lowest accessible frequency ($f_0 = 190MHz$) and high temperature ($T = 1.2K \simeq 17E_{Th}$), we find a cosine phase dependence (see fig.6.1) characteristic of the usual Josephson current-phase dependence, sinusoidal for $T \gtrsim E_g(\varphi = 0)$ [80]. At higher frequencies we find a greater harmonic content with an important contribution of the 2nd harmonic whereas the amplitude of the response does not change. A surprising feature is the appearance of dissipation even when χ'has recovered a purely sinusoidal phase dependence. χ"phase dependence strongly depends on the frequency with a signal dominated by its second harmonic at low frequency turning into a signal with an almost opposite phase dependence at high frequency (see fig.6.1). It is worth noting that even though at low frequency χ"strongly differs from what has been previously observed in W/Au rings (see fig.2.5), there is a regime where a similar phase dependence, close to the one of the minigap, is observed for these two different samples.

In the following, we analyze these data in the light of the Kubo formula approach we introduced in chapters 3 and 4. We show that our findings are well accounted for within this framework where the response is described as the sum of three contributions : the Josephson adiabatic response, the relaxation of populations and the induced transitions. We describe how these different contributions are deduced from the data and characterize them.

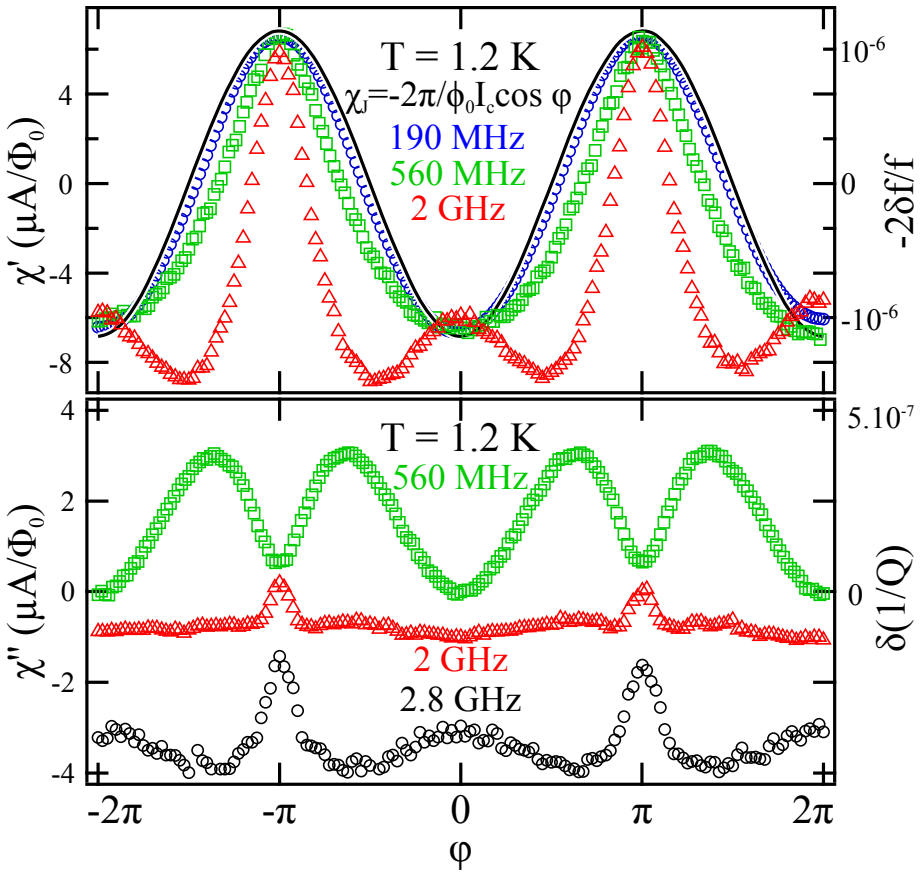

Figure 6.1: **Top:**Non-dissipative χ' and **Bottom:** dissipative χ" response at several frequencies and $T = 1.2K$. Note that the amplitude between 0 and π of χ' does not depends on frequency whereas its harmonic contents does. For the sake of clarity, χ"$(2GHz)$ is offset by -1 and χ"$(2.8GHz)$ by -3.

6.1 Josephson contribution: adiabatic response

The Josephson contribution :

$$\chi_J = -\frac{2\pi}{\Phi_0}\frac{\partial I_J}{\partial \varphi} \tag{6.1}$$

is related to the supercurrent and is therefore purely real (non-dissipative) and frequency independent. For frequencies such as $\omega\tau_{in} \ll 1$ diagonal and non-diagonal contributions are negligible (adiabatic regime) and so $\chi' = \chi_J$ is just a measure of the current-phase relation at equilibrium. In the case of a weak link being a diffusive N wire, the current-phase relation is $I_J(\varphi) = I_c \sin(\varphi)$ at temperatures sufficiently high to suppress higher harmonics of the current-phase relation [80]. $\delta_{\pi-0}\chi'$ is related to the critical current by:

$$\delta_{\pi-0}\chi' = \frac{4\pi}{\Phi_0} I_c \tag{6.2}$$

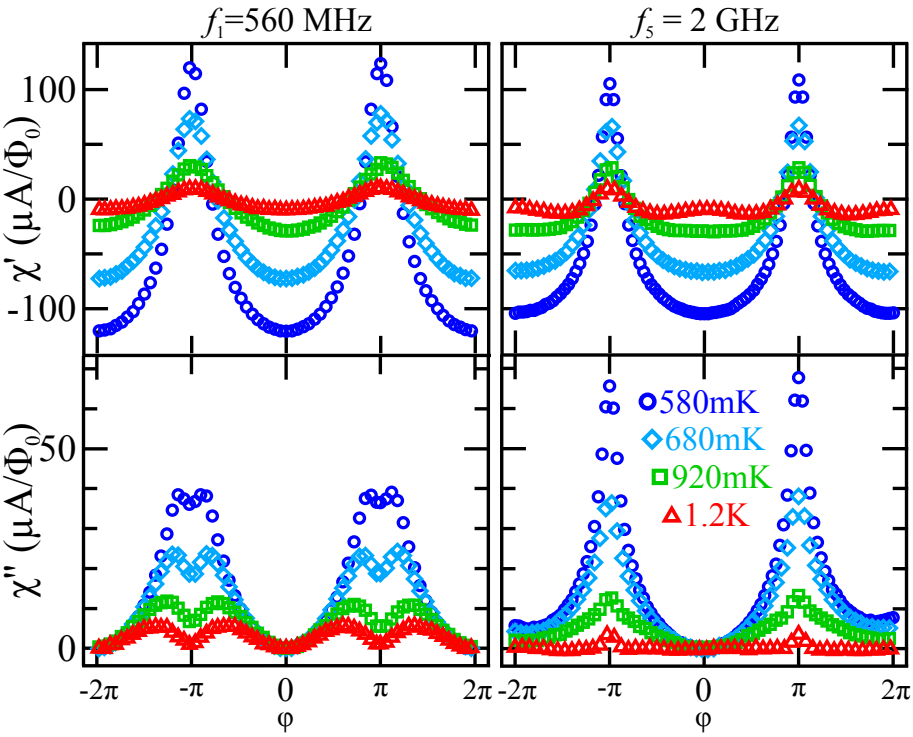

Figure 6.2: Evolution of χ' (top) and χ" (bottom) phase dependence with temperature at $f_1 = 560\,MHz < E_{Th}/h$ (left) and $f_5 = 2\,GHz \gtrsim E_{Th}/h$ (right). $\chi'(\varphi = \pi)$ and $\chi"(\varphi = \pi)$ increase with decreasing temperature. $\chi'(\varphi)$ and $\chi"(\varphi)$ strongly differ at low frequency and high temperature whereas they are similar with a shape reminiscent of the minigap at high frequency. Curves have been shifted so that $\chi'(\varphi = \pi) - \chi'(\varphi = 0) = 0$ and $\chi"(\varphi = 0) = 0$

This adiabatic limit is almost never reached in the current experiment but the conclusion remains unchanged since $\delta_{\pi-0}\chi'_D = 0$, χ'_Ddoes not modify the amplitude of the signal. This analysis is valid until the frequency is too high ($\omega \gtrsim E_g$) so that χ'_{ND}comes into play. We thus have access to the critical current temperature dependence via the amplitude of χ'.

$\delta_{\pi-0}\chi'(T)$ perfectly reflects the expected, roughly exponential, decay of the Josephson critical current with temperature $I_J(T) = I_J(0)\exp(-k_BT/3.6E_{Th})$ [72]. Fitting this dependence yields :

$$E_{Th} \equiv 71mK \tag{6.3}$$

The analysis of the amplitude of χ'in the low frequency regime thus allows to perfectly characterize the junction with the knowledge of the total minigap width :

$$2E_g(0)/h \equiv 9GHz \tag{6.4}$$

and the corresponding diffusion time across the junction :

$$\tau_D = 0.1ns \tag{6.5}$$

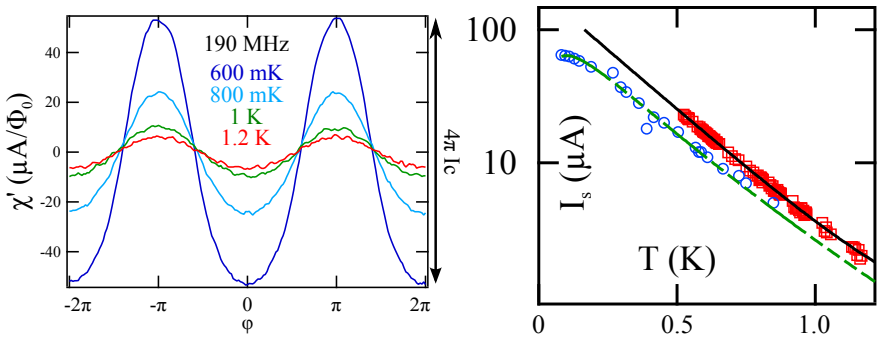

Figure 6.3: **Left:** $\chi'(\varphi)$ at several temperatures and $f = 190MHz$. The amplitude of χ' is related to the critical current of the NS ring by $\chi'(\pi)-\chi'(0) = \frac{4\pi I_c}{\Phi_0}$. **Right:** Temperature dependence in semi-log scale of the critical current of the ring (squares) and of the control sample (circles) along with their fit. Determination of the critical current of the ring is described in the main text. $E_{Th} = 71mK$ is found.

Critical current's temperature dependence

The amplitude of the signal is related to the critical current by $\delta\chi' = \frac{4\pi}{\Phi_0} I_c$. This relation yields the temperature dependence of the critical current and so the Thouless energy. Following [72], fitting this temperature dependence with $I_c \propto \exp(-\frac{\pi k_B T}{11.9 E_{Th}})$ yields $E_{Th} = 71mK = 1.5GHz$. It gives us a precious information since it sets the relevant scale for temperature and frequency.

Lastly, we can note that since the control sample and the PdNbAu ring share the same geometrical characteristics and similar critical current temperature dependences, a similar value for the resistance can be assumed.

We now turn to the diagonal contribution which is the first frequency-dependent term that contributes to χ'.

6.2 Diagonal contribution: relaxation of populations

This second contribution describes the relaxation of population driven out-of-equilibrium by the finite frequency phase biasing. It is called diagonal contribution since it only involves diagonal elements of the current operator. In the following we detail how this contribution is extracted from the data. The analysis of its phase, temperature and frequency dependence let's perfectly characterize this contribution and yields an important parameter: the inelastic scattering time τ_{in}. **This finite frequency contribution is also interpreted as a zero-frequency supercurrent noise. This is a central result of this work.**

Extraction of the diagonal contribution

Noting that $\delta_{\pi-0}\chi_D = 0$ (see for instance fig.3.2) whereas $\delta_{\pi-0}\chi_{ND} \neq 0$ (see for instance fig.3.4) and having an amplitude of χ'almost independent of frequency[1] for $f \leq 2.8GHz$ as shown in fig.6.4 proves χ'_{ND}can be neglected at

[1] a non-monotonic variation of about 10% is observed

low frequency. One can then access the non-dissipative part of the diagonal contribution : $\chi'_D = \chi' - \chi_J$ (see fig.6.5.b). The dissipative part of the diagonal contribution is more difficult to access since we still lack a good analytical prediction for $\chi_{ND}(\varphi)$, a term that gives a large contribution to $\chi''(\varphi)$ even at low frequency. χ'' is however dominated by χ''_D in the range of temperature and frequency where $\omega\tau_{in} \sim 1$. For instance, this is experimentally the case at $T = 1.2K$ and $f = 560MHz$ (see fig.6.1). Otherwise, we have overcome this difficulty by subtracting the flux dependence of χ''_{ND} estimated from the high frequency data (2.8 GHz) as shown in fig.6.5c and d . However this is not such a good approximation. Indeed, this assumes the phase dependence of $\chi''_{ND}$is frequency independent which is not well verified as detailed in sec. and can be easily inferred remembering χ''_{ND}describes microwave-induced transitions.

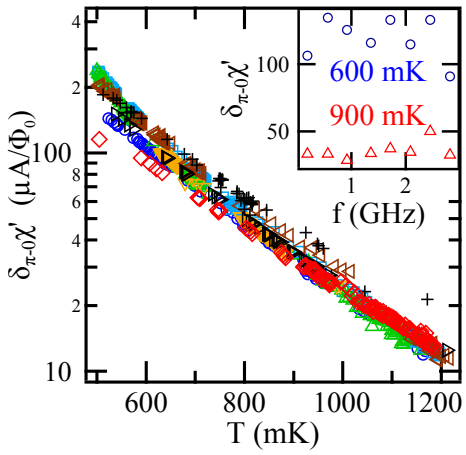

Figure 6.4: Temperature dependence of the amplitude of χ'at every explored frequency. $\delta_{\pi-0}\chi'$ does not depend on frequency in the range of temperatures and frequencies explored. The inset shows that the variations of $\delta_{\pi-0}\chi'$ are non-monotonic with frequency. This means χ'_{ND}can be neglected since it would manifest itself by a decreasing of $\delta_{\pi-0}\chi'$ with frequency.

Phase dependence of the diagonal contribution: dominant contribution of the 2^{nd} harmonic

The extracted $\chi'_D$and χ''_Dexhibit a sharp cusp at $\varphi = \pi$. These experimental phase dependences can be compared with the predicted flux dependence of χ_D, given by the function F

$$F(\varphi, T) = -\sum_n i_n^2 \frac{\partial f_n}{\partial \epsilon_n}, \tag{6.6}$$

As detailed in sec.2.2, this function was first introduced by Lempitsky [91] to describe the I(V) characteristics of SNS junctions, and was calculated numerically using Usadel equations by Virtanen et al.[95]. At large temperature compared to E_{Th}, $F(\varphi)$ can be approximated by the following analytical form:

$$F_U(\varphi) \propto [(-\pi + (\pi + \varphi)[2\pi])] \sin(\varphi) - |\sin(\varphi)| \sin^2(\varphi/2)/\pi \tag{6.7}$$

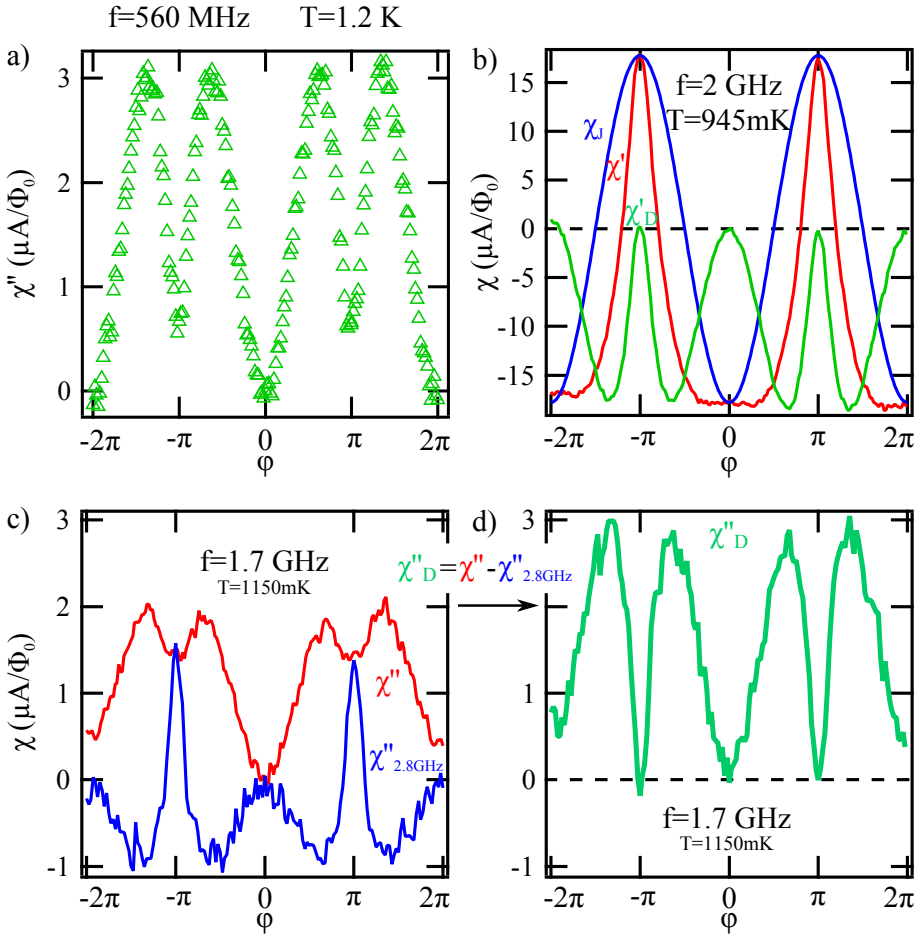

Figure 6.5: **a.** χ''_D is directly observed in the range of frequency and temperature such as $\omega\tau_{in} \sim 1$ when χ''_D dominates χ". **b.** Assuming χ'_{ND} is negligible, χ'_D is obtained by subtracting $\chi_J = -\delta_{\pi-0}\chi' \cos(\varphi)$ to χ'. This can be done at each frequency and temperature explored. **c.** Most of the time, χ"is not clearly dominated by χ''_D due to the compensation between χ''_D and χ''_{ND}. χ''_D is then extracted using $\chi''(f = 2.8GHz)$, the dissipative signal at 2.8 GHz, assuming that it is dominated by χ''_{ND} and that the phase dependence of χ''_{ND} does not depend on frequency. As shown is sec.6.3 this is not such a good approximation (see in particular fig.6.13). The resulting χ''_D is shown in **d.**

It is dominated by its second harmonics with in addition a sharp linear singularity at odd multiples of π (see Fig.6.6). This is due to the dominant contribution of Andreev levels close to the minigap whose flux dependence is singular as in a highly transmitting superconducting single channel point contact [116].

In fig.6.6 we compare the independently measured flux dependences of $\chi' - \chi_J$ and χ'' at high temperature (T=1.2 K) with theoretical predictions from the Usadel equations, $F_U(\varphi)$. This is done for several frequencies and a good agreement is found.

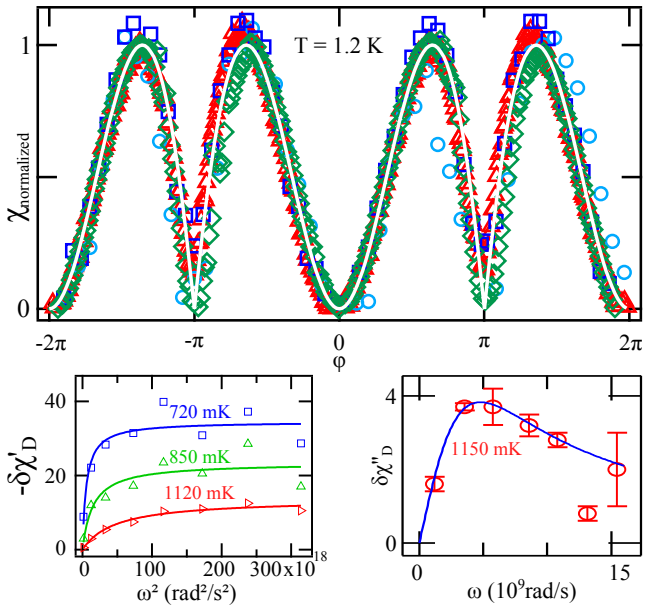

Figure 6.6: **Top:** Normalized experimental phase dependences at $T = 1.2\,K$ (open symbols) compared to F_U (solid). Data are χ" (squares), $|\chi'_D| = \chi_J - \chi'$ (circles) at $f_1 = 560\,MHz$ and χ" (triangles), $|\chi'_D| = \chi_J - \chi'$ (diamonds) at $f_3 = 1.35\,GHz$. At high temperature and for $f \lesssim E_{Th}/h$, experimental $\chi_J - \chi'$ and χ" are found to be in very good agreement with theoretical prediction of Usadel equations F_U. **Bottom left:** Frequency dependence of $\delta\chi'_D$: the maximum of $-\chi'_D(\varphi)$, at different temperatures (symbols) compared to the theoretical prediction from Eq.6.8. **Bottom right:** frequency dependence of $\delta\chi''_D$ at 1.15K (circles) compared to the theoretical prediction from Eq.6.9.

Frequency dependence of the diagonal contribution: extraction of τ_{in}

We now look at the frequency dependence of the diagonal contribution. We first follow the frequency dependence of the amplitude of $\chi'_D(\varphi) = \chi'(\varphi) - \chi_J(\varphi)$ at fixed temperature, and check that the shape of $\chi'_D(\varphi)$ does not change with frequency and is the same as that of χ''_D, as predicted for the temperature and frequency regime where the contribution of χ''_{ND} can be neglected. As shown on Fig.6.6 it is then possible to fit the frequency dependence of the amplitude of $\chi'_D(\varphi)$ by the expected

$$A'(\omega) = \frac{(\omega\tau_{in})^2}{1 + (\omega\tau_{in})^2} \tag{6.8}$$

and determine the characteristic time τ_{in} for several temperatures according to Eq.6.8 . We find values of τ_{in} varying between 0.2 and 0.8 ns. The temperature dependence of τ_{in} is shown in fig.6.7 and is consistent with a T^{-3} law. This dependence is discussed in more details in sec.6.2. Anticipating on the following, we represented in fig.6.7 the supercurrent noise frequency dependence which is related to τ_{in}.

It is interesting to note that our results can be described by a single inelastic time, independent of φ, whereas a phase dependent τ_{in} is expected for electron phonon collisions in SNS junctions [117]. This is probably due to the fact that temperature is larger than $E_g(0)$ in our case which somehow washes out the effect of the minigap.

A similar analysis can be done on χ'' , the quality of the calibration is however not as good as on χ'. Moreover $\chi''_D$is extracted using $\chi''_{ND}$from higher frequency measurements which is not such a good approximation. The resulting amplitude $\delta\chi''_D(\omega)$ however agrees with the expected frequency dependence in

$$A''(\omega) = \frac{\omega\tau_{in}}{1+(\omega\tau_{in})^2} \tag{6.9}$$

as shown in Fig. 6.6. At 1150 mK, a τ_{in} of about 0.1 ns is found from the frequency dependence of $-\delta\chi'_D$ whereas a τ_{in} of about 0.2 ns is found from the frequency dependence of $\delta\chi''_D$. These values are in reasonable agreement with one another, taking into account the delicate calibration of $\chi''_D(\varphi)$.

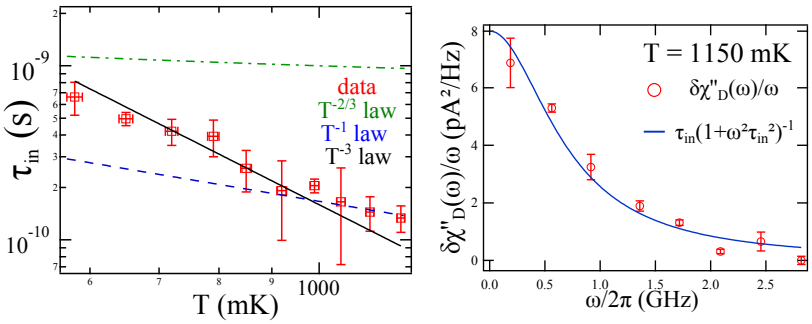

Figure 6.7: **Left:** Temperature dependence of the inelastic scattering time (symbols). It is extracted from the fits of $\delta\chi'_D$ frequency dependence at different temperatures. The black solid line is a T^{-3}, the blue dashed line is a T^{-1} law and the green dashed line is a $T^{-2/3}$ law. We offset the $T^{-2/3}$ law such as its value at 1K is the same as the one measured in Au 5.9 by Pierre *et al.* [118]. **Right:** Frequency dependence of supercurrent noise deduced from χ''_Dmeasurements. It is finite with amplitude $\sum i_n^2 \frac{\partial f_n}{\partial \epsilon_n}$ at zero frequency and depends on frequency as $(1+\omega^2\tau_{in}^2)^{-1}$.

The data agrees with the phase and frequency dependence expected from the relaxation of Andreev populations. This is the main source of dissipation when $\omega\tau_{in} \sim 1$ at high temperature.

Temperature dependence of the diagonal contribution

The non-dissipative diagonal contribution $\chi'_D$is shown for several temperatures in fig.6.8. In qualitative agreement with predictions by Virtanen *et al.*, the position of the first positive maximum φ_M slightly changes with temperature and saturates at high temperature [95]. As shown in fig.6.8, the amplitude of χ'_Ddecreases as a power law with temperature with an exponent that depends on frequency, increasing roughly linearly with frequency. The origin of this behavior remains unclear.

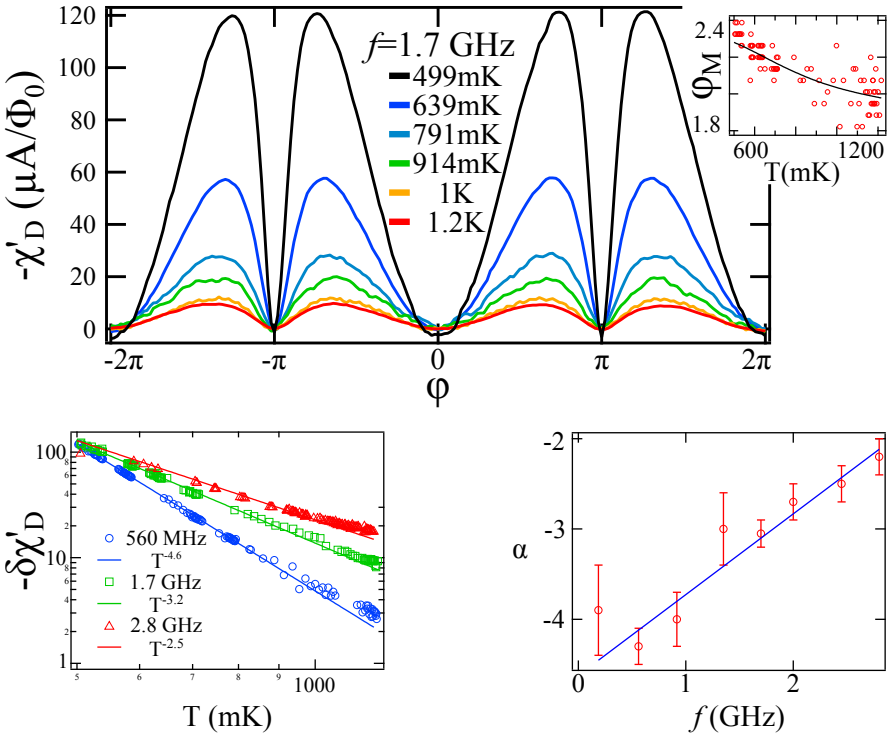

Figure 6.8: **Top:** -χ'_D at $f = 1.7GHz$ and several temperatures. Inset: In qualitative agreement with theoretical predictions [95], the position of the maximum φ_M slightly shifts with increasing temperature and saturates. **Bottom left:** Temperature dependence of the amplitude of -χ'_Dat several frequencies (symbols) along with their respective power law fits (solid lines). Data at 2.8 GHz have been offset by $53\mu A/\Phi_0$. **Bottom right:** Frequency dependence of the exponent α for the odd multiples of the fundamental frequency $f_0 = 190MHz$ up to 2.8 GHz (symbols). The evolution is consistent with a linear frequency dependence.

To compare the experimental temperature dependence of the diagonal contribution to theoretical predictions by Virtanen *et al.* [95], one has to input the experimentally determined Thouless energy E_{Th} and inelastic scattering time $\tau_{in}(T)$ into :

$$\chi'_{D,th} = \frac{\omega^2\tau_{in}^2}{1+\omega^2\tau_{in}^2}\frac{G_N E_{Th}^2}{\hbar k_B T}Q(\varphi,T) \tag{6.10}$$

where G_N is the normal state conductance and is taken as unity[2] and $Q(\varphi,T)$ has been calculated numerically by Virtanen *et al.* [95] (see fig.4.9).

The temperature dependence of the frequency dependent prefactor

$$A'(\omega,T) = \frac{\omega^2\tau_{in}^2}{1+\omega^2\tau_{in}^2} \tag{6.11}$$

[2]The exact value of the normal state conductance does not impact the temperature dependence of F

determined using the T^{-3} fit of the experimental $\tau_{in}(T)$ is displayed in fig.6.9. Whereas its amplitude strongly depends on temperature at low frequency (when $\omega\tau_{in} \lesssim 1$ in the whole temperature range), it is almost constant and equal to unity at high frequency (when $\omega\tau_{in} \gg 1$ in the whole temperature range).

The temperature dependence of $\chi'_{D,th}$ also comes from the one of

$$F = G_N \frac{E_{Th}^2}{\hbar k_B T} Q(\varphi, T) \tag{6.12}$$

Defining δF as the amplitude of the phase dependence of F and using the numerically determined $Q(\varphi, T)$, one can see that the temperature dependence of $-\delta F$ simply follows a $1/T$ law (see fig.6.9). Indeed, even though the amplitude of $Q(\varphi, T)$ strongly depends on temperature at low temperature compare to E_{Th}, it is almost temperature independent in the explored regime of temperatures of about 8 to 16 E_{Th}. This $1/T$ temperature dependence is the one of the energy derivative of the Fermi distribution at high temperature since F writes in the discrete spectrum limit:

$$F = -\sum_n i_n^2 \frac{\partial f_n}{\partial \epsilon_n} \tag{6.13}$$

The comparison between theoretical predictions and experiment is done for several frequencies in the middle and bottom panels of fig.6.9. One sees that at high temperature, when the prefactor $A'(\omega, T)$ is not saturated to 1, the temperature dependence of $-\delta\chi'_{D,th}$ is similar to the experimental one. This is however not the case at lower temperature when $A'(\omega, T)$ saturates to unity. This discrepancy can be due to an overestimated τ_{in} at low temperature, indeed if $A'(\omega, T)$ were smaller than 1, the temperature dependence of $-\delta\chi'_{D,th}$ would be larger. This overestimation could be due to the fact that the effect of screening of the applied magnetic field by the inductance of the ring is not totally taken into account at low temperature when screening is the strongest.

Interpretations of the diagonal contribution

Comparison with fractional Shapiro steps

As we have seen, the diagonal contribution related to the relaxation of Andreev states populations is dominated by its second harmonics. That means that when a SNS junction is voltage biased, the diagonal contribution modifies the current-phase relation with the addition of a 2^{nd} and higher harmonic contributions [91, 92]. This becomes important at voltages such as $\omega_J\tau_{in} \gtrsim 1$. Therefore, the relaxation of Andreev states populations could partly[3] explain the emergence of fractional Shapiro steps, as already mentioned in [96, 119]. A quantitative comparison between the temperature dependence of the harmonics of the diagonal contribution and the fractional Shapiro steps is necessary to confidently ascribe the origin of fractional Shapiro steps to this phenomenon. This has to be done in junctions made of the same materials due to the importance of the temperature dependence of the inelastic scattering time.

[3] Relaxation is one among other non-adiabatic effects that can change the harmonic contents of the current-phase relation.

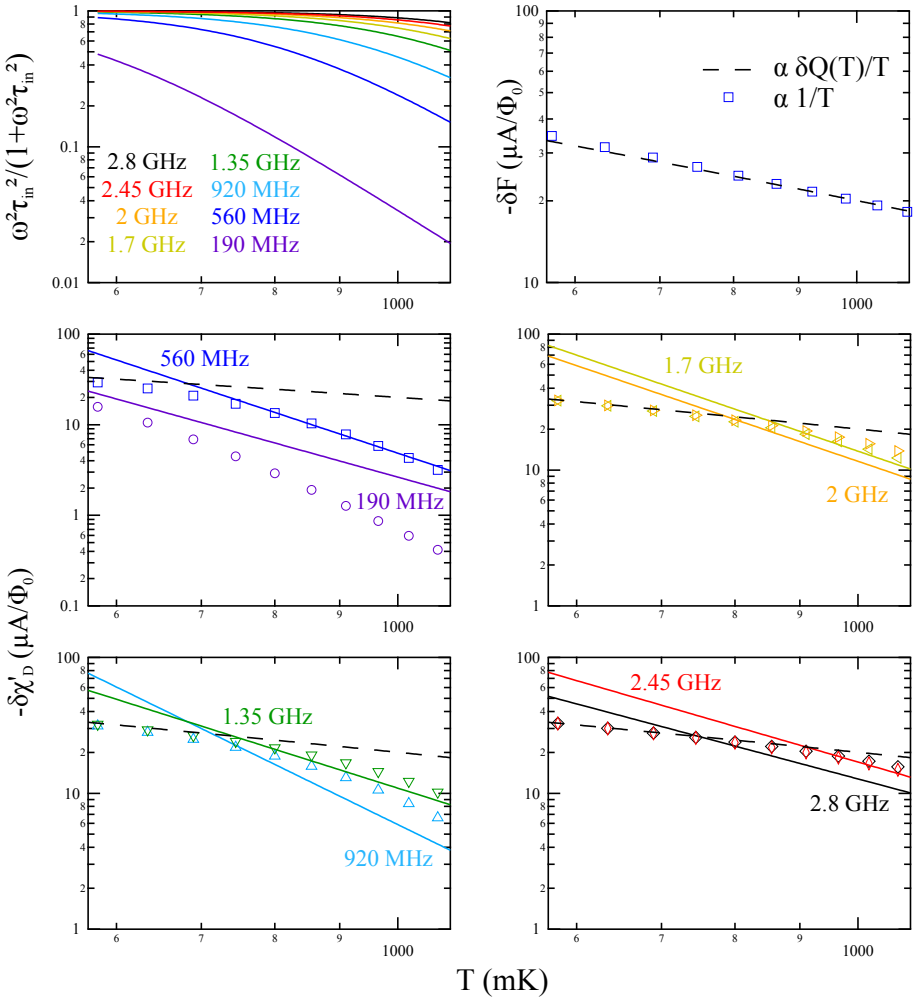

Figure 6.9: **Top left:** Temperature dependence of $\frac{\omega^2\tau_{in}(T)^2}{1+\omega^2\tau_{in}(T)^2}$ at several frequencies using the T^{-3} fit of the experimentally extracted $\tau_{in}(T)$. **Top right:** (dashed line) Expected temperature dependence of $-\delta F(T)$ the opposite of the amplitude of $F(\varphi,T) = G_N\frac{E_{Th}^2}{\hbar k_B T}Q(\varphi,T)$ with $Q(\varphi,T)$ given by eq.3.63 using $G_N = 1S$ and $E_{Th}/k_B = 71mK$. In the explored temperature range, the temperature dependence of $Q(\varphi,T)$ is negligible and so $-\delta F(T)$ follows a $1/T$ law (square) . **Middle left:** Experimental temperature dependences of the best fit of the amplitude of the diagonal contribution (solid) at $190MHz$ and $560MHz$ along with their respective predicted temperature dependences (symbols) using the experimental $\tau_{in}(T)$ and $E_{Th}/k_B = 71mK$. A $1/T$ law is displayed as a dashed line. Similar information is plotted in other panels but for $920MHz$ and $1.35GHz$ (**Bottom left**); $1.7GHz$ and $2GHz$ (**Middle right**); $2.45GHZ$ and $2.8GHz$ (**Bottom right**).

Fluctuations of the supercurrent

Theoretically, it was predicted that, in contrast to tunnel Josephson junctions [120] and because of the smallness of the induced gap, SNS junctions should exhibit low frequency supercurrent fluctuations at equilibrium [116]. According to the fluctuation dissipation theorem, in the linear response regime, such equilibrium fluctuations lead to a dissipative current under an ac flux excitation [71, 95]. This dissipative current is measured via χ''_D.

Using fluctuation-dissipation theorem, one can estimate the related thermodynamic current noise as:

$$S_I(\omega) = \frac{2}{\pi}\frac{k_B T \chi''_D(\omega)}{\omega} = \frac{2}{\pi} k_B T \sum_n i_n^2(\varphi) \frac{\partial f_n}{\partial \epsilon_n}\left[\frac{\tau_{in}}{1+(\omega\tau_{in})^2}\right] \tag{6.14}$$

This dissipative response is directly related to the low frequency thermal noise of the Josephson current, with a flux dependence proportional to the average square of the spectral (or single level) current, and can be precisely described by theoretical predictions.

Interestingly, the expression of this noise becomes particularly simple when temperature is much larger than the minigap, so that $\frac{\partial f_n}{\partial \epsilon_n} \equiv \frac{1}{k_B T}$. One then finds that the frequency integrated current noise is just

$$\delta I^2 = \sum i_n^2 \tag{6.15}$$

which corresponds to independent current fluctuations for each Andreev level.

It is interesting to compare our findings to earlier experiments specifically aiming at revealing the noise of a SNS junction [90, 85]. These experiments are done in a voltage biased regime and show a divergence of the noise at voltages smaller than E_{Th}. This divergence is due to Multiple Andreev Reflexion which exist whatever small the bias voltage is. This shows that, since MAR are a non-equilibrium process, equilibrium noise can not be measured in a voltage biased configuration. In this context, it should be emphasized that the equilibrium supercurrent noise revealed in our experiment is finite in the limit of zero frequency. In addition, in contrast with these voltage-biased experiments with no control over phase, measuring χ"yields the phase dependence of noise. This phase dependence is very recognizable : it has almost half the period of Josephson current due to its dependence on the square of the single levels and show cusps at odd multiples of π reflecting the closing of the minigap.

A new look over earlier results: a puzzling relaxation mechanism

In lights of the Kubo formula approach we developed, which agrees well with results of PdNbAu sample, we reconsidered the data from WAu1 and WAu2 samples. We got rid of calibration errors by normalizing their χ'. Then we follow the same method as for PdNbAu sample to extract the inelastic scattering time: we subtract a cosine to $\chi'$to extract the diagonal contribution (see fig.6.10); then the frequency dependence of the amplitude of the diagonal contribution is compared to the expected $\frac{\omega^2\tau_{in}^2}{1+\omega^2\tau_{in}^2}$. This analysis is performed at three different temperatures for sample WAu2. The resulting τ_{in} is shown in

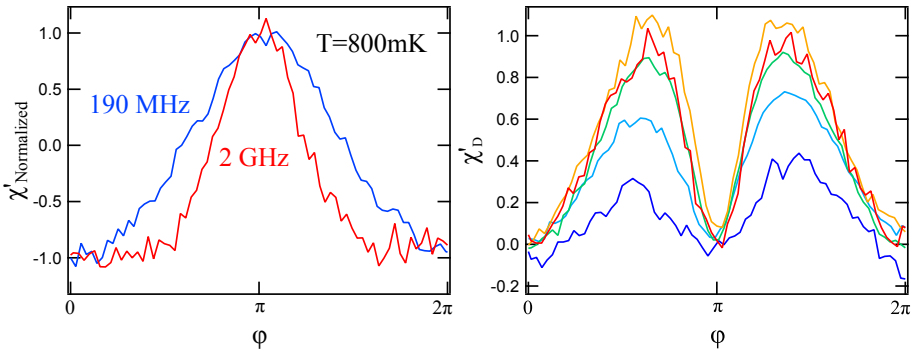

Figure 6.10: **Left:** Normalized χ'at f=190 MHz and f=2 GHz at 800mK for sample WAu2. **Right:** $-\chi'_D$ extracted from the normalized χ'at T=800mK and, from bottom to top, f=190 MHz,560 MHz,930 MHz,1.35 GHz

fig.6.11 along with the T^{-3} fit of τ_{in} in PdNbAu sample. They are of the same order of magnitude. A similar analysis could be performed for sample WAu1, there is unfortunately not enough data points to determine the inelastic scattering time. It can be noted though that they are expected to be of the same order of magnitude than the values measured in WAu1 and PdNbAu samples since a similar evolution of the phase dependence of $\chi'(\varphi)$ is observed for the three samples.

The inelastic scattering time extracted from these different experiments is quite surprising: its temperature dependence is consistent with a T^{-3} law whereas in this range of temperature ($T < 1K$) a T^{-1} law due to the dominant electron-electron interaction is expected [121, 122]. It could be argued that due to the weakness of electron-electron interaction the observed T^{-3} law is due to electron-phonon interaction. The magnitude of the extracted τ_{in} however disagrees with this picture: a τ_{in} one order of magnitude larger is expected at $1K$ [118].

In [123], inelastic scattering due to paramagnons, magnetic excitations in Pd [114, 115], was invoked to account for the observed short τ_{in}. This affirmation is contradicted by the observation of τ_{in} of similar magnitude in WAu samples. On the other hand, W is a disordered superconductor that exhibits subgap states which might induce relaxation [124].

Lastly, we emphasize that gold of different purities (5.9 for PdNbAu sample, 6.9 for WAu samples) have been deposited using different techniques (Joule heating for WAu, electron gun for PdNbAu) to fabricate the different samples.

6.3 Non-diagonal contribution: induced transitions

The last contribution χ_{ND}, called non-diagonal contribution since it only involves non-diagonal elements of the Hamiltonian, describes microwave induced transitions between different energy levels. Due to the great number of levels involved, its evolution with temperature and frequency is more complex than the diagonal contribution. As detailed in sec.3.4, it is important in the low frequency range ($\hbar\omega \lesssim E_g(0)$) only in the dissipative part of the response.

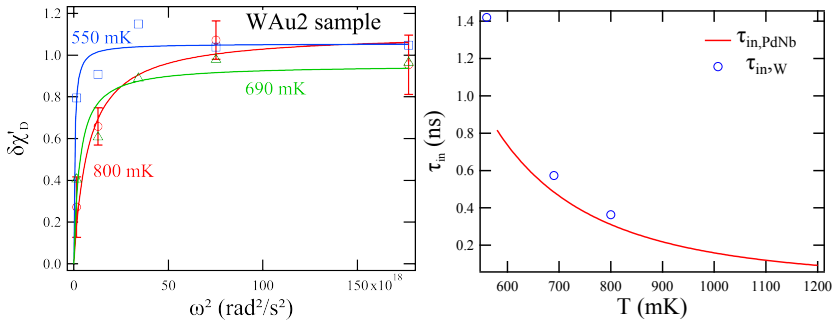

Figure 6.11: **Left:** Frequency dependence of $\delta\chi'_D$: the maximum of $-\chi'_D(\varphi)$, at different temperatures (symbols) along with their fit to eq.6.8. **Right:**Temperature dependence of the inelastic scattering time. It is extracted from the fits of the frequency dependence of $\delta\chi'_D$ at different temperatures. Solid line is a T^{-3} fit of data from PdNbAu sample, symbols from sample WAu2.

Extraction of the non-diagonal contribution

The dissipative response is dominated by this non-diagonal contribution at high frequency when $\omega\tau_{in} \gg 1$. As shown in fig.6.12a, the phase dependence of χ''_{ND}depends on temperature. At low temperature it is peaked at odd multiples of π whereas at high temperature there is the emergence of a local maximum around 0 in addition to the peak at π. At lower frequency $\chi''_{ND}$is extracted from the signal using χ_D. Indeed,

$$\chi''_{ND} = \chi'' + \frac{1}{\omega\tau_{in}}\chi'_D \tag{6.16}$$

since (see eq.3.68 and 3.69)

$$\chi''_D = -\frac{1}{\omega\tau_{in}}\chi'_D \tag{6.17}$$

A careful calibration of χ"is then necessary to obtain the right phase dependence. This has been done only for PdNbAu sample.

One can note that similar phase dependences, with a peak at π and a bump around 0, are observed either at low frequency ($\hbar\omega < E_g$) or high temperature ($k_BT > E_g$).

Phase dependence of the non-diagonal contribution

As shown in fig.6.13, χ''_{ND}phase dependence strongly depends on temperature and frequency. As shown in chapters 3 and 4 (see in particular fig.4.7), there are two limiting cases:

- at high temperature and low frequency, the contribution of non-diagonal elements of current operator is important which yields a phase dependence almost opposite in sign to the one of χ''_D
- at low temperature and high frequency, the current operator elements are considered as phase independent. It describes induced transitions

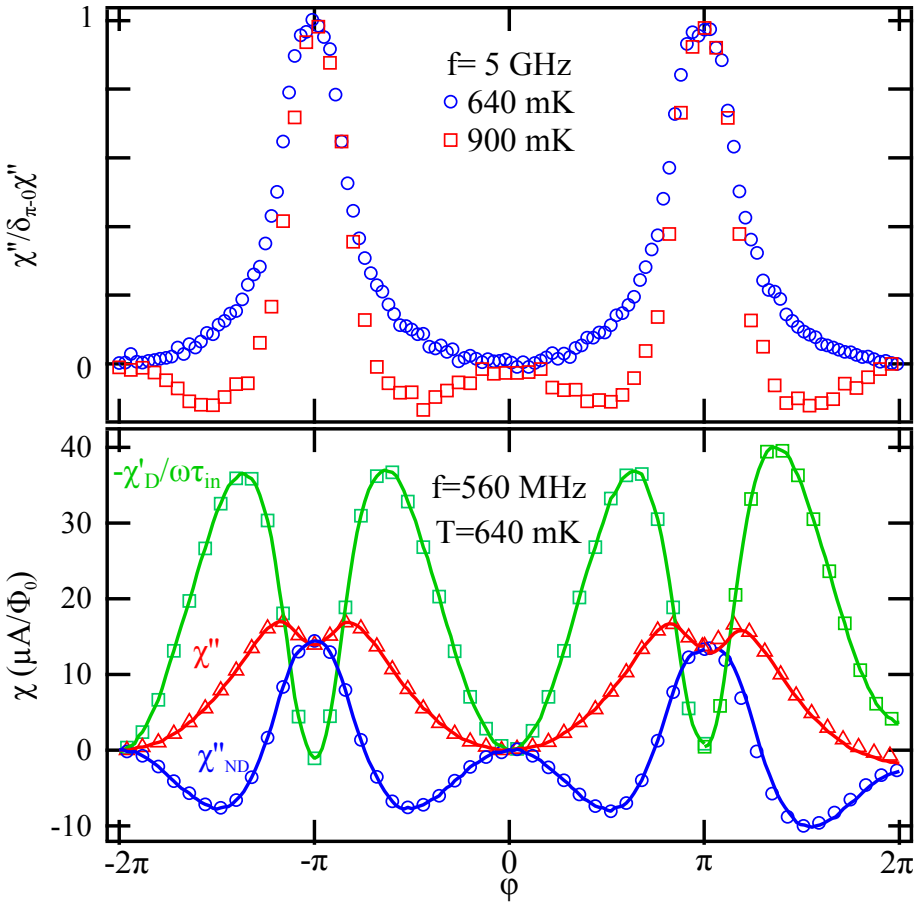

Figure 6.12: **Top:** At high frequency, χ"is dominated by χ''_{ND}; $\chi''_{ND}$is thus directly observed. **Bottom:** At low frequency, $\chi''_{ND}$is obtained subtracting $\chi''_D = -\frac{\chi'_D}{\omega\tau_{in}}$ to the measured χ". Note that the phase dependence of χ''_{ND}strongly depends on temperature and frequency contrary to the one of χ_D.

across the minigap between almost phase independent states deep in the spectrum.The phase dependence of $\chi''_{ND}$is then just peaked at $\varphi = \pi$. Its phase dependence is similar to the minigap's when $\hbar\omega \geq 2E_g(0)$

These two extreme cases are represented in fig.6.13 where χ''_{ND}exhibit a local maximum around $\varphi = 0$ that decreases with decreasing temperature at a given frequency or with increasing frequency at a given temperature.

Interestingly, as shown in fig.6.14, the similarity between χ" and the minigap can be accidental. If we were indeed performing the minigap spectroscopy, the phase dependence should not change with increasing frequency, even less sharpen. This similarity is actually due to the cancellation between the diagonal and non-diagonal contributions that have almost opposite phase dependences in the regime of high temperature.

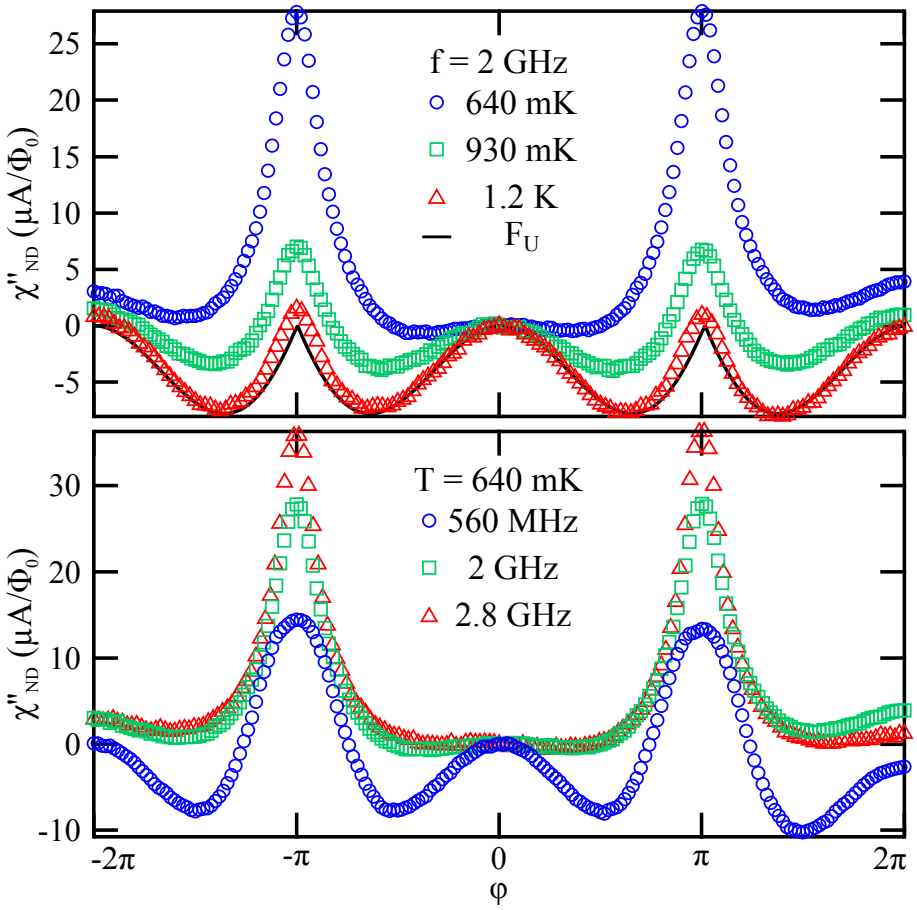

Figure 6.13: χ''_{ND}at several frequencies and temperatures. Note that the local maximum around zero increases with temperature and decreases with frequency.

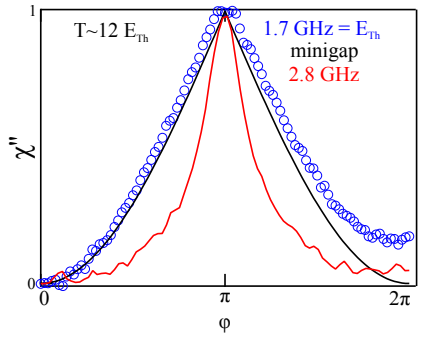

Figure 6.14: Due to the cancellation between $\chi''_D$and χ''_{ND}, the phase dependence of χ"can accidentally be similar to the minigap's.

frequency dependence of the non-diagonal contribution

In agreement with analytical predictions and numerical simulations, the amplitude of χ''_{ND}increases linearly with frequency for frequencies lower than $\frac{E_g}{\hbar} = 4.5Ghz$ as shown in fig.6.15.

Using the value of $R_N = 0.7\Omega$ deduced from the high temperature fit of the control sample's critical current temperature dependence, we found that ωG_N is larger than $\delta_{\pi-0}\chi$" at every explored frequency. We however expect that $\delta_{\pi-0}\chi" = \omega G_N$ at temperatures smaller than the minigap.

Relation between χ''_{ND} and χ'

As detailed in sec.3.1, Kramers-Kronig relation relates the frequency dependence of χ"to the one of χ'. Under the assumption that $|J(E,E')|^2$ does not depend much on the energy on a range k_BT, we predicted that the ratio $\delta_{\pi-0}\chi''_{ND}/\delta_{\pi-0}\chi'$ has two extreme behaviors:

- at low temperature $\delta_{\pi-0}\chi''_{ND}/\delta_{\pi-0}\chi' \propto \frac{\hbar\omega}{E_g}$
- at high temperature $\delta_{\pi-0}\chi''_{ND}/\delta_{\pi-0}\chi' \propto \frac{\hbar\omega}{k_BT}$

Therefore, at a given frequency and high temperature, the temperature dependence of $\delta_{\pi-0}\chi'' = \delta_{\pi-0}\chi''_{ND}$ is the same as the one of $\delta_{\pi-0}\chi'/T$ which is indeed observed experimentally (see fig.6.15).

As shown in fig.6.16, at a given temperature the ratio $\delta_{\pi-0}\chi''_{ND}/\delta_{\pi-0}\chi'$ depends linearly on the frequency. Let τ_{KK} be the slope of $\delta_{\pi-0}\chi''_{ND}/\delta_{\pi-0}\chi'$:

$$\delta_{\pi-0}\chi''_{ND}/\delta_{\pi-0}\chi' = \omega\tau_{KK} \tag{6.18}$$

We found that $1/\tau_{KK}$ increases linearly with temperature. It is always larger than the diffusion time estimated from the temperature dependence of χ'. This finding is consistent with the observation for WAu sample that $\delta_{\pi-0}\chi'' \propto \delta_{\pi-0}\chi'$ with the proportionality coefficient related to the diffusion time. This was accounted for by a phenomenological model and is actually related to the Kramers-Kronig relation.

In agreement with theoretical predictions presented in chap.4, one can easily imagine that there is a crossover from a temperature independent $1/\tau_{KK} = \frac{E_g}{\hbar}$ to a temperature dependent $1/\tau_{KK} = \frac{k_BT}{\hbar}$ at $T = 2E_g$.

6.4 High frequency / Low temperature response

In the preceding, we found that the response is well described in the regime $T \gtrsim 2E_g$ and $f \lesssim E_g$ by a model where the susceptibility is given by the sum of an adiabatic contribution, a diagonal contribution and a non-diagonal contribution. Here we report experiments at the frontier of this regime that does not seem to fit with that picture. As shown in fig.6.18, the non-dissipative response exhibits dips at odd multiple of π while the dissipative one displays broad maxima around odd multiples of π. The results presented here are still preliminary since their analysis is in progress. We however present some hypothesis about the origin of this response and describe qualitatively its evolution with temperature and frequency.

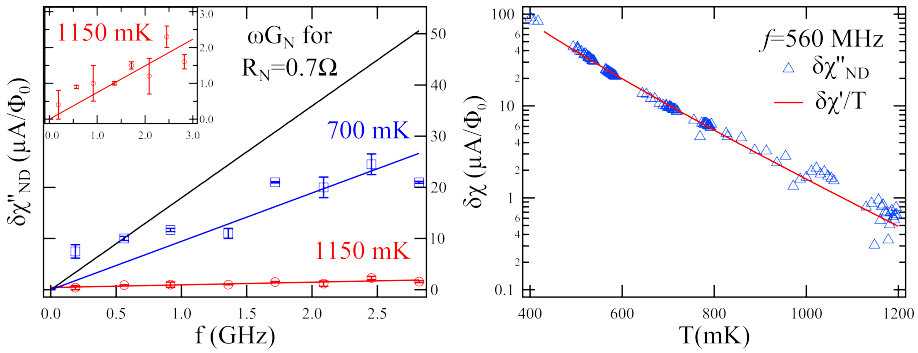

Figure 6.15: (**Left**) Frequency and (**Right**) temperature dependence of $\delta_{\pi-0}\chi"_{ND}$. Temperature dependence is for f=560 MHz . A close-up view of the frequency dependence of $\delta_{\pi-0}\chi"_{ND}$ at 1150 mK is shown in the inset.

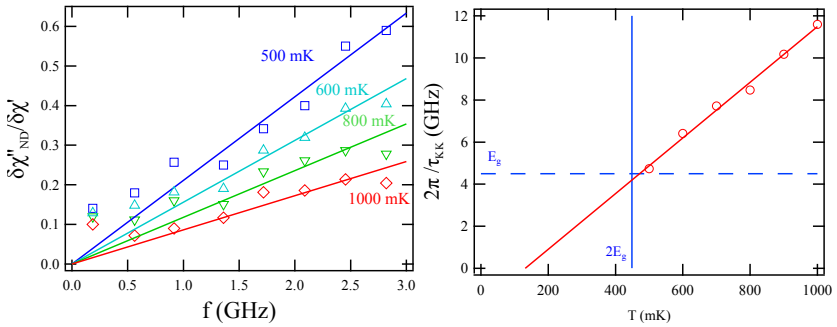

Figure 6.16: **Left:**Frequency dependence of $\delta_{\pi-0}\chi"_{ND}/\delta_{\pi-0}\chi'$ at several temperatures (symbols) along with their respective linear fits (lines). **Right:** Temperature dependence of $1/\tau_{KK}$, the inverse of the slope of $\frac{\delta_{\pi-0}\chi"_{ND}}{\delta_{\pi-0}\chi'}(\omega)$.

The dips in $\chi'(\varphi)$ in the vicinity of π are first observed at $f = 2.45GHz$ and $T = 430mK$ (see fig.6.17). They broaden with frequency and are more pronounced at low temperature (see fig.6.18). The latter is in contrast with experiments in non-linear regime [106] that display similar phase dependences but with a dip deepening when T increases. As shown in fig.6.19, we checked that experiments were carried in linear regime: the response does not depend on the applied power. Moreover spurious effects such as power being send to the sample through the mixer can be discarded since the amplitude of V_2, the second-harmonic of the signal, depends on the applied power.

At higher frequency (for instance at 14 GHz) the change of sign of χ' close to π corresponds to an inversion of the supercurrent; there is thus a $0-\pi$ transition. Such a $0-\pi$ transition has been observed in non-linear regime experiments where quasiparticles obeys a non-equilibrium double-step distribution function [76, 77] or in SNS junctions under microwave irradiation [80].

A tentative interpretation of our high frequency data would rely on Landau-Zener effect: at $\varphi = \pi$, quasiparticles do not adiabatically follow the low energy levels and have a finite probability to tunnel to the positive energy levels. The probability however depends on the applied power which is in contradiction

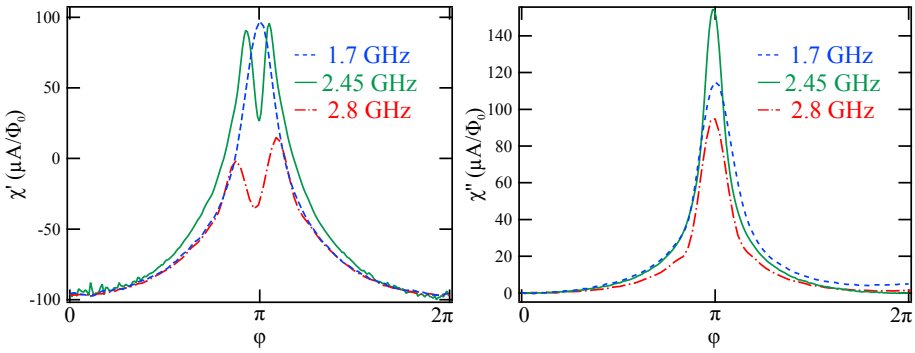

Figure 6.17: **Left:**Non-dissipative response χ' and **Right:** dissipative response χ'' at f=1.7 GHz and T=455 mK (dashed line), f=2.45 GHz and T=430 mK (solid line), f=2.8 GHz and T=435 mK (dashed dotted line)

with the observation of a linear response behavior.

An alternative explanation would be as follow: as put forward by Buttiker in the context of mesoscopic normal ring, a sinusoidal modulation of the phase of amplitude V_{ac} at frequency ω gives rise to sidebands at energies $E + \hbar\omega$ and $E - \hbar\omega$ [21]. Such sidebands would modify the spectrum by lowering the positive energy band and pulling up the negative energy band. This would be analogous to the Tien-Gordon effect [125] which is also a non-linear effect. Again, we emphasize that our experiments are in a linear regime. It seems reasonable to consider that the observed phase dependence are explained by an out-of-equilibrium distribution, we are however unable to describe a mechanism that would yield such a non-equilibrium distribution in a linear regime. It might be that we observed a non-linear effect in a saturated regime, thus explaining the absence of dependence on the applied power. We emphasize that these interpretations are still extremely preliminary. A complete investigation of these high frequency effects is left for future studies, all the more that a description of these features may be possible within Usadel formalism [126].

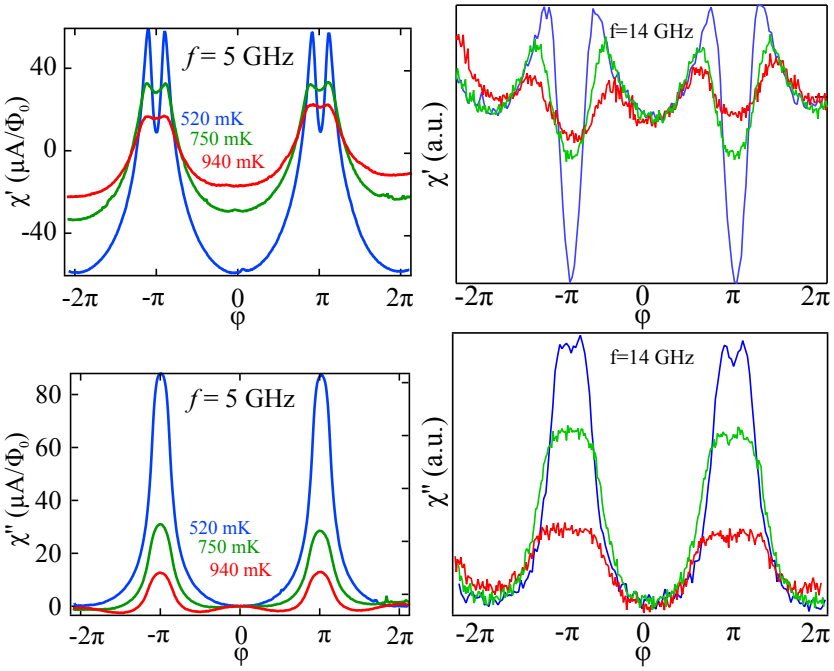

Figure 6.18: In-phase $\chi'$and out-of-phase χ"susceptibility at $f = 5GHz$ and $f = 14GHz$ for several temperatures.

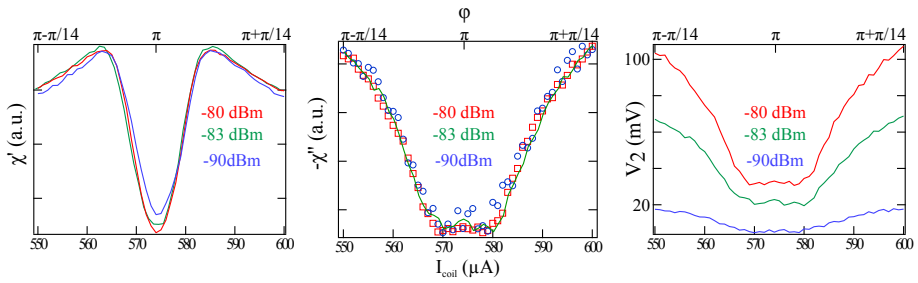

Figure 6.19: Close-up view of the response around $\varphi = \pi$ at $T = 445 \pm 2mK$, f=5 GHz for several powers. In phase and out-of-phase responses do not depend on the applied power. There are small deviations at $P_{att} = -100dB$ due to the looseness of the feedback loop.V_2, the voltage of the 2^{nd} harmonics, changes with power, indicating that the applied power effectively changes.

Conclusion

We probed the physics of a quantum system by playing with its *fundamental degree of freedom*, the phase of the wavefunctions, and by performing a non-invasive measurement of the ac susceptibility $\chi = \chi' + i\chi''$ *close to equilibrium*. Our results, made in the specific case of a long and diffusive SNS junction, should hold in any system provided it exhibits a phase-dependent spectrum. Such systems are, for instance, any Josephson junction or mesocopic normal rings. These systems exhibit non-dissipative currents at equilibrium due to the phase-dependence of their spectrum. In the case of long and diffusive SNS junctions the non-dissipative current is carried by Andreev pairs: a coherent superposition of electron and hole states. They populate Andreev bound states that form a quasi-continuous spectrum except for a phase-dependent gap at low energy: the minigap.

Our experiment revealed the evolution with phase, temperature and frequency of both the non-dissipative $\chi'$and dissipative χ"responses. We found out a wealth of behaviors related to the dynamics of Andreev pairs. We unveiled the existence of two timescales : the inelastic scattering time τ_{in} and a "minigap time" $\tau_g = \hbar/E_g = \tau_D/\pi$. These timescales are related to the onset of resistance in a phase-coherent system at finite frequency. To analyze the complex evolution of susceptibility we developed a Kubo-formula approach. Within this approach, we recast the susceptibility into three distinct contributions, related to distinct physical processes.

We called **Josephson contribution** χ_J the adiabatic response. It is purely non-dissipative and corresponds to the phase derivative of the supercurrent. It is frequency independent and has the temperature dependence of the critical current. The study of this contribution allows to characterize the system by determining the diffusion time τ_D and so the minigap $E_g/\hbar = \pi/\tau_D$.

The first frequency-dependent contribution is related to the **relaxation of Andreev pairs** driven out-of-equilibrium by the time-dependent phase biasing and therefore emerges on the timescale of the inelastic scattering time τ_{in}. We called this contribution the diagonal susceptibility $\chi_D$since it only involves the diagonal elements of the density matrix. $\chi_D$has a very specific double-peak phase dependence dominated by its second harmonic due to its dependence on the square of the single level currents. Its temperature dependence is related to the inelastic scattering and therefore depends on the relaxation mechanism relevant to the system. Its non-dissipative part χ'_Dmodifies the overall phase dependence of the adiabatic response,adding higher harmonics, but does not change its amplitude. The amplitude of χ'_Dsaturates at frequencies of a few τ_{in}. Its dissipative part χ''_Dcontributes the conductance and can be much larger

than the Drude conductance. It is peaked at frequencies close to the inelastic scattering rate. **The relaxation of Andreev pairs dominates the conductance at frequencies close to the inelastic scattering rate.** Using fluctuation-dissipation theorem, χ''_Dcan be related to **thermal noise at equilibrium** in a SNS junction. This noise may seem surprising since usually fluctuations are seen in systems having a resistance at zero frequency. In the present case there are fluctuations but no resistance at zero frequency.

The second frequency-dependent contribution described **microwave-induced transitions across the minigap** and is therefore related to E_g. We called this contribution the non-diagonal susceptibility χ_{ND} since it only involves the non-diagonal elements of the density matrix. Due to its dependence on the non-diagonal elements of the current operator as well as on the energies, it exhibits a rich behavior. At low temperature and high frequency it has a phase-dependence reminiscent of the minigap's. Its high temperature and low frequency phase dependence sharply contrasts: it is the opposite of the one of χ''_D. This surprising behavior is observed at high frequency and is supported by numerical simulations. These simulations pointed out the existence of **selections rules**: the amplitude of the non-diagonal current operator is non-negligible only for **transitions between electron-hole symmetric Andreev states**.

Since the non-dissipative part of the non-diagonal susceptibility $\chi'_{ND}$is negligible in the regime of high temperature and low frequency we focused on, we only considered the evolution its dissipative part χ''_{ND}. It has been studied via Kramers-Kronig relations that relates the non-dissipative susceptibility to the dissipative one. We found the ratio of the amplitudes to be proportional to the frequency $\frac{\delta_{\pi-0}\chi"_{ND}}{\delta_{\pi-0}\chi'} = \frac{1}{\tau_{KK}(T)}\omega$ with $\tau_{KK} \propto T$ in the high temperature regime. Our experimental findings are consistent with the prediction that τ_{KK} saturates at low temperature ($T < 2E_g$) with $\tau_{KK} = \frac{E_g}{\hbar}$, **reflecting the presence of the minigap in the density of states of the normal metal.**

We have thus developed a robust set of theory and experiment which accounts for the linear response of a quantum system under a frequency-dependent phase driving. It gives a very simple picture that consists in describing a system by its spectrum and its occupation, as in many quantum physics problem. It however suffers from some flaws: the non-dissipative response is still puzzling in the low temperature / high frequency regime with the emergence of a dip where the minigap closes. This feature may be described by our model but a more thorough study is necessary. In addition, we found a surprisingly short τ_{in} whose temperature dependence in T^{-3} is not yet understood.

Before concluding this dissertation with the perspectives offered by this work, we want to emphasize the fundamental difference between phase biasing and voltage biasing. **In contrast with voltage biasing, phase biasing is free of any non-equilibrium spurious effect** such as multiple Andreev reflections and solely probe the dynamics of Andreev pairs. Dynamical effects lead to the emergence of higher harmonics in the current-phase relation and may explain the appearance of fractional Shapiro steps in the current-voltage characteristics of microwave-irradiated SNS junctions. We thus emphasize this **limit to the usage of Shapiro steps to determine equilibrium properties of Josephson junctions** all the more in the current context where one

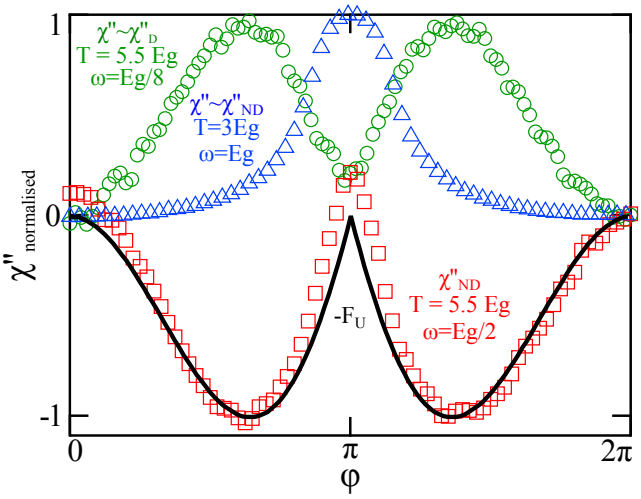

Figure 6.20: Typical phase dependences of χ". At frequencies close to τ_{in} ($\omega\tau_{in} \sim 1$) and high temperature ($T > E_g$), χ"can be dominated by its diagonal contribution χ''_D. At high frequency ($\omega \gtrsim E_g$) , the phase dependence of χ"is almost the minigap's. At low frequency and high temperature, χ''_{ND}phase dependence is almost the opposite of the one of the diagonal contribution. In this regime $\chi''_{ND}$and χ''_Dnearly cancel each other.

of the expected signature of novel excitations such as Majorana fermions is a 4π-periodic current-phase relation [127].

This work also opens new perspectives: at the time of writing this dissertation, we have not been able to go to the quantum regime where the temperature is much smaller than the excitation frequency even though it is currently within reach. It has been predicted that the spectroscopy of the minigap could be achievable in this regime. A direct improvement would also be the implementation of a tunable resonator with the use of Josephson junctions as non-linear impedance. This would allow to explore more precisely the low frequency regime.

This setup would prove of great interest to determine the properties of exotic materials. For instance there are several exciting predictions for SNS junctions where the weak-link is a wire with strong spin-orbit scattering or a topological insulator [128, 129, 130, 131].

Appendix: Focused Ion Beam fabrication technique

Focused Ion Beam (FIB) is a versatile technique: it allows to etch a surface and to deposit material. We used it to deposit W wires that are superconducting at $4K$ and have a critical field of $H_c \sim 7T$. It has been used in the group for several years [132] and more recently to make SNS junctions and NS rings [106]. We start using this technique to make NS rings embed into resonators because it yields good interfaces between W (S) and Au (N) thanks to an etching step prior to deposition and also because it is a mask-free technique that allows to easily redesign a sample.

In the following we detail the technique and balance its pros and cons to make SNS junctions and NS rings.

A brief description of the technique

A metallo-organic vapor of tungsten hexacarbonyl is injected over the sample. This vapor is decomposed by a focused Ga^+ ion beam, and a disordered W alloy is deposited on the substrate (see fig.1). The wires produced are composed of tungsten, carbon and gallium in varying proportions (in our case, the atomic concentrations are roughly 30% W, 50% C and 20% Ga). The superconducting critical temperature of the wires produced is $T_c \sim 4K$, an order of magnitude higher than the bulk T_c of W. This could be due to the inclusion of Ga, which is itself a superconductor with $T_c = 1K$. The W wires are 200 nm wide and 100 nm thick. There is a "contaminated" conducting area of about $200nm$ around the W wire (see fig.2). The dependence of the superconducting properties of these wires on the deposition conditions have been investigated in detail by W. Li *et al.* [133].

Another difficulty arose in our case: since we are using sapphire substrates which are insulating, charges cannot evacuate easily. Such a charging effect leads to image distortions and to the deposition of W wires of poor quality. It can be avoided by grounding the sample (see fig.1).

Characterization of WAuW junctions

We have measured the temperature dependence of the critical current of several junctions whose geometrical characteristics are gathered in table 1 (see caption for the definition of the different parameters). Even though these different junctions have similar geometrical properties (i.e. similar length, thickness and

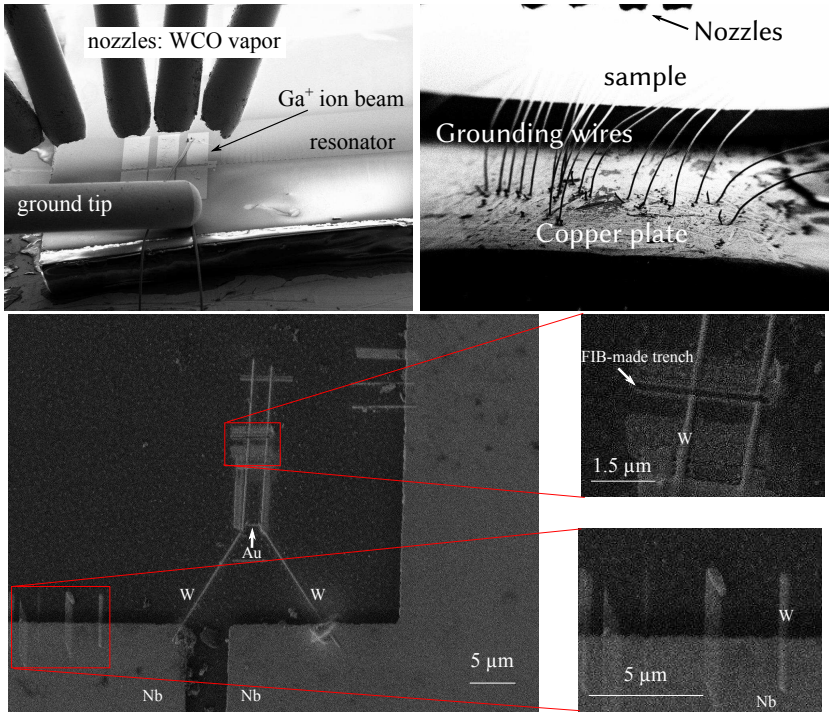

Figure 1: **Top left:**Nozzles inject a WCO vapor which is decomposed by a Ga^+ ion beam. A disordered W alloy is then deposited on the substrate (see bottom panel). Sample has to be grounded to avoid shifting during W deposition. If the grounding is not good enough, deposited wires are not well defined. **Top right:** To efficiently ground the sample, all contact pads of the resonator have to be connected to a copper plate. **Bottom:** Overview of a WAu ring embed into a Nb resonator. The top close-up view shows the possibility to redesign a sample by cutting wires somewhere using the Ga^+ ion beam and depositing another W wire elsewhere. Bottom close-up view shows that deposited wires can be not well-defined. This shifting can be due to a poorly grounded sample or to the fact that the sample's temperature is not stable yet: it takes some time before temperature stabilizes after the nozzles have been brought close to the sample for deposition.

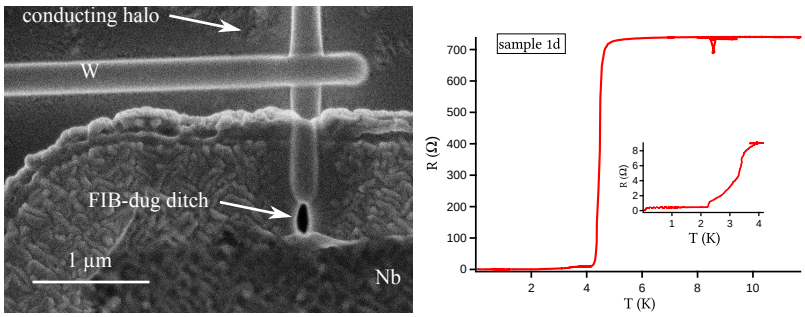

Figure 2: **Left:** FIB allows to deposit W wires and also to deeply etch a material. For instance here, a 1 micron thick Nb film has been dug and then filled by W. A halo of about $200nm$ around the W wire correspond to a "contaminated" conducting area. **Right:** Temperature dependence of the resistance of a WAuW junction. W wires turn superconducting at $T_c \sim 4K$.

sample	L_N (μm)	t (nm)	w (nm)	R_N (Ω)	$I_c(T=0)$ (μA)	E_{Th} (mK)
F	1.5	50	340	X	2.4	35
1d	1.3	50	230	4.5	1.8	22
1m	1.3	50	230	4	3.2	79
1j	1.4	50	390	2.8	40	75
1k	1.2	50	340	2.5	86	68

Table 1: Characteristics of several WAu junctions. Parameters are: the distance between superconducting leads L_N; the thickness t, the width w and the normal state resistance R_N of the normal wire; the critical current at zero temperature $I_c(T=0)$ and the Thouless energy E_{Th} of the junction. Different batches are separated by double lines.

width), we observe large sample-to-sample variations for the critical currents and the Thouless energy (see table 1). It may be due to the variations of deposition conditions that play a role on the superconducting properties of W or a variation of the interfaces quality. One may also have to consider the asymmetry between left and right contacts: as shown in the top left panel of fig.3, there is an extra length of Au on the left-hand side of the left contact whereas the right contact is almost at the end of the Au wire. Such an asymmetry vary from junction to junction and its effect is difficult to take into account.

Kinetic inductance of W wires

The concept of inductance reflects the fact that electric circuits oppose to a change in electromotive force which results in a phase lag in voltage. A change in electromotive force can be opposed either by the finite rate of change of magnetic flux in an inductor, this is the magnetic self-inductance and is a consequence of Faraday's law, either by the inertia of the charge carriers, this is the kinetic inductance.

Kinetic inductance (L_K) arises naturally in the Drude model. In the ex-

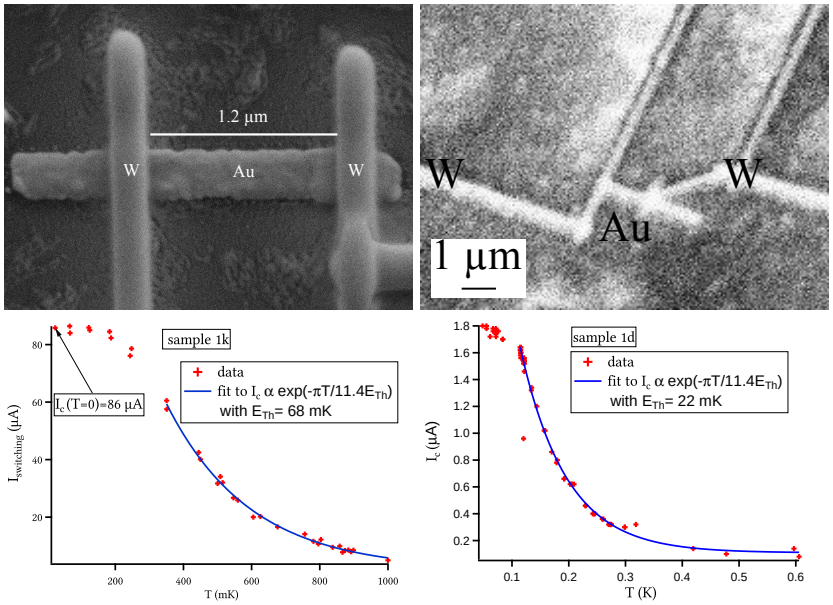

Figure 3: **Top:** Micrographs of sample 1k (left) and sample 1d (right, the poor quality of the micrograph is due to charging effect).**Bottom:** temperature dependence of the critical current of two similar WAu junctions: **Left:** sample 1k and **Right:** sample 1d. Whereas they have similar geometrical properties, their critical current and Thouless energy strongly differ from one another (see table 1).

pression of the conductivity σ, given by

$$\sigma = \frac{ne^2\tau}{m(1+\omega^2\tau^2)} - i\frac{ne^2\omega\tau^2}{m(1+\omega^2\tau^2)} \tag{6.19}$$

the imaginary part arises from kinetic inductance. In normal metals the collision time τ is typically $\approx 10^{-14}s$, so for frequencies < 100 GHz the term $\omega^2\tau^2$ is very small and can be ignored, leaving the magnetic self-inductance alone. In a superconductor, however, the dc resistance is zero and the impedance from dc to GHz frequencies can be dominated by the kinetic inductance of the supercurrent.

For a superconducting wire, the kinetic inductance can be calculated by equating the total kinetic energy of the Cooper pairs with an equivalent inductive energy[134]:

$$\frac{1}{2}(2mv^2)(n_s l A) = \frac{1}{2}L_K I^2 \tag{6.20}$$

where m is the electron mass, v is the average Cooper pair velocity, n_s is the density of Cooper pairs, l is the length of the wire, A is the wire cross-sectional area, and I is the current. Using the fact that the current $I = 2evn_sA$, where e is the electron charge, this yields:

$$L_K = \left(\frac{m}{2n_s e^2}\right)\left(\frac{l}{A}\right) \tag{6.21}$$

The kinetic inductance increases as the carrier density decreases. Physically, this is because a smaller number of carriers must have a greater velocity than a larger number of carriers in order to achieve the same current. As a consequence, superconductors with a small carrier density such as FIB-deposited W should display a large kinetic inductance.

Estimation of the kinetic inductance of W wires

In the low frequency limit ($hf \ll k_B T$), the Mattis-Bardeen formula for the complex conductivity can be written in terms of the ratio of the imaginary conductivity σ_2 to the normal state conductivity σ_N as [101]

$$\frac{\sigma_2}{\sigma_N} = \frac{\pi\Delta}{hf}\tanh(\frac{\Delta}{2k_B T}) \tag{6.22}$$

where Δ is superconducting energy gap[4]. The imaginary component of the impedance is due to kinetic inductance, and hence we can write equation 6.22 as

$$L_K = \frac{R_N h}{2\pi^2\Delta}\frac{1}{\tanh(\frac{\Delta}{2k_B T})} \tag{6.23}$$

where R_N is the resistance in the non-superconducting state. In the limit of low temperature ($k_B T \ll \Delta$), it simply reads:

$$L_K = \frac{R_N h}{2\pi^2\Delta} \tag{6.24}$$

The kinetic inductance of the FIB-deposited W wires can be estimated using that $\Delta/k_B = 1.76T_c \simeq 7K$ and using that the resistance of a 200 nm wide and 100 nm thick wire is about $100\Omega/\mu m$. These numbers yield a kinetic inductance of

$$L_K \sim 210pH \tag{6.25}$$

for a 600 nm wide, 100 nm thick and $18\mu m$ long wire such as the one used for the NS ring in sample 1m (see fig.1).

Experimental observation of the kinetic inductance of W wires

Kinetic inductance can lead to hysteresis in the magnetic susceptibility of a NS ring. Due to screening of the magnetic field by the ring the effective flux experienced by the ring Φ_{int} is different from the applied flux Φ_{ext}. Assuming a sinusoidal current-phase relation, the relation between the two reads :

$$\Phi_{ext} = \Phi_{int} + L_l I_c \sin(2\pi\Phi_{int}/\Phi_0) \tag{6.26}$$

where L_l is the loop's inductance and I_c the critical current of the weak link. Hysteresis appears when the parameter

$$\beta = \frac{2\pi L_l I_c}{\Phi_0} \tag{6.27}$$

[4] we assume here a temperature independent gap in absence of bias current

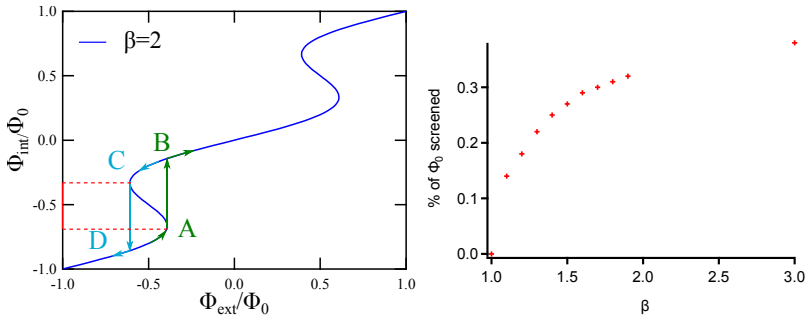

Figure 4: **Top left:** Internal flux vs. external flux for $\beta = 2$. When increasing the external flux, the internal flux follows up to A, where it jumps to B. Decreasing the external flux, the internal flux only jumps back to D in C, creating an hysteresis cycle. The red lines mark the internal flux range not accessible. **Top right:** Internal flux range not accessible Φ_s vs. $\beta = \frac{2\pi L_l I_c}{\Phi_0}$.

is larger than 1. Indeed, as shown in fig.4, when $\beta \geq 1$ the function $\Phi_{int}(\Phi_{ext})$ is no more single valued for Φ_{ext} close to odd multiples of Φ_0 and hysteresis appears. One can then associate a given value of β to a given amount of screened flux which is the experimentally accessible quantity.

To avoid the presence of hysteresis in the phase dependence of WAu rings' susceptibility, we have measured first the temperature dependence of a WAuW junction's critical current and close it afterward. To determine the perimeter of the loop to be made, we had wrongly considered only the magnetic self-inductance of the wire L_g which is typically $1pH/\mu m$ and therefore fabricated a loop such as

$$\frac{2\pi L_g I_c(T=0)}{\Phi_0} \lesssim 1 \tag{6.28}$$

During our first set of experiments we found a large hysteresis at low temperature. Unfortunately due to a leakage in the dilution fridge the experiment had to stop and this hysteresis could not be well estimated. We however decided to reduce the size of the ring (sample 1m) and make the wires three times larger (see fig.1). Then after we observed hysteresis at temperatures below 390 mK. Using the temperature dependence of Φ_s, the range of flux which is not accessible due to hysteresis, we could determined the temperature dependence of β at several frequencies. Knowing the critical current previously measured by transport experiments, we could determined the kinetic inductance of the ring (see fig.5). It is about $220pH$, ten times larger than the magnetic inductance.

Conclusion

In conclusion, FIB-deposition is a technique that allows to deeply etch already present structures, thus ensuring a transparent interface between the structure and the deposited wire. It also allows to easily redesign sample. Moreover, FIB-deposited W wires have a rather large critical temperature $T_c \simeq 4K$ and a large critical magnetic field $H_c \simeq 7T$. We however found a lack of reproducibility for the WAuW we have made with a large variation of the critical current

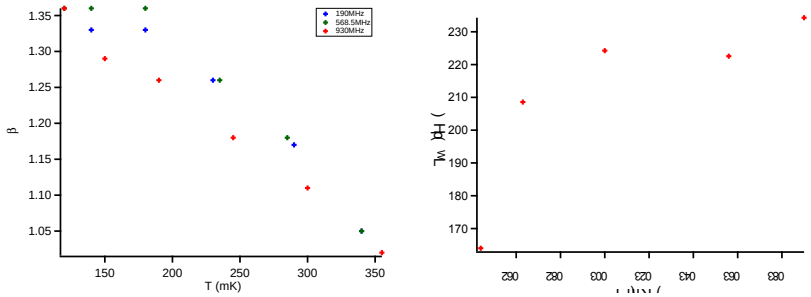

Figure 5: **Bottom left:** Experimental temperature dependence of β. **Bottom right:** Experimentally determined inductance of a 600 nm wide, 100 nm thick and 18μm long W wire.

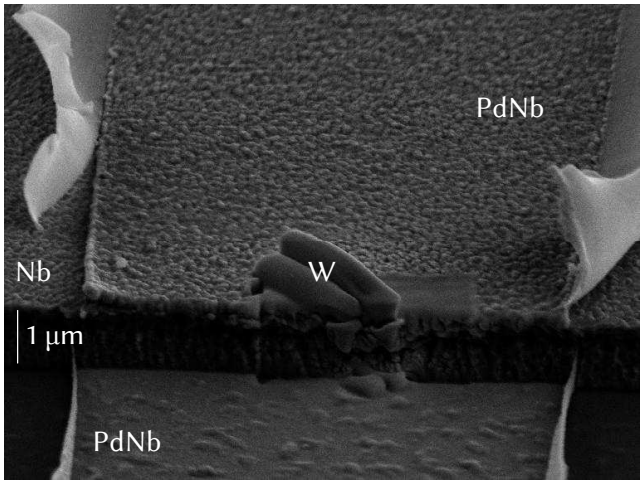

Figure 6: FIB-deposited W is used to connect a PdNbAu ring to a 1μ thick Nb resonator

and Thouless energy of apparently similar junctions. Yet there is room from improvement if care is taken about the position of the contacts.

Concerning the use of W wires for the fabrication of NS rings, we observed that they have a large inductance that is not compatible with the condition of a small LI_c product necessary avoid a hysteretic behavior. That is why we abandoned this technique to make NS ring, replacing W by a PdNb bilayer. It is however still used to obtain a good contact between the resonator and the NS ring (see fig.6). Indeed, the resonator is 1μm thick and its surface is oxidized, etching before deposition is thus necessary to obtain a good contact.

Lastly, along the lines of [134], it is worth mentioning that superconducting nanowires offer a large inductance that depends only weakly on current in a geometry that is relatively easy to fabricate. This makes them attractive for use in a variety of superconducting microwave circuits, including photon detectors [135], metamaterials [136], low-loss compact filters [137], and quantum bits [138].

Bibliography

[1] J.File and R.G. Mills. *Physical Review Letters*, 10:93, 1963. *Cited page 1*

[2] W. Meissner and R. Ochsenfeld. *Naturwissenschaften*, 21:787, 1933. *Cited page 1*

[3] V.L. Ginzburg and L.D. Landau. *JETP*, 20:1064, 1950. *Cited page 1*

[4] J Bardeen, LN Cooper, and JR Schrieffer. Theory of superconductivity. *Physical Review*, 108:1175, 1957. *2 citations pages 1 and 45*

[5] P. Dubos. *Transport électronique dans des nanojonctions supraconducteur - métal normal - supraconducteur*. PhD thesis, 2000. Available at http://tel.archives-ouvertes.fr/tel-00004264. *5 citations pages 2, 19, 34, 50, and 84*

[6] Richard Deblock. *Cohérence aux échelles mésoscopiques : réponse électromagnétique d'anneaux isolés et supercourants dans les nanotubes de carbone*. PhD thesis, 2001. Available at http://tel.archives-ouvertes.fr/tel-00002327. *3 citations pages 2, 8, and 9*

[7] B. Josephson. Possible new effects in superconductive tunnelling. *Physics Letters*, 1:251, 1962. *Cited page 1*

[8] P. W. Anderson and J. M. Rowell. Probable observation of the josephson superconducting tunneling effect. *Physical Review Letters*, 10:230–232, 1963. *Cited page 1*

[9] P. G. De Gennes. *Superconductivity of Metals and Alloys*. Westview Press, 1999. *3 citations pages 1, 13, and 45*

[10] F Bloch. Off-Diagonal Long-Range Order and Persistent Currents in a Hollow Cylinder. *Physical Review*, 137:A787, 1965. *Cited page 2*

[11] M Büttiker, Y Imry, and R Landauer. Josephson behavior in small normal one-dimensional rings. *Physics letters a*, 96(7):365–367, 1983. *3 citations pages 2, 3, and 4*

[12] R Landauer and M Büttiker. Resistance of small metallic loops. *Physical review letters*, 54(18):2049–2052, May 1985. *4 citations pages 2, 3, 5, and 12*

[13] RA Webb and S Washburn. Observation of h/e Aharonov-Bohm oscillations in normal-metal rings. *Physical review Letters*, 54(25), 1985. *Cited page 2*

[14] LP Levy, G Dolan, J Dunsmuir, and H Bouchiat. Magnetization of mesoscopic copper rings: Evidence for persistent currents. *Physical review letters*, 64(17):2074–2077, 1990. *Cited page 2*

[15] D Mailly, C Chapelier, and A Benoit. Experimental observation of persistent currents in GaAs-AlGaAs single loop. *Physical review letters*, 70(13):2020, 1993. *Cited page 2*

[16] V Chandrasekhar, RA Webb, and MJ Brady. Magnetic response of a single, isolated gold loop. *Physical review Letters*, 67(25):3578–3581, 1991. *Cited page 2*

[17] K. Lehnert, N. Argaman, H.-R. Blank, K. Wong, S. Allen, E. Hu, and H. Kroemer. Nonequilibrium ac Josephson Effect in Mesoscopic Nb-InAs-Nb Junctions. *Physical Review Letters*, 82(6):1265–1268, February 1999. *3 citations pages 2, 23, and 82*

[18] P. Dubos, H. Courtois, O. Buisson, and B. Pannetier. Coherent Low-Energy Charge Transport in a Diffusive S-N-S Junction. *Physical Review Letters*, 87(20):1–4, October 2001. *4 citations pages 2, 23, 82, and 83*

[19] L. Angers, F. Chiodi, G. Montambaux, M. Ferrier, S. Guéron, H. Bouchiat, and J. Cuevas. Proximity dc squids in the long-junction limit. *Physical Review B*, 77(16):165408, April 2008. *Cited page 2*

[20] M Büttiker. Flux-Sensitive Effects in Normal Metal Loops. *Annals of the New York Academy of Sciences*, 480:194–209, 1986. *6 citations pages 2, 5, 6, 7, 35, and 50*

[21] M Büttiker. Small normal-metal loop coupled to an electron reservoir. *Physical Review B*, 32(3):2–5, 1985. *2 citations pages 2 and 105*

[22] Y Imry and NS Shiren. Energy averaging and the flux-periodic phenomena in small normal-metal rings. *Physical Review B*, 33(12), 1986. *3 citations pages 2, 7, and 32*

[23] N Trivedi and DA Browne. Mesoscopic ring in a magnetic field: Reactive and dissipative response. *Physical Review B*, 38(14), 1988. *8 citations pages 2, 7, 23, 27, 32, 33, 34, and 42*

[24] JM Rowell. Tunneling Observation of Bound States in a Normal Metal -Superconductor Sandwich. *Physical Review Letters*, 30:167–170, 1973. *2 citations pages 3 and 13*

[25] H. le Sueur, P. Joyez, H. Pothier, C. Urbina, and D. Esteve. Phase Controlled Superconducting Proximity Effect Probed by Tunneling Spectroscopy. *Physical Review Letters*, 100(19):1–4, May 2008. *3 citations pages 3, 18, and 23*

[26] J-D. Pillet, C. H. L. Quay, P. Morfin, C. Bena, A. Levy Yeyati, and P. Joyez. Andreev bound states in supercurrent-carrying carbon nanotubes revealed. *Nature Physics*, 6(12):965–969, November 2010. *Cited page 3*

[27] L Bretheau, Ç Ö Girit, H Pothier, D Esteve, and C Urbina. Exciting Andreev pairs in a superconducting atomic contact. *Nature*, 499(7458):312–5, July 2013. *Cited page 3*

[28] PF Bagwell. Suppression of the Josephson current through a narrow, mesoscopic, semiconductor channel by a single impurity. *Physical Review B*, 46:12573, 1992. *4 citations pages 3, 15, 16, and 17*

[29] J Bardeen and JL Johnson. Josephson current flow in pure superconducting-normal-superconducting junctions. *Physical Review B*, 5:72, 1972. *4 citations pages 3, 13, 16, and 18*

[30] J Cayssol. *Etudes de propriétés thermodynamiques de structures hybrides métal normal/métal ferromagnétique-supraconducteur*. PhD thesis, 2003. Available at http://tel.archives-ouvertes.fr/tel-00008723. *Cited page 3*

[31] M Büttiker and TM Klapwijk. Flux sensitivity of a piecewise normal and superconducting metal loop. *Physical Review B*, 33:5114–5117, 1986. *2 citations pages 3 and 13*

[32] Hendrik Bluhm, Nicholas Koshnick, Julie Bert, Martin Huber, and Kathryn Moler. Persistent Currents in Normal Metal Rings. *Physical Review Letters*, 102(13):136802, March 2009. *Cited page 3*

[33] N Byers and CN Yang. Theoretical considerations concerning quantized magnetic flux in superconducting cylinders. *Physical review letters*, 7(2):2–5, 1961. *Cited page 4*

[34] F Bloch. Simple interpretation of the Josephson effect. *Physical Review Letters*, 21(17):1241–1243, 1968. *2 citations pages 4 and 20*

[35] F Bloch. Josephson effect in a superconducting ring. *Physical Review B*, 2(1):109, 1970. *Cited page 4*

[36] B Reulet. *Susceptibilité magnétique orbitale et Conductivité AC d'Anneaux mésoscopiques isolés*. PhD thesis, 1994. Available at http://cat.inist.fr/?aModele=afficheN&cpsidt=162288. *3 citations pages 8, 59, and 65*

[37] Y Noat. *Réponse électrique et magnétique de systèmes mésoscopiques isolés*. PhD thesis, 1999. Available at https://www.equipes.lps.u-psud.fr/spm/IMG/pdf/pdf_theseYves.pdf. *3 citations pages 8, 12, and 59*

[38] *Les Houches, session LXI, mesoscopic quantum physics*. Amsterdam ; North-Holland, 1994. *Cited page 11*

[39] Y. Aharonov A. Stern and Y. Imry. *Phys. Rev. A*, 41:3436, 1990. *Cited page 11*

[40] R. Landauer. Spatial variation of currents and fields due to localized scatterers in metallic conduction. *IBM J. Res. Develop.*, 1:233, 1957. *Cited page 12*

[41] R. Landauer. Electrical resistance of didisorder one-dimensional lattices. *Phil. Mag.*, 21:863, 1970. *Cited page 12*

[42] Rolf Landauer. Residual resistivity dipoles. *Zeitschrift fur Physik B Condensed Matter and Quanta*, 21(3):247–254, September 1975. *Cited page 12*

[43] R. Kubo. *J. Phys. Soc. Japan*, 12:570, 1957. *Cited page 12*

[44] Greenwood. *Proc. Phys. Soc. London*, 71:585, 1958. *Cited page 12*

[45] DS Fisher and PA Lee. Relation between conductivity and transmission matrix. *Physical Review B*, 23(12):6851, 1981. *Cited page 12*

[46] IO Kulik. Macroscopic quantization and the proximity effect in SNS junctions. *Soviet Journal of Experimental and Theoretical Physics*, 30(5):944, 1970. *4 citations pages 13, 14, 16, and 18*

[47] C Ishii. Josephson currents through junctions with normal metal barriers. *Progress of theoretical Physics*, 44(6), 1970. *2 citations pages 13 and 16*

[48] BJ Van Wees, KMH Lenssen, and C Harmans. Transmission formalism for supercurrent flow in multiprobe superconductor-semiconductor-superconductor devices. *Physical Review B*, 44(1):470, 1991. *Cited page 13*

[49] CWJ Beenakker and H Van Houten. Josephson current through a superconducting quantum point contact shorter than the coherence length. *Physical review letters*, 66(23):3056, 1991. *Cited page 13*

[50] U Gunsenheimer, U Schüssler, and R Kümmel. Symmetry breaking, off-diagonal scattering, and Josephson currents in mesoscopic weak links. *Physical Review B*, 49(9), 1994. *Cited page 13*

[51] AF Andreev. Thermal conductivity of the intermediate state of superconductors. *Soviet physics JETP*, 19:1228, 1964. *Cited page 13*

[52] PG De Gennes and D Saint-James. Elementary excitations in the vicinity of a normal metal-superconducting metal contact. *Physics Letters*, 4:4–5, 1963. *Cited page 13*

[53] D Saint-James. Excitations élémentaires au voisinage de la surface de séparation d'un métal normal et d'un métal supraconducteur. *Journal de Physique*, 25(1):899, 1964. *Cited page 13*

[54] X Jehl, M Sanquer, R Calemczuk, and D Mailly. Detection of doubled shot noise in short normal-metal/superconductor junctions. *Nature*, 405(6782):50–3, May 2000. *Cited page 13*

[55] S. Guéron, H. Pothier, N. Birge, D. Esteve, and M. Devoret. Superconducting Proximity Effect Probed on a Mesoscopic Length Scale. *Physical review letters*, 77(14):3025–3028, September 1996. *Cited page 13*

[56] L. Angers. *Rectification et supraconductivité de proximité dans des anneaux mésoscopiques*. PhD thesis, 2007. Available at http://tel.archives-ouvertes.fr/tel-00156703. *Cited page 14*

[57] CWJ Beenakker. Universal limit of critical-current fluctuations in mesoscopic Josephson junctions. *Physical review letters*, 67(27):3836–3839, 1991. *3 citations pages 16, 17, and 18*

[58] AV Zaitsev. Quasiclassical equations of the theory of superconductivity for contiguous metals and the properties of constricted microcontacts. *Zh. Eksp. Teor. Fiz*, 59(May 1984):1015, 1984. *Cited page 16*

[59] E. Scheer, W. Belzig, Y. Naveh, M. Devoret, D. Esteve, and C. Urbina. Proximity Effect and Multiple Andreev Reflections in Gold Atomic Contacts. *Physical Review Letters*, 86(2):284–287, January 2001. *2 citations pages 16 and 20*

[60] L. Bretheau, Ç. Girit, C. Urbina, D. Esteve, and H. Pothier. Supercurrent Spectroscopy of Andreev States. *Physical Review X*, 3(4):041034, December 2013. *2 citations pages 16 and 58*

[61] M Ferrier, B Dassonneville, S. Guéron, and H Bouchiat. Phase-dependent Andreev spectrum in a diffusive SNS junction : Static and dynamic current response. *Phys. Rev. B*, 88:174505, 2013. *Cited page 17*

[62] Y. Imry. *Introduction to mesoscopic physics*. Oxford University Press, 1997. *Cited page 16*

[63] A. Golubov, M. Kupriyanov, and E. Ilichev. The current-phase relation in Josephson junctions. *Reviews of Modern Physics*, 76(2):411–469, April 2004. *2 citations pages 17 and 19*

[64] YV Nazarov. Limits of universality in disordered conductors. *Physical review letters*, 73(1):134–137, 1994. *2 citations pages 17 and 49*

[65] ON Dorokhov. On the coexistence of localized and extended electronic states in the metallic phase. *Solid state communications*, 51(6):381–384, 1984. *2 citations pages 17 and 49*

[66] Nathan Argaman. Random scattering matrices and the circuit theory of Andreev conductances. *EPL (Europhysics Letters)*, pages 1–12, 1997. *Cited page 18*

[67] F Zhou, P Charlat, B Spivak, and B Pannetier. Density of states in superconductor-normal metal-superconductor junctions. *Journal of Low Temperature Physics*, 110:841–850, 1998. *2 citations pages 18 and 49*

[68] Dmitri Ivanov, Raphael von Roten, and Gianni Blatter. Minigap in a long disordered SNS junction: Analytical results. *Physical Review B*, 66(5):052507, August 2002. *Cited page 18*

[69] KK Likharev. Superconducting weak links. *Reviews of Modern Physics*, page 101, 1979. *Cited page 18*

[70] I. Kulik and A. Omel'yanchhuk. *JETP Lett.*, 21:96, 1975. *Cited page 18*

[71] I. Kulik and A. Omel'yanchuk. *Sov. J. Low. Temp. Phys.*, 3:459, 1977. *3 citations pages 18, 35, and 98*

[72] P Dubos, H Courtois, and B Pannetier. Josephson critical current in a long mesoscopic SNS junction. *Physical Review B*, 63:1–5, 2001. *5 citations pages 18, 19, 83, 89, and 90*

[73] Alex Levchenko, Alex Kamenev, and Leonid Glazman. Singular length dependence of critical current in superconductor/normal-metal/superconductor bridges. *Physical Review B*, 74(21):212509, December 2006. *Cited page 18*

[74] W Belzig, C Bruder, and G Schön. Local density of states in a dirty normal metal connected to a superconductor. *Physical review. B, Condensed matter*, 54(13):9443–9448, October 1996. *Cited page 18*

[75] W Belzig, FK Wilhelm, and C Bruder. Quasiclassical Green's function approach to mesoscopic superconductivity. *Superlattices and microstructures*, 25(5):1251, 1999. *Cited page 18*

[76] JJA Baselmans and AF Morpurgo. Reversing the direction of the supercurrent in a controllable Josephson junction. *Nature*, 397(March 1979):1998–2000, 1999. *2 citations pages 19 and 104*

[77] J. Baselmans, T. Heikkilä, B. van Wees, and T. Klapwijk. Direct Observation of the Transition from the Conventional Superconducting State to the π State in a Controllable Josephson Junction. *Physical Review Letters*, 89(20):207002, October 2002. *2 citations pages 19 and 104*

[78] Sophie Guéron. *Quasiparticles in a diffusive conductor : Interaction and pairing.* PhD thesis, 1997. Available at http://tel.archives-ouvertes.fr/tel-00185371. *Cited page 19*

[79] Tero Heikkilä, Jani Särkkä, and Frank Wilhelm. Supercurrent-carrying density of states in diffusive mesoscopic Josephson weak links. *Physical Review B*, 66(18):184513, November 2002. *3 citations pages 19, 50, and 84*

[80] M. Fuechsle, J. Bentner, D. Ryndyk, M. Reinwald, W. Wegscheider, and C. Strunk. Effect of Microwaves on the Current-Phase Relation of Superconductor/Normal Metal/Superconductor Josephson Junctions. *Physical Review Letters*, 102(12):9–12, March 2009. *7 citations pages 19, 23, 34, 82, 87, 88, and 104*

[81] GE Blonder, M Tinkham, and TM Klapwijk. Transition from metallic to tunneling regimes in superconducting microconstrictions: Excess current, charge imbalance, and supercurrent conversion. *Physical Review B*, 25(April):4515, 1982. *Cited page 20*

[82] D. Averin and A. Bardas. ac Josephson Effect in a Single Quantum Channel. *Phys. Rev. Lett.*, 75(9):1831–1834, 1995. *Cited page 20*

[83] M Chauvin, P Vom Stein, D Esteve, C. Urbina, J. C. Cuevas, and Levy Yeyati A. Crossover from Josephson to multiple Andreev reflection currents in atomic contacts. *Physical Review Letters*, 99:067008, 2007. *Cited page 20*

[84] C. Hoffmann, F. Lefloch, M. Sanquer, and B. Pannetier. Mesoscopic transition in the shot noise of diffusive superconductor/normal metal/superconductor junctions. *Physical Review B*, 70(18):180503, November 2004. *2 citations pages 20 and 23*

[85] E. Lhotel, O. Coupiac, F. Lefloch, H. Courtois, and M. Sanquer. Divergence at Low Bias and Down-Mixing of the Current Noise in a Diffusive Superconductor–Normal-Metal–Superconductor Junction. *Physical Review Letters*, 99(11):117002, September 2007. *3 citations pages 20, 23, and 98*

[86] E. Bezuglyi, E. Bratus, V. Shumeiko, G. Wendin, and H. Takayanagi. Circuit theory of multiple Andreev reflections in diffusive SNS junctions: The incoherent case. *Physical Review B*, 62(21):14439–14451, December 2000. *2 citations pages 20 and 23*

[87] K. Nagaev. Frequency-Dependent Shot Noise in Long Disordered Superconductor/Normal Metal/Superconductor Contacts. *Physical Review Letters*, 86(14):3112–3115, April 2001. *2 citations pages 20 and 23*

[88] S. Pilgram and P. Samuelsson. Noise and Full Counting Statistics of Incoherent Multiple Andreev Reflection. *Physical Review Letters*, 94(8):086806, March 2005. *2 citations pages 20 and 23*

[89] J. Cuevas, J. Hammer, J. Kopu, J. Viljas, and M. Eschrig. Proximity effect and multiple Andreev reflections in diffusive superconductor/normal metal/superconductor junctions. *Physical Review B*, 73(18):184505, May 2006. *2 citations pages 20 and 23*

[90] T Hoss, C Strunk, T Nussbaumer, and R Huber. Multiple Andreev reflection and giant excess noise in diffusive superconductor/normal-metal/superconductor junctions. *Physical Review B*, 62(6):4079–4085, 2000. *3 citations pages 20, 23, and 98*

[91] SV Lempitskii. Stimulation of superconductivity by a direct current in a superconductor-normal metal-superconductor junction. *Sov. Phys.-JETP (Engl. Transl.)*, 58(3):624–628, 1983. *6 citations pages 20, 21, 35, 50, 91, and 96*

[92] F Zhou and B Spivak. Resistance of superconductor-normal-metal-superconductor (SNS) junctions. *Journal of Experimental and Theoretical Physics Letters*, (January):369–374, 1997. *2 citations pages 20 and 96*

[93] N Argaman. Nonequilibrium Josephson-like effects in wide mesoscopic SNS junctions. *Superlattices and microstructures*, 25(5), 1999. *Cited page 20*

[94] K. Tikhonov. *Proximity effect and fluctuations in superconducting structures with disorder*. PhD thesis, 2012. Available at http://qmeso.itp.ac.ru/eng/index.html. *Cited page 20*

[95] Pauli Virtanen, F. Sebastián Bergeret, Juan Cuevas, and Tero Heikkilä. Linear ac response of diffusive SNS junctions. *Physical Review B*, 83(14), April 2011. *13 citations pages 23, 24, 35, 36, 42, 50, 51, 56, 58, 91, 94, 95, and 98*

[96] F Chiodi, M Ferrier, K Tikhonov, P Virtanen, T T Heikkilä, M Feigelman, S Guéron, and H Bouchiat. Probing the dynamics of Andreev states in a coherent Normal/Superconducting ring. *Scientific reports*, 1:3, January 2011. *5 citations pages 23, 24, 35, 65, and 96*

[97] B Reulet and H Bouchiat. ac conductivity of mesoscopic rings: The discrete-spectrum limit. *Physical Review B*, 1994. *4 citations pages 23, 33, 42, and 62*

[98] F. Chiodi, M. Aprili, and B. Reulet. Evidence for Two Time Scales in Long SNS Junctions. *Physical Review Letters*, 103(17):177002, October 2009. *Cited page 23*

[99] Christophe Texier. Physique statistique des systèmes (faiblement) hors équilibre : formalisme de la réponse linéaire. Dissipation quantique. Transport électronique. 2013. Available at http://lptms.u-psud.fr/christophe_texier/enseignements/enseignements-en-master/physique-statistique-hors-equilibre/. *Cited page 27*

[100] G Montambaux, H Bouchiat, D Sigeti, and R Friesner. Persistent currents in mesoscopic metallic rings: Ensemble average. *Physical Review B*, 42(12):7647, 1990. *2 citations pages 34 and 47*

[101] M. Tinkham. *Introduction to superconductivity (2nd edition)*. Dover Publications, 1996. *2 citations pages 45 and 115*

[102] S Datta and PF Bagwell. Can the Bogoliubov - de Gennes equation be interpreted as a 'one-particle'wave equation? *Superlattices and microstructures*, 25(5), 1999. *Cited page 45*

[103] I. O. Kulik and A. N. Omelyanchuk. *Sov. J. Low Temp.Phys.*, 3:459, 1977. *Cited page 50*

[104] F. Kos, S. E. Nigg, and L. I. Glazman. Frequency-dependent admittance of a short superconducting weak link. *Physical Review B*, 87(17):174521, May 2013. *Cited page 57*

[105] R Deblock, Y Noat, H Bouchiat, B Reulet, and D Mailly. Measurements of flux-dependent screening in aharonov-bohm rings. *Physical review letters*, 84(23):5379–82, June 2000. *Cited page 59*

[106] F Chiodi. *Dynamical effects in Superconductor / Normal metal / Superconductor long Josephson Junctions*. PhD thesis, 2010. *4 citations pages 59, 61, 104, and 111*

[107] G. Feher. Sensitivity considerations in microwave paramagnetic resonance absorption techniques. *Bell System Technical Journal*, 36:449, 1957. *Cited page 66*

[108] M. Göppl, A. Fragner, M. Baur, R. Bianchetti, S. Filipp, J. M. Fink, P. J. Leek, G. Puebla, L. Steffen, and A. Wallraff. Coplanar waveguide resonators for circuit quantum electrodynamics. *Journal of Applied Physics*, 104(11):113904, 2008. *Cited page 68*

[109] F. W. Grover. *Inductance calculations*. 1947. *Cited page 77*

[110] Gilles Montambaux. Interference pattern of a long diffusive Josephson junction. *arXiv preprint arXiv:0707.0411*, pages 1–4, 2007. *Cited page 81*

[111] J. Cuevas and F. Bergeret. Magnetic Interference Patterns and Vortices in Diffusive SNS Junctions. *Physical Review Letters*, 99(21):217002, November 2007. *Cited page 81*

[112] S Shapiro. Josephson currents in superconducting tunneling: The effect of microwaves and other observations. *Phys. Rev. Letters*, 1(2), 1963. *Cited page 82*

[113] F Chiodi, M Ferrier, and S Guéron. Geometry-related magnetic interference patterns in long SNS Josephson junctions. *Physical Review B*, pages 1–5, 2012. *Cited page 82*

[114] W. Belzig M. Wolz, C. Debuschewitz and E. Scheer. *Phys. Rev.B*, 84:104516, 2011. *2 citations pages 84 and 99*

[115] H. Raffy et al. *J. Physique*, 46:627, 1985. *2 citations pages 84 and 99*

[116] A Martín-Rodero, Levy Yeyati A, and Fj García-Vidal. Thermal noise in superconducting quantum point contacts. *Physical review. B, Condensed matter*, 53(14):R8891–R8894, April 1996. *2 citations pages 92 and 98*

[117] T. Heikkilä and Francesco Giazotto. Phase sensitive electron-phonon coupling in a superconducting proximity structure. *Physical Review B*, 79(9):094514, March 2009. *Cited page 94*

[118] F Pierre. *Interactions électron-électron dans les fils mésoscopiques*. PhD thesis, 2001. Available at http://tel.archives-ouvertes.fr/tel-00591514. *2 citations pages 94 and 99*

[119] KS Tikhonov and MV Feigel'man. AC Josephson effect in the long voltage-biased SINIS junction. *JETP letters*, 89(4):205–211, 2009. *Cited page 96*

[120] D Rogovin and DJ Scalapino. Fluctuation phenomena in tunnel junctions. *Annals of Physics*, 90:1–90, 1974. *Cited page 98*

[121] Y. Blanter. electron-electron scattering rate in didisorder mesoscopic systems. *Phys. Rev. B*, 54:12807, 1997. *Cited page 99*

[122] Christophe Texier and Gilles Montambaux. Dephasing due to electron-electron interaction in a diffusive ring. *Physical Review B*, 72(11):1–20, September 2005. *Cited page 99*

[123] B. Dassonneville, M. Ferrier, S. Guéron, and H. Bouchiat. Dissipation and Supercurrent Fluctuations in a Diffusive Normal Metal/Superconductor Ring. *Physical Review Letters*, 110(21):217001, May 2013. *Cited page 99*

[124] MA Skvortsov and MV Feigel'man. Subgap states in disordered superconductors. *arXiv preprint arXiv:1305.6300*, pages 1–12, 2013. *Cited page 99*

[125] PK Tien and JP Gordon. Multiphoton process observed in the interaction of microwave fields with the tunneling between superconductor films. *Physical Review*, 129:647, 1963. *Cited page 105*

[126] K Tikhonov. private communications. *Cited page 105*

[127] Leonid P. Rokhinson, Xinyu Liu, and Jacek K. Furdyna. The fractional a.c. Josephson effect in a semiconductor/superconductor nanowire as a signature of Majorana particles. *Nature Physics*, 8(11):795–799, September 2012. *Cited page 109*

[128] A. Buzdin. Direct Coupling Between Magnetism and Superconducting Current in the Josephson $varphi_0$ Junction. *Physical Review Letters*, 101(10):107005, September 2008. *Cited page 109*

[129] Jay D. Sau, Roman M. Lutchyn, Sumanta Tewari, and S. Das Sarma. Generic new platform for topological quantum computation using semiconductor heterostructures. *Phys. Rev. Lett.*, 104:040502, Jan 2010. *Cited page 109*

[130] Meng Cheng and Roman M. Lutchyn. Josephson current through a superconductor/semiconductor-nanowire/superconductor junction: Effects of strong spin-orbit coupling and zeeman splitting. *Phys. Rev. B*, 86:134522, Oct 2012. *Cited page 109*

[131] Liang Fu and C. Kane. Superconducting Proximity Effect and Majorana Fermions at the Surface of a Topological Insulator. *Physical Review Letters*, 100(9):096407, March 2008. *Cited page 109*

[132] A. Kasumov, K. Tsukagoshi, M. Kawamura, T. Kobayashi, Y. Aoyagi, K. Senba, T. Kodama, H. Nishikawa, I. Ikemoto, K. Kikuchi, V. Volkov, Yu. Kasumov, R. Deblock, S. Guéron, and H. Bouchiat. Proximity effect in a superconductor-metallofullerene-superconductor molecular junction. *Physical Review B*, 72(3):033414, July 2005. *Cited page 111*

[133] Wuxia Li, J. C. Fenton, Yiqian Wang, D. W. McComb, and P. a. Warburton. Tunability of the superconductivity of tungsten films grown by focused-ion-beam direct writing. *Journal of Applied Physics*, 104(9):093913, 2008. *Cited page 111*

[134] Anthony J Annunziata, Daniel F Santavicca, Luigi Frunzio, Gianluigi Catelani, Michael J Rooks, Aviad Frydman, and Daniel E Prober. Tunable superconducting nanoinductors. *Nanotechnology*, 21(44):445202, November 2010. *2 citations pages 114 and 117*

[135] PK Day, HG LeDuc, and BA Mazin. A broadband superconducting detector suitable for use in large arrays. *Nature*, 425(October):12–14, 2003. *Cited page 117*

[136] Cihan Kurter, John Abrahams, and Steven M. Anlage. Miniaturized superconducting metamaterials for radio frequencies. *Applied Physics Letters*, 96(25):253504, 2010. *Cited page 117*

[137] K D Irwin, M D Niemack, J Beyer, H M Cho, W B Doriese, G C Hilton, C D Reintsema, D R Schmidt, J N Ullom, and L R Vale. Code-division multiplexing of superconducting transition-edge sensor arrays. *Superconductor Science and Technology*, 23(3):034004, March 2010. *Cited page 117*

[138] Vladimir E Manucharyan, Jens Koch, Leonid I Glazman, and Michel H Devoret. Fluxonium: single cooper-pair circuit free of charge offsets. *Science (New York, N.Y.)*, 326(5949):113–6, October 2009. *Cited page 117*